LA-4749-MS

C.3

Quarterly Status Report on the

Advanced Plutonium Fuels Program

April 1 to June 30, 1971

and Fifth Annual Report, FY 1971

los alamos
scientific laboratory
of the University of California
LOS ALAMOS, NEW MEXICO 87544

UNITED STATES
ATOMIC ENERGY COMMISSION
CONTRACT W-7405-ENG. 36

This LA. . .MS report presents the status of the LASL Advanced Plutonium Fuels Program. The four most recent Quarterly Status Reports in this series, all unclassified, are:

LA-4494-MS	LA-4595-MS
LA-4546-MS	LA-4693-MS

This report, like other special-purpose documents in the LA. . .MS series, has not been reviewed or verified for accuracy in the interest of prompt distribution.

Printed in the United States of America. Available from
National Technical Information Service
U. S. Department of Commerce
5285 Port Royal Road
Springfield, Virginia 22151
Price: Printed Copy $3.00; Microfiche $0.95

LA-4749-MS
UC-80
FAST REACTOR REPORT
SPECIAL DISTRIBUTION

ISSUED: August 1971

los alamos
scientific laboratory
of the University of California
LOS ALAMOS, NEW MEXICO 87544

Quarterly Status Report on the

Advanced Plutonium Fuels Program

April 1 to June 30, 1971

and Fifth Annual Report, FY 1971

compiled by

R. D. Baker

FOREWORD

This is the fifth annual report on the Advanced Plutonium Fuels Program conducted at the Los Alamos Scientific Laboratory. Results of the current quarter's work has been in most cases incorporated into the summary of the year's work, and is therefore specifically identified.

Most of the investigations discussed are of the continuing type. Results and conclusions described may therefore be changed or augmented as the work continues. Published reference to results cited in the report should not be made without obtaining explicit permission to do so from the persons in charge of the work.

TABLE OF CONTENTS

PROJECT 401

EXAMINATION OF FAST REACTOR FUELS

Person in Charge: R. D. Baker
Principal Investigators: J. W. Schulte
K. A. Johnson
G. R. Waterbury

I. INTRODUCTION

This project is directed toward the examination and comparison of the effects of neutron irradiation on LMFBR Program fuel materials. Unirradiated and irradiated materials will be examined as requested by the Fuels and Materials Branch of DRDT. Capabilities are established and are being expanded for providing conventional preirradiation and postirradiation examinations. Nondestructive tests will be conducted in a hot cell facility specifically modified for examining irradiated prototype fuel pins at a rate commensurate with schedules established by DRDT.

Characterization of unirradiated and irradiated fuels by analytical chemistry methods will continue, and additional methods will be modified and mechanized for hot cell application. Macro- and micro-examinations will be made on fuel and cladding using the shielded electron microprobe, emission spectrograph, radiochemistry, gamma scanner, mass spectrometers, and other analytical facilities. New capabilities will be developed in: gamma scanning, analyses to assess spatial distributions of fuel and fission products, mass spectrometric measurements of burnup and fission gas constituents, chemical analyses, and measurement of carbon in irradiated fuels.

Microstructural analyses of unirradiated and irradiated materials will continue using optical and electron microscopy, and autoradiographic and x-ray techniques. Special emphasis will be placed on numerical representation of microstructures and its relationship to fabrication and irradiation parameters. New etching and mounting techniques will be developed for high burnup materials.

II. EQUIPMENT DEVELOPMENT

A. Inert Atmosphere Systems

(C. E. Frantz, P. A. Mason, R. F. Velkinburg, L. A. Waldschmidt)

The difficulties experienced in FY 1970 with the purification systems and leaks in the containment boxes were largely overcome during FY 1971. The goal of providing the containment boxes with inert atmospheres having less than 100 ppm O_2 + H_2O was achieved during this period by improvements to the recirculating systems, transfer systems, and box penetrations.

Special seal collars for the manipulator boots were installed in the disassembly cell and the two metallography cells. These collars are composed of a floating assembly which provides a multiple seal in the annulus between the manipulator through-tube and the manipulator port in the alpha box. The installation of the collars resulted in a significant reduction in the air leak rate.

Since August 1970, the atmosphere in the disassembly cell has been maintained almost continuously by a Vacuum Atmosphere Corporation HE-293A Purifier System capable of removing oxygen and moisture. The concentration of nitrogen has been maintained below 1% by the use of a 2 to 5 SCFH Ar purge of the system. Concentrations as low as 1.7 ppm O_2 and 0.8 ppm H_2O have been achieved during the report period. Except for an occasional spike in the O_2 and H_2O levels due to poor sealing

during some transfer operations, levels of < 10 ppm O_2 and ~ 2 ppm H_2O are being maintained.

In November 1970 the two metallography cells and metallograph blister were taken out of service to permit extensive leak checking and the change-out of some equipment. Major leaks were located at manipulator ports in the alpha boxes. Other significant leaks were located and corrected at the rubber gaskets for the sealed panels and the O-ring-sealed flanges of the two intercell pass-throughs. Leaks were also located at the window seals which were inaccessible for correction. The leaks at the manipulator ports were corrected by installing specially cast lead weights (35 lbs per manipulator) in the slave end of the manipulator through-tubes. This permitted relocation of the center of gravity of the manipulator to a point between the sets of support rollers. A correct alignment of the through-tube in the boot seal collar assembly was thus provided. Subsequent tests indicated that the major leaks were corrected since it was possible to attain O_2 and H_2O concentrations as low as 1.5 ppm and 0.7 ppm, respectively, with the two boxes and blister on the recirculating purifier.

The Freon TF which was used as a grinding lubricant and in the ultrasonic cleaners caused severe corrosion in the gas purification systems. Consequently, a search was initiated for a replacement solvent which would have the following characteristics: minimum reaction with the specimens and mounting materials, high purity, low vapor pressure, desirable cavitation properties in ultrasonic cleaners, halogen-free, ready availability, and moderate price. Several compounds were tested, and the solvent that met most of the requirements was n-butyl acetate. It was expected that acetic acid would be formed from the decomposition of the butyl acetate in the purifier; however, no deleterious effects on the recirculating system have been observed after several months.

Operation of the cells for approximately four weeks did show, however, that the butyl acetate caused rapid deterioration of the PVC in the manipulator gauntlets. Preliminary tests indicated that polyurethane is considerably more resistant to the solvent. Efforts are being made to find a commercial supplier for polyurethane gauntlets or booting. The boots which were provided with the Model L manipulators, obtained from Central Research Laboratories, have molded polyurethane gauntlets which appear to be performing satisfactorily after six weeks of service in one of the metallography cells where high concentrations of butyl acetate are present.

Further efforts are being made to minimize the buildup of butyl acetate in the boxes and to obviate any deleterious effect of the solvent on the recirculating system and the manipulator boots. A refrigeration system is being designed which will remove 90% of the butyl acetate from the atmosphere of the metallography cells. The principle of operation is to cool the effluent atmosphere from the boxes to the "dew point" which will condense the solvent for collection and removal as a liquid.

A station and control panel have been installed to permit remote operation for providing inert atmosphere for the transfer containers by either a once-through purge mode or a repetitive evacuation and back-fill method.

A modification to the U. S. Dynamics RSD Purifier System for moisture gettering has been fabricated to convert from a purge to an evacuation type of regeneration cycle. This will permit a reduction of 40 SCFH of Ar in the purge requirements. Installation has been postponed for further evaluation of the effect of a probable increase in the evaporated solvent concentrations in the metallography cells.

The two containment boxes used for analytical chemistry have been equipped to permit an Ar purge for those operations in which an inert atmosphere may be required. Of the eight containment boxes now equipped for handling irradiated plutonium fuels, seven can be provided with inert atmosphere. The eighth box,which is used for emission spectrography of irradiated fuels, could be altered for inert atmosphere capability within a few days if required.

B. Sealed Manipulators

(P. A. Mason, C. D. Montgomery, R. F. Velkinburg)

One pair of CRL Model "L" sealed manipulators was received in November 1970. Special adapter tubes to accommodate these manipulators in the cell walls and alpha

containment boxes were designed and built. Extensive tests were performed on these manipulators in the mock-up area. A boot assembly was attached to each manipulator arm and the boot was purged and pressurized to 5 in. of water. No significant leakage was observed through either manipulator assembly using a VEECO helium leak detector.

These manipulators were installed in one of the inert atmosphere metallography cells on May 25, 1971. Experience since this time indicates that it is possible to achieve an Ar atmosphere of < 10 ppm $O_2 + H_2O$ with the use of Model L manipulators and the type of containment box used in the LASL Wing 9 Hot Cell Facility. Additional manipulators have been ordered for equipping other boxes requiring high-purity atmospheres.

C. Thermal Diffusivity

(M. E. Lazarus, R. F. Velkinburg)

The high temperature vacuum furnace, ordered for the thermal diffusivity measurements on irradiated Pu bearing fuels, has been modified to incorporate an additional power transformer supplied by the vendor. With this modification the furnace now attains the guaranteed temperature of 3000°C. Tests have shown that the furnace meets the required specifications.

D. In-Cell Equipment

(J. W. Dahlby, E. L. Ekberg, F. J. Fitzgibbon, M. E. Lazarus, J. L. Lehmann, P. A. Mason, C. D. Montgomery, A. E. Tafoya, J. R. Trujillo)

1. Sodium Distillation Apparatus. A new sodium distillation apparatus has been designed, built, and installed in the DTA cell. The unit was designed to provide more effective and rapid sodium removal from sodium-bonded fuel-clad sections.

2. Optical Gauge for Diameter Measurements. A Bausch and Lomb DR 25B optical gauge was modified for use in a beta-gamma cell for making diameter measurements on capsules and unbreached pins. The device replaces the remotely operated micrometers now being used for these measurements. The instrument which has a claimed accuracy of better than ± 0.0001 in. will also be considered as back-up equipment for the optical profilometer installed in the DP West Facility. The unit, as installed, considerably decreases the time required to make fuel element diameter measurements. Further modifications are planned to increase the versatility and operating speed of the equipment.

3. Remote Cut-Off Saw. This new saw for use in sectioning pins and capsules in the disassembly cell has been tested extensively out of cell. Modifications made to improve the reliability and extend the service life of the saw are: a redesigned actuator for the power feed engagement which is controlled by a standard manipulator rather than a solenoid; and a rolling closure curtain over the table feed and ball bushing mechanism to protect the sensitive parts from dust and film accumulations.

4. Sealed Tube System for Chemical Dissolution. A sealed tube method for the dissolution of fuel samples was adapted for remote operation and has been in service for about four months. The principal items of the system are as follows:

a. A high pressure, high temperature furnace to accomplish the rapid dissolution of samples in acid within a sealed quartz tube. The furnace can be pressurized to 4000 psi and can attain a temperature of 300°C.

b. A powered, rotation fixture for flame-sealing the tube and for scribing the surface prior to opening.

c. A fracturing anvil for breaking the tube at the scribed ring.

d. A 4000 psi Ar supply system with attendant controls, safety devices, filter and pressure release.

e. Cooling water supply for the furnace and a gas supply for the heating torch on the sealing fixture.

5. Improved Method for Sealing Gas Sampling Holes. A new means of sealing the holes in capsules or pin cladding following gas sampling was developed to assure that the pin was tightly sealed with a radiation resistant material during storage. Such materials as Silicone RTV, rubber tubing, and Apiezon Q had been considered for use, but each had some deficiency. A new heat-shrinkable rubber tubing which appeared promising was also investigated.

Hot air from a blower type heat gun was passed over a 2-in. length of heat-shrinkable silicone rubber tubing which had been placed on a capsule or pin cladding in the punctured area. The heat caused the silicone tubing to shrink uniformly onto the cladding and effect a seal. A

sample of silicone tubing shrank from 3/8-in. i.d. to 3/16-in. i.d. when subjected to this heat treatment.

A stainless steel tube covered with a shrunken silicone tubing was exposed to 4 x 10^8 r with a ^{60}Co source. Following exposure the silicone tubing was resilient and adhered to the stainless steel tubing as firmly as in the unirradiated condition.

6. Micro-Sampling System. Work has continued on a low priority basis toward development of a micro-sampling system. A precision X-Y coordinate positioning stage has been received for incorporation into the sampling system. Slo-Syn stepping motors and a control unit are also on hand. Preliminary experiments with a rotary ultrasonic coring device have not been too successful with the unirradiated UC pellets used as simulants. Additional tests with this method will be made on cores > 0.020 in. in diameter to show what is the smallest diameter that will provide an intact sample.

Tests were performed on mounts molded from "Noryl" plastic. Although the material withstood 1.4 x 10^8 r gamma exposure from a ^{60}Co source and was resistant to the customary acid etch solutions and some solvents, it was not compatible with the butyl acetate and Hyprez solutions currently being used as vehicles for the grinding-polishing operations. Consequently, other plastics will be tested to find a suitable material.

7. New Metallography Sample Holders. The metallography sample holders presently in use have had the inherent problem of clamping only on the periphery of the 1.25-in.-diam sample casting in two places. Experience has shown that this sometimes allows a rocking motion to develop which results in a sample being held insecurely.

A new design has been developed and is in fabrication which hopefully will ensure three-point clamping and eliminate this problem. A preliminary model is being made for testing.

E. New Metallograph Installation

(K. A. Johnson, C. D. Montgomery, T. Romanik, R. F. Velkinburg)

The design of the new metallograph blister assembly, mentioned in the FY 1970 Annual Report, has been completed. Shop fabrication of the new alpha containment box is completed.

1. The shielding modules to accommodate the containment box and various penetrations are nearly completed. A window salvaged from the dismantled "Beetle" at Jackass Flats, Nevada, is being modified for use in a module of the shielding. The viewing window contains 11.5 in. of 6.2 density Pb glass plus two 1-in.-thick cover plates of cerium-stabilized glass. This design provides shielding equivalent to approximately 6-tenth-value thicknesses which should be adequate for an activity of 3000 curies of 1.3 MeV (assumed average fission product energy) gamma-emitting materials.

The shielding enclosure is of modular construction which allows removal of separate sections for maintenance of the equipment.

2. The two mini-manipulators are in place in the mockup assembly and have performed satisfactorily. An adjustment will be made for vertical displacement between the master and slave ends.

3. The new Leitz metallograph was received from Germany, checked out with the company engineering representative, and is ready for installation.

4. The major components for an ion beam etching device have been procured, and space for such a unit has been designed into the new blister. The application, of course, is pending actual useful developments in a technique which appears to have a very high potential with respect to the difficult problem of etching irradiated fuels.

5. The image analysis equipment, which was assembled and checked out, is ready for application to irradiated materials when the Leitz remote metallograph is installed in the new blister. A data analysis program has been written and an advanced programmable desk top calculator has been procured to process the image analysis data.

6. A new stage of improved design is being investigated for possible use on the existing Bausch and Lomb remotized metallograph.

F. Scanning Electron Microscope

An SEM has been installed and operated on alpha active materials. Several important accessories have also been installed including an energy dispersive x-ray

analyzer (EDX), a high temperature stage (1100°C), a tensile stage (250 kg), a transmission detector, and solid pair detectors. A shielded transport cask and specimen holder for irradiated samples has been designed.

G. Shipping Casks

(C. D. Montgomery, J. W. Schulte)

A second cask (Type DOT SP 5885) for shipping irradiated EBR-II fuel capsules, up to 42 in. in length, will be available during the first quarter of FY 1972.

Approval (DOT SP 6421) was received for the small cask (2000 lbs) intended for off-site shipment of short sections of fuel pins. This cask will also be available early in FY 1972.

An insert and tubes have been provided for shipping 61-in.-long unencapsulated, EBR-II fuel pins in a 21-ton Rover cask.

H. Miscellaneous Improvements

(M. E. Lazarus, J. M. Ledbetter, J. R. Trujillo, C. D. Montgomery, R. F. Velkinburg)

1. Betatron Radiography. Sometime during 1970 it was observed that the negatives obtained from radiography with the Betatron were not as "sharp" as usual. Although the exact source of the trouble was not determined, it was concluded that the capsule was vibrating during the 2 to 3-minute exposure to the beam. The difficulty was eliminated by placing a 3/4-in.-thick felt pad under the lead cask and by strengthening the supports which hold the 5-ft.-long positioning device above the cask.

2. Cooling System for the Top of Alpha Boxes. Excessive heat build-up, principally from the mercury vapor lighting within the boxes, has been a cause of concern for some time. This heat has an adverse effect on the equipment within the boxes, the manipulator boots, and the purifier systems. Preliminary tests were conducted with chilled water flowing through copper tubing attached to the top of a stainless steel containment box. The tubing was mechanically fastened to the box, and an overspray of aluminum from a metal spray gun provided the contact and thermal path for dissipating the heat. Temperature reductions of approximately 20°F were observed near the top of the box with the system in operation.

The results of subsequent tests will influence the design of future alpha containment boxes.

3. Alternate Method for Removing Sodium from Capsules. The method previously developed for removing sodium from a capsule entailed melting the sodium in hot mineral oil with the capsule maintained in a horizontal position. Although this method was effective, it introduced the possibility of melting and redistributing the bonding-sodium used in some experimental mixed-carbide fuel pins. It is desirable to maintain the postirradiation configuration of the sodium within the pin to comply with data preservation practices. This requirement is especially important if there is a possibility that the fuel pins will be re-encapsulated for TREAT irradiations. Consequently, equipment has been fabricated and has been used to melt sodium in an irradiated fuel capsule held vertically.

It is also desirable to remove residual sodium from the fuel pin surface in an environment which protects that surface from exposure to moist air in the presence of sodium. The procedure, developed to accomplish this, entails removing the bottom end-plug of the capsule using a saw and placing the capsule assembly quickly in the well of the vertical heater containing mineral oil. The temperature of the oil is raised to about 130°C to melt the sodium which is removed through a valve system. After cooling, the capsule cladding is removed and the remaining sodium in the mineral oil and on the fuel pin cladding is reacted with Dowanol EB. The fuel pin is then removed from the bath and washed with water and alcohol (in the same manner used with the "horizontal bath" method) to remove water-soluble deposits and films.

4. Development of Other Equipment. A tool was developed to remove fuel from the inner surface of a section of fuel pin cladding prior to making density measurements and other tests. A small-diameter, motor-operated, wire brush was used successfully as a reaming tool for in-cell use.

A suggestion was made by ANL (Ill.) personnel to scribe a fiducial mark on the cladding at a known distance from the bottom of the fuel pin prior to profilometry measurements. This mark would serve as an accurate reference point and would be reproduced on each profilometer

chart. Various tools and fixtures are being considered for applying the fiducial mark in an area which will not disturb other measurements or the integrity of the pin.

5. Miscellaneous. Components for high pressure equipment to impregnate metallographic specimens are being procured. It is expected that high-pressure impregnation (~ 3000 psi) of irradiated metallographic specimens will aid in improving microstructural analysis.

Low magnification units and a 35 mm automatic camera were purchased for the Reichert unit used for unirradiated fuel materials.

III. HOT CELL FACILITY AT DP WEST

(F. J. Fitzgibbon, M. E. Lazarus, J. M. Ledbetter, C. D. Montgomery, J. R. Phillips, J. W. Schulte, J. R. Trujillo, R. F. Velkinburg)

Modification and activation of the four hot cells at the DP West facility have experienced many delays due to strikes, procurement problems, and reductions in personnel. The installation of equipment will be started the first part of July. The plan view of this facility is shown in Fig. 401-1.

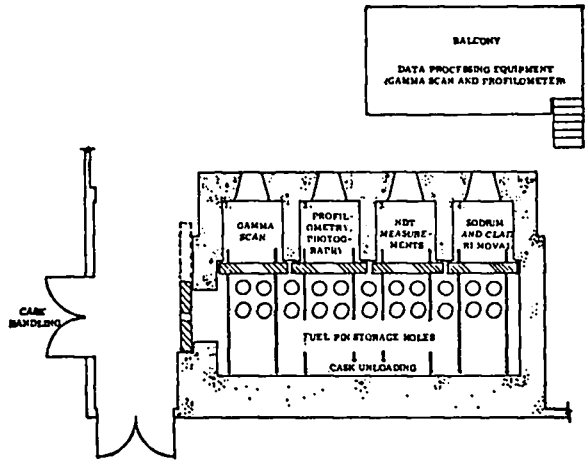

Fig. 401-1. Hot Cell Facility at DP West.

A. Structures and Building Equipment

1. Core drilling of 4-in. and 8-in. holes through the high density concrete of the cells was completed, and steel liners were grouted and welded in place.

2. A 25-ton hoist structure for handling shipping casks was completed on the north side of the building. The hoist, which has been installed and tested, is shown in Fig. 401-2.

Fig. 401-2. 25-Ton Hoist at DP West Hot Cells.

3. A double door, 8 ft. wide by 8 ft. high, was placed in the north wall to provide access from the hoist area into the corridor behind the hot cells.

4. A 36-wheel, free-running cart (see Fig. 401-3) to be moved with a forklift was fabricated for moving casks between the 25-ton hoist and the hot cell corridor. Tests were made in which the cart, loaded with > 22 tons, was moved between the 25-ton hoist position and the normal load/unload position in the corridor and then returned to the starting position. This movement was found to be reproducible within ± 2 in. which is satisfactory.

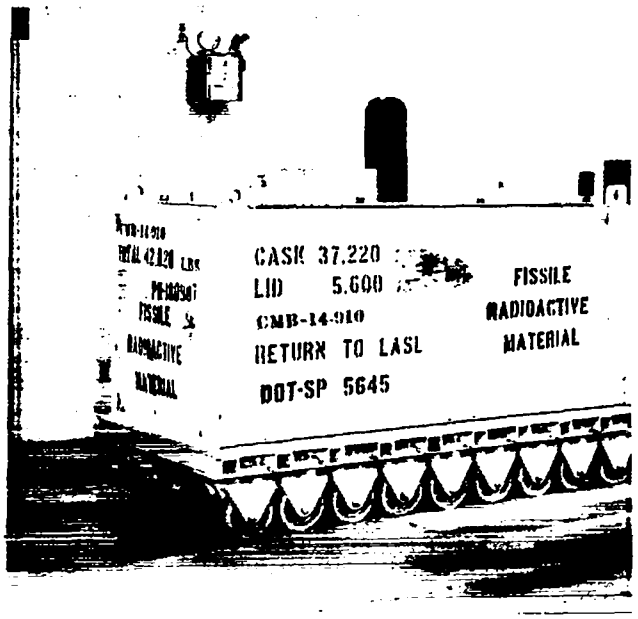

Fig. 401-3. Cart for Moving Casks at DP West Hot Cells.

5. A 3-ton corridor crane was procured and installed. A 200-lb hoist was added to the crane to provide additional height for removing cask inserts from tall casks. The hoist has been installed but wiring and final check-out remain to be completed.

6. A 1/2-ton hoist, with its attendant support for bridge and trolley travel to accommodate the handling of manipulators, periscopes, and wall plugs, was installed and satisfactorily tested.

7. The exhaust ducts in the floor of Cells 1 and 2 were modified to accommodate 18-in. x 18-in. HEPA filters. This change was necessary to allow installation of anchors for the gamma scanner and profilometer equipment.

8. Design, fabrication and installation were completed on 12 storage hole adapters for accommodating 6-in. -diam inserts for use with EBR-II fuel pins and capsules. Studies have shown that as many as 25 fuel elements in each of the 4 cells and 25 elements in each of 22 corridor storage holes may be stored simultaneously without incurring a criticality risk.

9. A 6000-lb-capacity forklift for general work and for moving the cask has been received and used. A fork adapter was fabricated to clamp to the forklift and engage the 36-wheel cart for movement.

10. Modifications of the air handling system, the radiation monitoring system, the air sampling system, and the fire alarm system have been completed.

11. The balcony area has been enclosed, except for the west side, and provided with power outlets and new lighting fixtures. This area will house electronic components for the gamma scanning system including data acquisition and processing equipment. Since the accuracy of this equipment is temperature dependent, the west side will be enclosed, and an air conditioner will be installed in the near future to maintain a relatively constant room temperature.

B. Hot Cell Equipment

1. Gamma Scanning System. The pin-handling portion of the gamma scanner has been completed and is in use presently with the Nuclear Data 50/50 system at a temporary location. The heavy metal platform and track for the scanner-shield assembly have been set in place. Installation of equipment will begin during the first part of July. The fabrication of collimators is approximately 75% complete.

2. Fission Gas Sampling System. Figure 401-4 shows the fission gas sampling system that will be installed

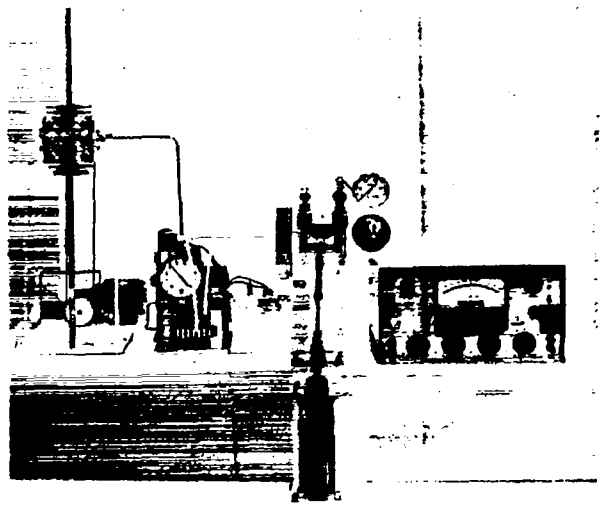

Fig. 401-4. System for Fission Gas Sampling at DP West.

at DP West. The fuel element drill is at the left of the figure with the drill motor below. To the right of this is the Baratron pressure sensing head and remote isolation valves, followed by the sample flask and calibration system, and finally the Baratron read-out unit.

3. Sodium Dissolution. A system for removal and dissolution of sodium between the capsule and pin has been fabricated. A cover of inert gas is maintained by a hood which fits over the dissolution tray. Equipment for removing pins in both the horizontal and vertical positions will be provided.

4. Macrophotography. The system for photographing unbreached fuel pins, shown in Fig. 401-5, is ready for installation. The equipment consists of:

a) A pin transport mechanism which precisely aligns the pin for each sectional photograph. This facilitates the preparation of photographic montages.

b) Two first-surface mirrors which provide three views of the pin on one photograph.

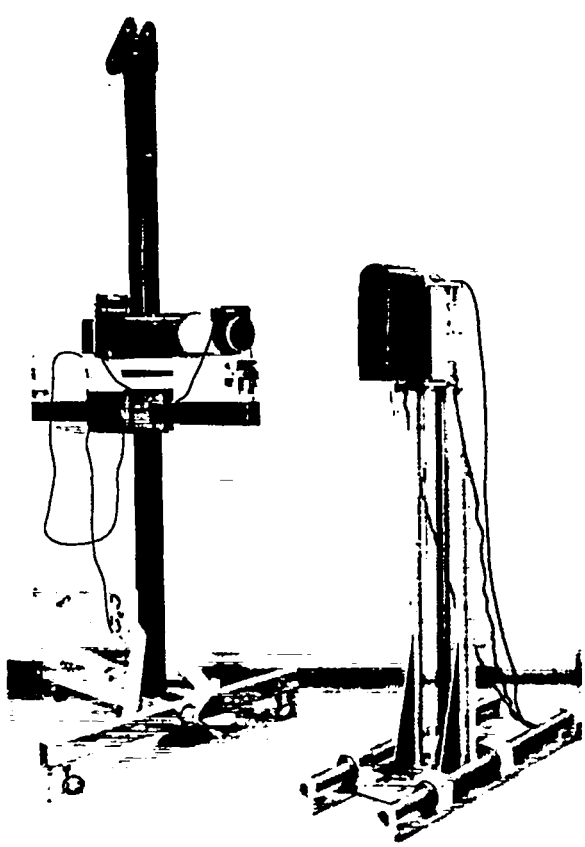

Fig. 401-5. Components for Macrophotography of Pins at DP West.

c) A lighting system which consists of 18 fluorescent lamps and a xenon flash lamp. The fluorescent lamps are oriented in a circle around the back and sides of the pin. The flash tube is located above the section of the pin being photographed and provides frontal lighting by means of light being reflected onto the pin with a beam-splitting mirror.

The system works well on dull or dirty surfaces but gives poor detail on shiny mirror surfaces. On this three-view system the lighting on the pin must be uniform around its entire circumference. The two mirrors block areas of the pin from the lighting. This nonuniformity results in bright and dark lines along the length of the pin in photographs of pins with mirror-like surfaces. Means for correcting the nonuniformity are being investigated.

5. Profilometer. The Electro-Optical Profilometer has been assembled, tested (except for the data storage system), and is now being installed. It was observed during testing that fuel element motion in the front to back and side directions caused significant data errors, and,further, that the bulk of these errors was caused by nonuniform, poorly collimated light. Tests were run on many different light sources. A high-intensity, short-arc xenon lamp was ordered. Delivery of the xenon lamp was a month late, and testing disclosed that it did not meet specifications. The optical section of the lamp is now at the factory for modifications, and the profilometer will be used with the original Quartz-Iodine lamp until the xenon lamp is ready for use. A Brown strip chart recorder will be used to record data at a maximum fuel element speed of 4 in./min until the high-speed data storage system is ready. The high-speed system should be able to record data at a fuel pin speed of 60 in./min. Figure 401-6 is a schematic of this profilometer setup showing the various components and their relative positions in the hot cell. The optical sensor is positioned to look directly into the profilometer wall periscope. This positioning must be done to better than ± 0.002 in. The fuel pin support fixture (see Fig. 401-7) positions and moves the fuel pin in front of the viewing periscope and transmits electrical signals to indicate the exact position and orientation of the fuel pin.

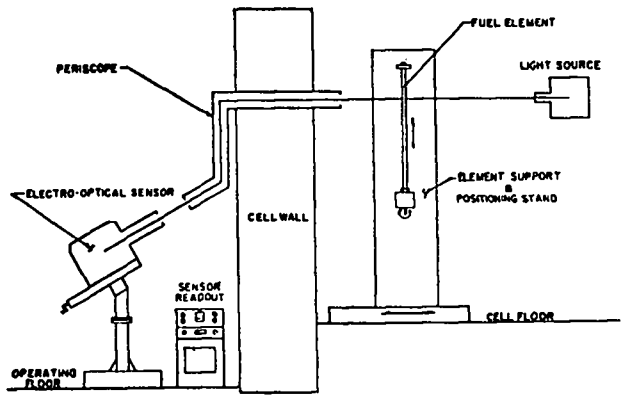

Fig. 401-6. Schematic of the Electro-Optical Profilometer System for DP West Hot Cells.

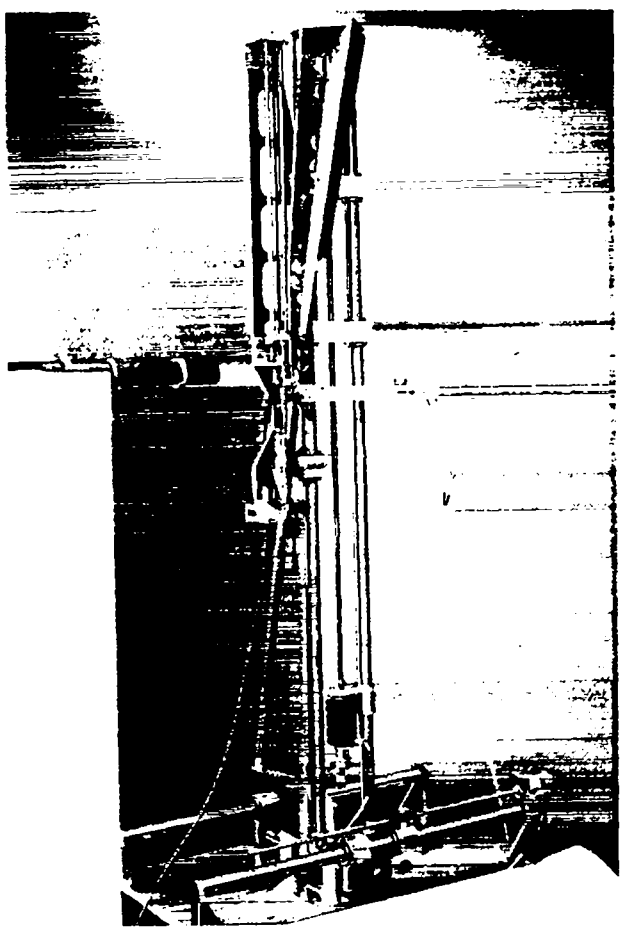

Fig. 401-7. Fuel Pin Support Fixture for DP West Hot Cells.

IV. METHODS OF ANALYSIS

A. Measurement of U and Pu
(J. W. Dahlby)

Controlled-potential coulometric equipment, which was previously modified for titrating U and Pu in the chemical characterization of irradiated mixed oxide or carbide fuels, was applied successfully to the measurement of each metal without chemical separation in $(U,Pu)O_2$ fuels having undergone as much as 6 at.% burnup. The Pu was measured by integrating the current for the coulometric oxidation of Pu(III) to Pu(IV) at a Pt electrode and then integrating the current for the coulometric reduction of Pu(IV) to Pu(III). The oxidation-reduction cycles were repeated until consecutive values for the Pu titrated during oxidation cycles differed by less than 2 μg. The U was measured by integrating the current for the coulometric reduction of U(VI) at a Hg electrode to U(IV), following a preliminary reduction of more-easily reduced impurities.[1] The aliquot was left in the titration cell for a time equal to that required for the original titration, and then the titration was repeated to obtain a blank. The value of this blank was used to correct for the effect of peroxides generated radiolytically.

Analysis for U and Pu in samples taken at five locations on a failed $(U,Pu)O_2$ fuel pin having undergone 6 at.% burnup showed variations in uranium contents between 64.3 and 66.4% and in plutonium contents between 16.8 and 17.6% among the five samples. As the samples were quantitatively dissolved and the precisions (1 σ) of the methods were 0.3% for the U titration and 0.1% for the Pu titration, the large ranges in contents for the two metals indicated either variable amounts of Na in the fuel because of the cladding failure or nonuniformity of the fuel itself.

Spectrographic measurement of Na in eight samples from this fuel pin showed that the Na content was significant and variable, ranging between 1.1 and 2.3%. The observed variations in U and Pu contents probably were the result of the large variation in Na content. Repeated measurements of U and Pu in a solution prepared from a mixed oxide fuel having undergone 6 at.% burnup verified that the previous (1 σ) were 0.3% for titrating U and 0.1% for titrating Pu.

Three samples of mixed oxide fuel having undergone 8 at.% burnup also were analyzed for U by this method. The average of eight measurements for each sample was 69.7%, 70.0% and 71.3% uranium, and the standard deviations were 0.5%, 1.6%, and 1.7%, respectively. This precision was poorer than that for the analyses of the 6 at.% burnup samples and indicated that a separation of the U and Pu from the highly radioactive fission products would be necessary for fuel having undergone burnups greater than 6 at.%. A separation scheme has been worked out and will be tested for this purpose in the near future.

One problem in coulometric titrations is the difficulty in detecting malfunction of the reference calomel electrode. Two simple tests were developed for determining satisfactory operation of the electrode. In one test, a solution containing exactly equal amounts of Pu(III) and Pu(IV) was prepared by coulometric oxidation of half of the Pu in a solution originally containing only Pu(III), and the potential was measured between the calomel electrode and a Pt electrode dipping into this solution. Under the particular conditions used, the measured potentials for satisfactory electrode systems were 500 ± 3 mV.

In the second test, the potential drop across this system was measured while a known resistance was connected in series with the reference electrode. The internal resistance of the calomel electrode, which should be less than 5000 ohms, was calculated from these measurements. Electrodes which tested within the stated electrical limits operated satisfactorily in coulometric titrations.

As a further check on the reliability of the coulometric titration method, known quantities of U and Pu will be added to analyzed aliquots of solutions of the irradiated fuels, and the resulting solutions will be analyzed again for total U and total Pu. The results will show if the added U and Pu are being measured quantitatively under the conditions existing in the irradiated fuel solutions. Attempts are continuing to obtain fuels having undergone burnups greater than 8 at.% for further tests of the method and separation schemes.

B. Sealed-Tube Dissolution of Refractory Materials

(J. W. Dahlby, G. R. Waterbury (CMB-1); C. D. Montgomery (CMB-14); and T. Romanik (CMB-7)

Some irradiated sintered oxide fuels and metallic inclusions composed of fission-product Mo, Rh, Ru, and Tc found in fuels having undergone several percent burnup reportedly resist dissolution by all methods previously tried. For this reason, two more strenuous dissolution methods were tested using alloys made from nonradioactive Mo, Rh, Ru, and Tc metals for test samples. The first dissolution method tried used an a.c. electrolytic dissolver at an applied potential of 5 V between two vitreous carbon electrodes. Most of the sample dissolved in 15 h, but in all cases a slight amount of residue remained. Quantitative dissolution in HCl was attained by the second method in which the refractory sample and a measured volume of 12M HCl and $HClO_4$ oxidant were sealed in a thick-walled silica tube and heated at 300°C in a sealed, steel shell containing a compensating gas pressure.[2]

Equipment was remotized and mechanized for sealing the silica tubes and heating the samples in-cell. Dry ice was added to the lower compartment of the motorized sealing equipment, shown in Figure 401-8, to surround the silica tube and reduce internal pressure during sealing. The sealing tube was placed in the furnace (Fig. 401-9), a cap having an "O" ring seal was attached remotely, and a high pressure Ar system supplied the 3000 to 4000 lb./in.^{2} compensating pressure needed around the tube. Initial tests showed that various alloys composed of Ru, Tc, Rh, and Mo were quantitatively dissolved in 2 to 12 h by this method. Four samples containing up to 0.6 g of mixed oxide fuel having about 8% burnup were each completely dissolved in about 4 h. This compares to an elapsed time of several days for the various operations needed to dissolve the same material by more conventional methods. In addition to the time element, the sealed tube method produces "clean" solutions, directly usable for most chemical analyses. This method is now in regular use in the hot cell.

C. Determination of O_2 in Irradiated Materials

(C. S. MacDougall, M. E. Smith, G. R. Waterbury)

The dependence of the physical properties of various fuels and claddings upon their O_2 contents, and the

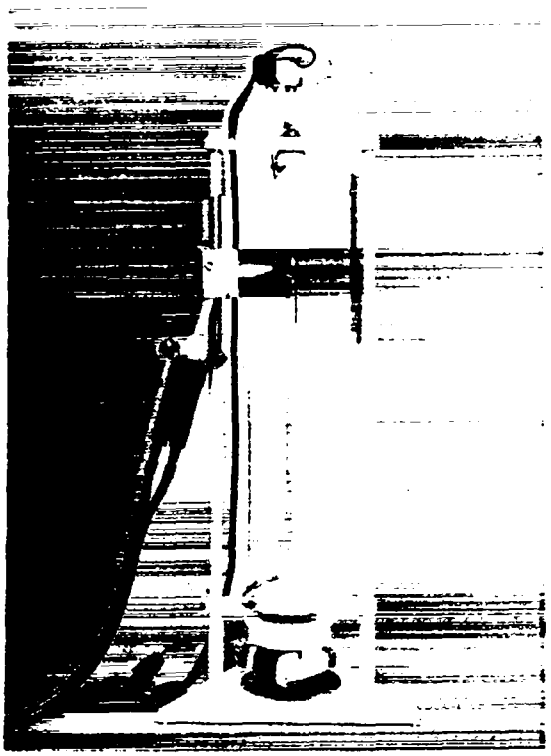

Fig. 401-8. Apparatus for Sealing Fused Silica Tubes Remotely.

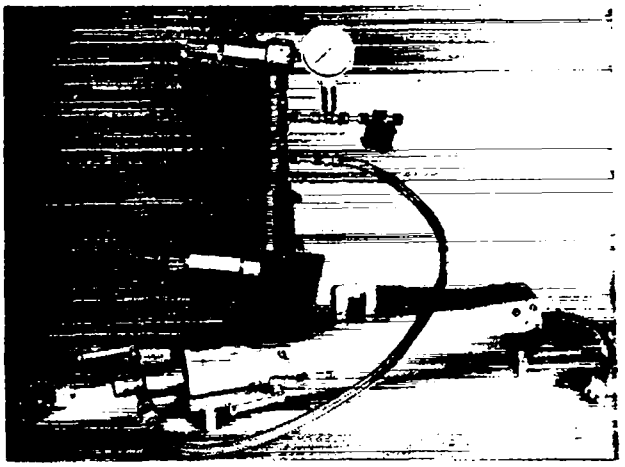

Fig. 401-9. Furnace and Components of High Pressure Gas System.

migration of O_2 in these materials during irradiation, make the reliable measurement of O_2 necessary for the proper interpretation of data obtained during irradiation or in-pile tests. For this reason, two proven methods[3,4] for measuring O_2 were adapted and remotized for hot cell use. In either method, the sample is reacted with C at 2000°C, and the CO and CO_2 produced are swept from the furnace by Ar and measured either gravimetrically or manometrically

Oxide fuels are ground, blended with C, and pressed into pellets prior to heating inductively at 2000°C. The O_2 is evolved from the pellet as CO and CO_2 which are swept by Ar carrier gas into an ascarite absorption tube to trap the CO_2 fraction. The remaining CO is oxidized over hot CuO to CO_2, which is trapped in a similar absorption tube, and the O_2 content is calculated from the weight increases of the two tubes. The apparatus was tested by analyzing U_3O_8 prepared by oxidation of U metal containing less than 100 ppm total impurities. The O_2 calculated from the weight increase upon oxidation was 15.24%. Analysis of this sample in the hot cell yielded an experimental value of 15.25%, and the precision (1 σ) was 0.1 to 0.2 relative percent. Analyses of irradiated oxide samples having undergone as much as 8.5 at.% burnup, Table 401-I, showed that the precision (1 σ) of the method ranged between 0.2 and 0.4 relative percent as compared to the 0.1 to 0.2 relative percent for similar analyses out-of-cell. The averages of repeated analyses on four samples ranged between 11.74 and 11.97% oxygen.

TABLE 401-I

OXYGEN CONTENTS OF IRRADIATED OXIDE FUELS

Sample	Burnup, %	Oxygen, %	No. of Analyses	Rel. Std Dev
1	6.29	11.97	3	—
2	6.06	11.74	8	0.4%
3	a	11.95	6	0.3%
4	8.50	11.94	5	0.2%

[a]Not measured

Carbide fuels and cladding samples are inductively heated to 2000°C in a graphite crucible containing molten Pt. The CO formed is swept from the reaction furnace by an Ar carrier gas through an I_2O_5 reagent, where it is oxidized to CO_2 which is measured manometrically.

Approximately 42 pieces of irradiated stainless steel cladding have been analyzed for O_2 contents ranging between 250 and 2800 ppm.

Unfortunately, samples of irradiated oxide fuels or cladding are not available to determine the accuracy of the methods. Analyses of unirradiated U_3O_8 and of samples of Ta, Nb, and steel indicate that the methods are not biased. Difficulties attributable to high radiation levels have not been experienced, and the methods are assumed to be unbiased for analyses of irradiated materials.

Testing of the method will be resumed when oxide fuels having undergone burnups higher than 8.5 at.% or helium-bonded irradiated carbide fuels become available. No difficulties are foreseen and the methods are in regular use.

D. Gamma Scanning

(J. R. Phillips, G. H. Mottaz, J. W. Schulte, G. R. Waterbury)

Gross gamma scanning of irradiated fuel elements provides information about the fission product and fuel distributions which is helpful in selecting areas for sectioning and for further analyses. The relative spatial distribution of specific isotopes can be determined by high-resolution gamma scanning. A new gamma scanning system consisting of a Nuclear Data 50/50 data acquisition system, a Ge(Li) anticoincidence system and a precision scanning mechanism was assembled and satisfactorily operated. This state-of-the-art system,which supplements the gross gamma scanner and the previous complex system for detailed gamma scanning, permits the automatic accumulation and reduction of data for up to 30 individual full-energy peaks and may be used for either one-dimensional or two-dimensional high-resolution gamma scans. The new scanning mechanism will be installed in the hot cell early in FY 1972.

The radial distributions of fission products provide information about the migrating properties of individual isotopes, mass transfer mechanisms, and fuel stoichiometry. Both a destructive and nondestructive method have been developed to determine isotopic distributions across the diameter of an irradiated fuel element. The destructive method consists of excising a 0.25-in.-thick disk from the fuel column which is reduced to about 0.050 in. in thickness by repeatedly impregnating with epoxy and grinding. The disk is scanned with a conical-pinhole collimator fabricated of gold and tantalum. The data is reduced by a computer code and presented as density and isometric projection plots.

The nondestructive method involves diametrally scanning the fuel element at different angles around the outside of the fuel capsule and using this data as input for a computer code. The code determines the radial distribution of each isotope of interest over a cross section of the fuel element. This method requires less scanning time but has a lower spatial resolution than the destructive technique.

A nondestructive gamma scanning method was developed for detecting fuel cladding failure in doubly encapsulated fuel elements. Detection of fission products, in particular ^{137}Cs, outside the fuel pin envelope was used to indicate the failure. The method was tested by examining eleven fuel elements fueled by (U,Pu)C and two fueled with $(U,Pu)O_2$. Gamma-ray scanning indicated that six of the thirteen fuel envelopes had failed. These results were confirmed by mass spectrometric analyses of the gases in the outer encapsulation which were found to contain 11.7 to 65.0% of the fission product xenon and 1.76 to 9.31% krypton. The cover gas from a seventh element contained only 0.016% xenon and < 0.003% krypton, and the presence of ^{137}Cs outside the fuel cladding was not conclusively shown by gamma scanning. The presence of ^{137}Cs was not detected in the other encapsulation of the six other fuel elements, and mass spectrometric analyses confirmed that the cladding had not failed.

E. Spectrochemical Analyses of Irradiated Materials

(O. R. Simi and R. T. Phelps)

Analyses for trace impurities in fuels, claddings, and other reactor components provide important data to assist in the interpretation of irradiation test results. The emission spectrography hot cell facility was used for simultaneously measuring several impurities in the chemical characterization of various irradiated materials during the past year, and the capabilities were extended or improved by reducing in-cell contamination and developing a method for measuring Na.

1. Reduction of Random Contamination. Random contamination of NaCl samples with the elements Al, Ca, Fe, Mg, and Si has been observed. Spot impurities in electrodes were identified as one source of the contamination. By changing the electrode shape so as to burn less graphite and by choosing high-purity lots of graphite, the effect of electrode contamination was reduced to an acceptable level. Another source of random contamination was identified as a dust or talc coating on the plastic manipulator covers (booties). The presence of the contaminating elements was demonstrated by spectrographically analyzing the coating removed with an alcohol wash from new booties. The gauntlet portion of the bootie carried more dust (80 mg as oxide) than the sleeve (4 mg). Two new booties have been cleaned with alcohol and detergent washes and have been installed. Further tests will be made for contamination that is related to operation of the cell.

2. Spectrochemical Measurement of Na in Irradiated $(U,Pu)O_2$. A method was developed for the spectrochemical determination of Na in irradiated $(U,Pu)O_2$ following dissolution of the fuel in HNO_3-H_2SO_4. A small aliquot of the $(U,Pu)O_2$ solution is added to enough $Pb(NO_3)_2$ solution to produce a sample containing the equivalent of 1% of $(U,Pu)O_2$ in $PbSO_4$ when the solution is acidified with H_2SO_4 and dried. Dilutions of the samples with pure $PbSO_4$ are made as required to reduce the Na content of the mixtures to the range of 1 to 100 ppm Na, which is suitable for spectrographic measurement.

The $PbSO_4$ is mixed with graphite powder and excited with an 8 amp d.c. arc using a 30-sec exposure time. The Na 5890 Å line is measured photometrically and the Na content is determined by reference to an analytical curve(plot of optical density vs log concentration) which is established by spectrography of $PbSO_4$-base calibration materials.

The $PbSO_4$ matrix was chosen following tests showing that 1% total U and Pu in $PbSO_4$ would not interfere with the spectrographic determination of Na. Using purified reagents, a detection limit of 100 ppm Na in $PbSO_4$ was attained, corresponding to a detection limit of 100 ppm Na in $(U,Pu)O_2$. This limit was considerably lower than the expected 0.1 to 1% Na content of the samples. Average deviations of duplicate measurements were between 4 and 11% in applications to analyses of six $(U,Pu)O_2$ fuels containing 1.1 to 2.3% Na.

V. REQUESTS FROM DRDT

A. Examination of Irradiated Material

(K. A. Johnson, E. D. Loughran, R. A. Morris, J. R. Phillips, J. W. Schulte, G. R. Waterbury)

Argonne National Laboratory (Illinois). Forty-six samples of stainless steel cladding from irradiated fuel elements were analyzed in-cell for oxygen by an inert-gas-fusion method.

Atomics International. The remaining sections of irradiated UC-W fuel pellets from NRX-101 were released by AI personnel for disposition in the contaminated waste pits at LASL.

General Electric Company. Seven irradiated and three unirradiated mixed oxide fuel specimens were received in June 1971. Melting point determinations and possibly other tests are to be performed on these samples.

Los Alamos Scientific Laboratory. OWREX-15 and -16 were received on July 22 and December 28, 1970, respectively. LASL Capsules 36-B and 42-B were received from the EBR-II on September 29.

Axial and diametral gamma scanning of OWREX-15 and -16 and LASL-36B and -42B was completed. In addition, a two-dimensional measurement of distributions of fission products was made by gamma scanning a cross section from LASL-42B.

The following nondestructive tests and other operations were completed on OWREX-15 and -16 and on LASL-36B and -42B. (See Table 401-II)

Microstructural examinations in an inert atmosphere consisting of macrophotography, alpha and beta-gamma autoradiography, and optical microscopy (including mosaic preparation) were completed on the samples tabulated in Table 401-III.

The shielded electron microprobe was used to examine a cross-section sample of 42B; a fuel section and stainless steel pellet from OWREX-15; and two fuel samples from OWREX-16.

TABLE 401-II

POST-IRRADIATION EXAMINATIONS OF LASL EXPERIMENTS

	Examinations and Operations[a]	OWREX -15	OWREX -16	Capsules 36B	Capsules 42B	Pin 42B
1.	Visual Inspection and Photography	X	X	X	X	X
2.	Measurements of Contamination and Radiation	X	X	X	X	--
3.	Radiography	X	X	X	X	--
4.	Diameter by Micrometer Measurements	--	--	X	X	--
5.	Na and Clad Removal	X	X	--	X	--
6.	Sectioning	X	X	--	--	X
7.	Na Removal from Fuel by Heat and Dissolution	X	--	--	--	--
8.	Na Removal from Fuel by Distillation	--	X	--	--	X
9.	Analysis of Cover Gas	--	--	--	X	--

[a]The operations of center point balance, profilometry, temperature, fission gas sampling, and sectioning were all carried out on pin LASL-42B in an inert atmosphere.

TABLE 401-III

MICROSTRUCTURAL EXAMINATION OF LASL SAMPLES

Experiment No.	Type and No. of Samples: Spacer	Fuel + Clad	Clad	EMX[a]
OWREX-14	1	1	3	--
OWREX-15	1	2	3	2
OWREX-16	2	2	2	2
LASL-42B	--	4	1	3

[a]Special preparations were required for microprobe examinations.

Density measurements by immersion were made on sections of cladding from pin 42B.

Capsule 36B was stored for possible reinsertion in EBR-II during the first quarter of FY 1972.

Nuclear Materials and Equipment Corporation.

A-Series Pins: Eleven pins were received on November 25, 1970. The following program had been agreed upon by representatives of ANL, LASL, and ORNL and approved by DRDT.

1. Nondestructive and destructive tests will be conducted at LASL on pins A-5, A-8, A-9, A-10 and A-11; sections of fuel will be shipped to ORNL after July 1, 1971.

2. Pins A-4 and A-7 will be shipped intact to ANL for processing studies. (Pins A-4 and A-7 were shipped to ANL on March 16, 1971.)

3. Routine nondestructive tests will be conducted on pins A-1, A-2, A-3, A-4, A-6, and A-7.

Tests performed on these pins are shown in Table 401-IV.

TABLE 401-IV

POST IRRADIATION EXAMINATION OF NUMEC MATERIALS

	Tests	NUMEC Pin No.
1.	Visual Inspection and Photography	A-1 through A-11
2.	Measurements of Contamination and Radiation	A-1 through A-11
3.	Measurements of Temperature	A-1 through A-11
4.	Center Point Balance	A-1 through A-11
5.	Betatron Radiography	A-1 through A-11
6.	Gamma Scanning[a]	A-1 through A-11
7.	Measurements of Temperature	A-1 through A-11
8.	Center Point Balance	A-1 through A-11
9.	Profilometry	A-1 through A-11
10.	Fission Gas Analysis	A-5, -8, -9, -10, -11
11.	Sectioning	A-5, -8, -9, -10, -11

Operations 7 through 11 were carried out in an Ar atmosphere.

[a]Three diametral and one axial gross gamma scans were made on each of the mixed-oxide fuel pins. In addition, multispectral gamma scans were made on the fuel regions of eight pins.

Microstructural examinations in an argon atmosphere consisting of macrophotography, alpha and beta-gamma autoradiography, and optical microscopy (including mosaic preparation) were completed on five specimens each from the following pins: NUMEC A-5, A-8, and A-9. Examinations are nearly finished on five specimens each from NUMEC A-10 and A-11.

Measurements of density by immersion were made on cladding specimens from the fuel regions of NUMEC A-5, -8, -9, -10, and -11.

B-Series Pins: One sample each from NUMEC-B-9D and -B-11 was prepared in an inert argon atmosphere for examination on the microprobe. Microprobe examinations were also completed and the reports written and distributed.

Microstructural examinations, as described for the NUMEC-A Series Pins, were applied to two specimens resulting from DTA tests.

United Nuclear Corporation. Nine EBR-II capsules were received on September 29, 1970, and 2 EBR capsules on December 28, 1970. Twelve "Rabbit pins", irradiated in GETR, were received on August 20, 1970. Table 401-V lists the examinations made on the UNC materials.

TABLE 401-V

POSTIRRADIATION EXAMINATION OF UNC MATERIAL

	Examination	UNC Number
1.	Visual Inspection and Photography	92, 96, 99, 104, 107, 108, 109, 111, 112, 138, 146, 210 through 221
2.	Measurements of Contamination and Radiation	Same as in "1".
3.	Measurement of Temperature (capsule)	Same as in "1".
4.	Betatron Radiography	Same as in "1".
5.	Micrometer Measurements	Same as in "1".
6.	Gamma Scanning[a]	See footnote "a"
7.	Cover Gas Analysis	92, 96, 99, 104, 107, 108, 109, 111, 112, 125 through 128, 138, 146, 210 through 221
8.	Na Melting, Clad Removal[b]	92, 96, 99, 104, 125 through 128, 138, 146
9.	NaK and Clad Removal	210 through 221
10.	Profilometry[c]	92, 96, 99, 104, 107, 108, 109, 111, 112, 125 through 128, 210 through 221
11.	Fission Gas Analysis	92, 96, 99, 104, 125 through 128, 210 through 221
12.	Temperature and Center Point	92, 96, 99, 104, 125 through 128, 210 through 221
13.	Sectioning	125 through 128, 210 through 221

[a] Gamma scanning was completed on the following 16 fuel elements: UNC-213, -125 through -128, -92, -96, -99, -104, -107, -108, -109, -111, -112, -138, and -146. Multispectral gamma scanning was applied to the nondestructive examination of three of these fuel elements, UNC-107, -109, and -111. In addition, measurements were made to locate ^{137}Cs near the capsule endplugs as a means of detecting failure of the fuel cladding on elements UNC-107, -109, -111, -138, and -146.

[b] This was performed with UNC-138 and -146 in a vertical position to prevent movement of the Na bond during the heating cycle of the capsule clad removal operation.

[c] The pin diameters of UNC-107 and -112 were taken with a micrometer because the ruptured condition of the pin clad prohibited use of the profilometer.

Microstructural examinations consisting of macrophotography, alpha and beta-gamma autoradiography, and optical microscopy (including mosaic preparation) were carried out in an argon atmosphere on the samples as tabulated in Table 401-VI

TABLE 401-VI

MICROSTRUCTURAL EXAMINATION OF UNC SAMPLES

UNC Experiment No.	Type and No. of Samples		
	Spacer	Fuel + Clad	EMX[a]
125	1	5	1
126	1	4	2
127	1	4	2
128	1	4	3
210		1	
211		1	
212		2	
213		2	
214		2	
215		2	1
216		2	3
217		2	
218		2	
219		2	
220		2	
221		2	

[a] Special preparations were required for microprobe examination.

One cross section from each fuel element UNC-125, -215, and -216, two cross sections from each fuel element UNC-126, -127, and three cross sections from UNC-128 were examined using the shielded electron microprobe.

A sample of fuel from each of UNC-125 through -128 pins was shipped to INC for burnup determination.

Measurements of density by immersion were made on fuel fragments of UNC-125 through -128, and clad samples from both the fuel area and the gas plenum area of UNC-81 through -86.

Twelve cladding specimens, one each from the gas plenum section and the burnup fuel section of UNC-81 through -86 were shipped to ORNL on October 20, 1970. Additional tests on this cladding will be performed at ORNL as requested by UNC personnel.

B. DRDT - LASL Meeting

On June 22-23, 1971, a meeting was held at LASL at the request of DRDT. This meeting was to acquaint various experimenters with the capabilities at LASL for examining irradiated fuel pins, and to obtain from the experimenters what additional capabilities they felt were most needed for effectively pursuing the fuel element development program.

Representatives from the following organizations were present: AEC - Division of Reactor Development and Technology; Argonne National Laboratory, Illinois; Argonne National Laboratory, Idaho; Battelle Memorial Institute, Columbus; General Electric, Sunnyvale; Gulf General Atomic, La Jolla; Hanford Experimental Development Laboratory, WADCO; LASL; ORNL; Westinghouse, WARD; United Nuclear did not send a representative, but did supply comments.

VI. REFERENCES

1. G. R. Waterbury, G. B. Nelson, K. S. Bergstresser, C. F. Metz, LA-4537, Los Alamos Scientific Laboratory (1970).
2. C. F. Metz, G. R. Waterbury, LA-3554, Los Alamos Scientific Laboratory (1966).
3. C. S. MacDougall, M. E. Smith, G. R. Waterbury, Anal. Chem. 41, 372 (1969).
4. W. G. Smiley, Anal. Chem. 27, 1098 (1955).

VII. PUBLICATIONS

1. B. K. Barnes and J. R. Phillips, "TWODIM, a Computer Code for Unfolding Diametral Gamma-Ray Scans on Reactor Fuel Elements," LA-4676, Los Alamos Scientific Laboratory (1971).
2. J. R. Phillips, J. W. Schulte, and G. R. Waterbury, "The Use of High-Resolution Gamma-Ray Spectrometry for Detecting Failure of Cladding in Encapsulated Fast Reactor Fuel Pins," to be published in the Proceedings of the 19th Conference on Remote Systems Technology, American Nuclear Society, October 1971.
3. J. W. Dahlby, G. R. Waterbury, C. D. Montgomery, and T. Romanik, "Application of the Sealed-Tube Method to Remote Dissolution of Irradiated Refractory Materials," to be published in the Proceedings of the 19th Conference on Remote Systems Technology, American Nuclear Society, October 1971
4. M. E. Lazarus, "Electro-Optical Profilometer," submitted for publication in the Proceedings of the 19th Conference on Remote Systems Technology, American Nuclear Society, October 1971.
5. C. E. Frantz, "Apparatus for Determining Heat Content on Irradiated Fuels," submitted for publication in the Proceedings of the 19th Conference on Remote Systems Technology, American Nuclear Society, October 1971.
6. D. D. Jeffries and L. A. Waldschmidt, "A Technique for Hot Cell Autoradiography," Proceedings of the Third Annual Technical Meeting of the International Metallographic Society, November 1970.
7. C. D. Montgomery, T. Romanik, and J. R. Trujillo, "Equipment for Preparing Sealed Metal Tubes for Long-Term Storage of Irradiated Uranium-Plutonium Fuel Element Sections," submitted for publication in the Proceedings of the 19th Conference on Remote Systems Technology, American Nuclear Society, October 1971.
8. P. A. Mason, C. E. Frantz, and C. D. Montgomery, "Inert Atmosphere Hot Cells for Examination of Irradiated U-Pu Fuel Elements," submitted for publication in the Proceedings of the 19th Conference on Remote Systems Technology, American Nuclear Society, October 1971.

PROJECT 463

CERAMIC PLUTONIUM FUEL MATERIALS

Person in Charge: R.D. Baker
Principal Investigator: J.L. Green

I. INTRODUCTION

The primary objective of this program is the overall evaluation of the most promising of the candidate fuel systems for advanced LMFBR application. Emphasis currently is placed on the study of the relative merits of stainless steel clad nitride and carbide fuels under conditions that appropriately exploit the potential of these materials to operate to high burnup at high power densities. The major portion of the program is the evaluation of the irradiation performance of these fuel element systems. A continuing series of irradiation experiments is being carried out under steady state conditions in fast reactor environments to assess the effects of damage and burnup on stainless steel clad, sodium bonded, monocarbide fuel elements. These experiments are designed to investigate fuel swelling, interactions between the fuel and clad and thermal bonding medium, fission gas release, and the migration of fuel material and fission products as a function of burnup and irradiation conditions. In addition, experiments are being designed to allow the study of the effects of rapid, overpower, reactor transients on sodium bonded monocarbide fuel assemblies. Contiguous efforts are necessary in the development of fuel material preparation and fabrication procedures as well as the techniques required for the characterization of fuel materials both before and after irradiation.

A second objective in the program is the determination of thermophysical, mechanical and chemical properties and characteristics of plutonium-containing ceramics that are required for their evaluation and use as fuel materials. A broad range of capabilities in this area has been developed, including the study of (1) phase relationships using differential thermal analysis, (2) thermal transport, (3) thermal stability and compatibility, (4) hot hardness and its temperature dependence, (5) structure and phase relationships using high temperature x-ray and neutron diffraction, (6) thermal expansion, and (7) compressive creep rates as a function of temperature and stress. These techniques are available for use with irradiated fuels.

II. IRRADIATION TESTING

The objective of the irradiation testing program is the overall evaluation of the most promising of the candidate fuel systems for advanced LMFBR application. The irradiation experiments are carried out under conditions that take advantage of the potential of these materials to operate to high burnup at high power densities.

A. Synthesis and Fabrication

(R. Honnell, C. Baker, W. Hayes, G. Moore, and R. Walker)

1. (U, Pu) C Pellets for EBR-II Irradiations

Well-characterized (U, Pu) C fuel pellets for EBR-II irradiation experiments were prepared using the basic LASL synthesis process.[1,2] Pellets are currently prepared with chamfered ends to reduce edge chipping during the loading and centrifuging of fuel pins. This is accomplished using die sets such as those shown in Fig. 463-1. The punches are machined to leave a small 45° chamfered edge on the ends of the green pellet. The use of recessed end punches requires that higher slugging pressures--4.3×10^3 kg/cm^2--be used to minimize end capping effects.

A total of 260 usable chamfered (^{235}U, ^{239}Pu) C fuel pellets was fabricated during FY 1971. The chemical compositions and physical properties of these pellets are shown in Table 463-I. The tabulated values are weighted averages calculated from the analytical results obtained on pellets randomly selected from each of the pellet lots. Other trace impurities detected in some of the pellets were 10-50 ppm Ni, 10-150 ppm W, 20-50 ppm Si, 2-4 ppm Cu, and 10 ppm Al.

2. (U, Pu) C Development

A blended powder technique was evaluated as a possible method for the preparation of fuel material containing small amounts of sesquicarbide but not containing acicular phases. The experimental procedure consisted of the preparation of pellets from powder blends of single phase $(U_{0.8}Pu_{0.2})C$ and $(U_{0.8}Pu_{0.2})_2C_3$. The metallographic results showed pellet microstructures containing acicular phases for all temperature ranges and carbon compositions investigated, i.e., 1900-1350°C and 4.84 to 4.75 wt% C. Oxygen and nitrogen concentrations in the sintered pellets totaled 600 ppm or less. As applied, this technique does not appear to be a suitable method for the preparation of carbon-rich fuels which are free of acicular phases. The mechanism responsible for the formation of the acicular phase is not known.

Current fuel specifications require the fabrication of pellets having sintered densities of 95% of theoretical. Developmental studies are in progress to define the process parameters necessary to meet this requirement. The effect of sintering temperature and milling procedures on sintered density, purity, and microstructure are of primary interest. The experimental procedure used to date has consisted of pressing pellets from powders vibratory milled for intervals of 1 and 3 hours, and from powder ball milled for 60 hours in a tungsten carbide jar with stainless steel balls. The pellets were placed in carburized tantalum tubes and sintered in a graphite tube furnace at either 1800 or 1900°C for 10 hours in a flowing argon atmosphere. All process parameters were held constant except milling techniques and sintering temperature. The same batch of (U, Pu) C starting material was used throughout the study. Characterization of the

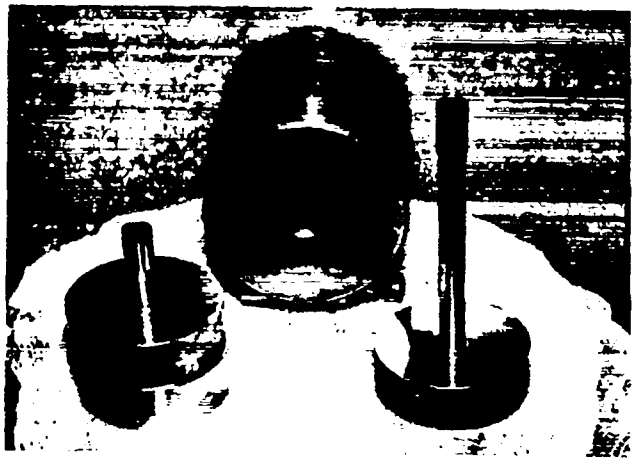

Fig. 463-1. Die and end punches for pressing chamfered pellets.

TABLE 463-I

COMPOSITIONS OF (^{235}U, ^{239}Pu C) PELLETS (WEIGHTED AVERAGES)

U	76.0 wt%	^{234}U	1.17 wt%
Pu	19.39 wt%	^{235}U	92.69 wt%
C	4.68 wt%	^{236}U	0.25 wt%
O	313[a]	^{238}U	5.86 wt%
N	384	^{239}Pu	93.85 wt%
Fe	47	^{240}Pu	5.67 wt%
Mo	25	^{241}Pu	0.47 wt%
V	24	^{242}Pu	0.01 wt%

Immersion Density:	12.40 g/cm^3
Lattice Constant:	4.964 Å

[a] ppm by weight unless otherwise specified.

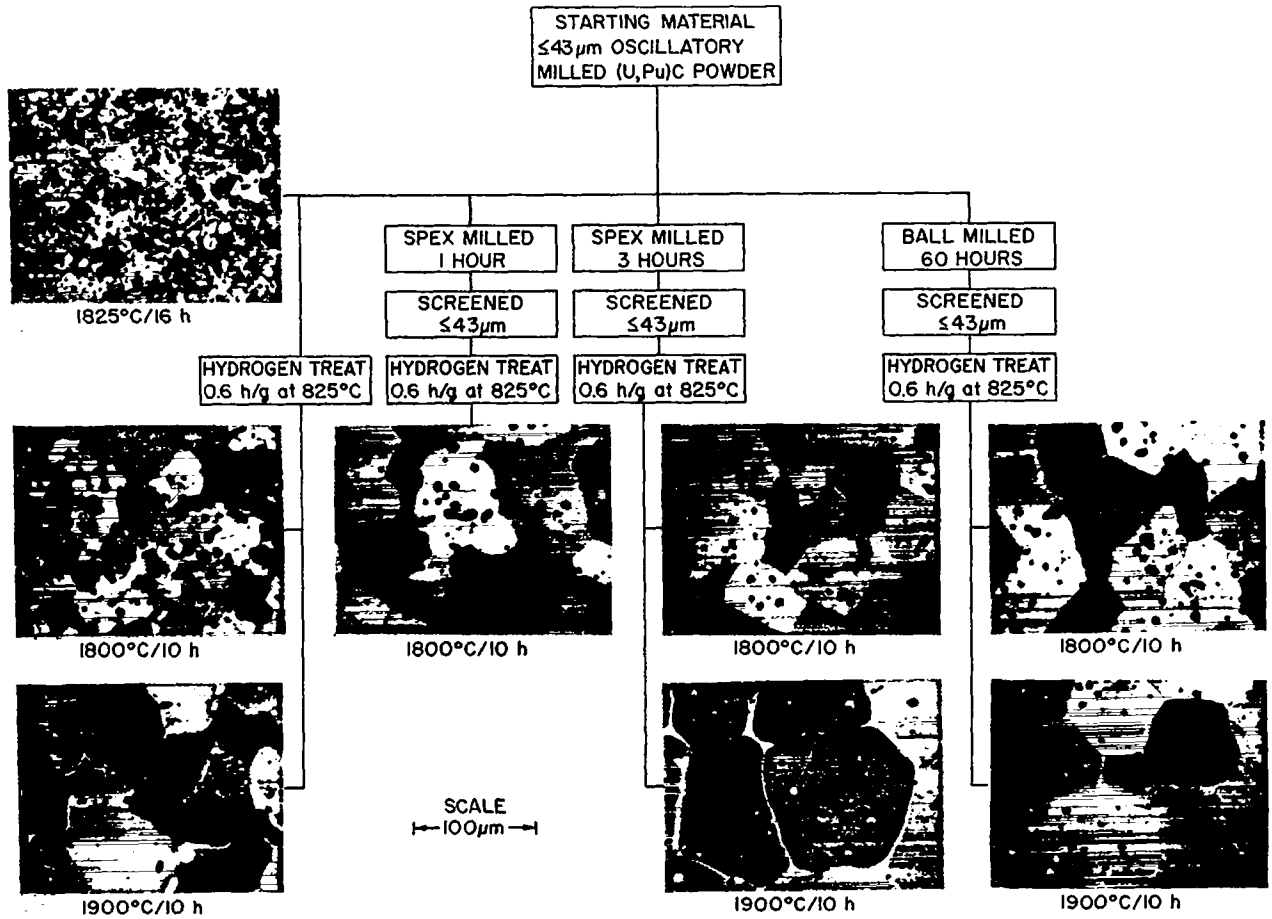

Fig. 463-2. Flow diagram summary of a study of the effect of powder milling techniques and sintering temperature on the preparation of high density $(U_{0.8}Pu_{0.2})C$.

powders and pellets is not complete, but metallographic examinations and density measurements have been made. These are presented in the flow diagram summary of the study which is shown in Fig. 463-2 and Table 463-II. As seen in the figure, pellets sintered at 1800°C are either single phase or contain a small amount of an acicular phase. The pellets sintered at 1900°C have a grain boundary precipitate which has been identified using microprobe analysis as having an approximate chemical composition of Pu-15 wt% U with little, if any, carbon. A second sintering run was made at 1900°C for 15 hours using pellets pressed from powder prepared by vibratory milling for 3 hours. An induction furnace was used in conjunction with a tantalum carbide container in a static argon atmosphere. The pellet microstructure of this second preparation contained a small amount of an acicular phase indicating that a slight excess of carbon was present. Consequently, the carbon loss from the material sintered at 1900°C in the graphite furnace in a carburized Ta crucible does not appear to be a characteristic of the U-Pu-C system. A comparison of these experiments does indicate that an interaction can occur between the fuel and the furnace atmosphere and crucible which affects

TABLE 463-II

$(U_{0.8}Pu_{0.2})C$ PELLETS
SINTERED AT 1800°C

Milling Treatment	Mean Particle Size, μm	Density, g/cm³
Vibratory	*	12.2
1 hr. Vibratory	5.9	12.5
3 hr. Vibratory	*	12.8
60 hr. Ball Mill	*	12.6

* Analysis not complete.

the carbon content of the sintered fuel. The mechanism of carbon transport is not understood at present.

3. Carbide Samples for Property Measurements

A number of different uranium, plutonium and solid-solution carbide compositions were synthesized, characterized and fabricated into test specimens for physical property measurements. Descriptions of these materials are contained in the various property measurement sections.

B. EBR-II Irradiation Testing
(J. O. Barner)

The purpose of the EBR-II irradiations is the evaluation of candidate fuel/sodium/cladding systems for application in advanced LMFBR reactors. In the designs currently under investigation, fuel pellets of single-phase, solid-solution $(U_{0.8}Pu_{0.2})C$ or $(U_{0.8}Pu_{0.2})N$ are sodium bonded to Type 316 stainless steel claddings. Four series of experiments are planned. The three series for which approval-in-principle has been received from the AEC are described in Table 463-III. The fourth series is a singly encapsulated, combination carbide-nitride subassembly.

Two capsules from Series 1, designated K-36B and K-42B, were removed from the EBR-II reactor after maximum calculated burnups of 3.7 and 5.0 at.%, respectively. Both capsules were non-destructively examined utilizing neutron radiography, x-ray radiography, and gamma scanning techniques. Capsule K-42B was destructively examined utilizing gas sampling, element profilometry, metallographic and electron microprobe techniques, and α and β-γ autoradiography.

The following observations were made:

1. No clad failures occurred in the inner elements of either capsule as a result of operating in EBR-II at maximum heating rates of ~ 30 kW/ft.

2. Fuel swelling rates (assuming isototropic swelling) were in the range 1.5 to 2.5 vol% per at.% burnup.

3. Some mechanical interaction between fuel and cladding was observed. This interaction resulted in cladding ovality over lengths up to 3 inches. (See Fig. 463-3.)

4. The maximum cladding deformation observed (including cladding swelling) was 1.3%.

TABLE 463-III

DESCRIPTION OF EXPERIMENTS

	Condition	Series 1	Series 2	Series 3
1.	Lineal Power, kW/ft	~30	~45	~30
2.	Fuel Composition	--$(U_{0.8}Pu_{0.2})C$, Solid-Solution, Sintered--		
3.	Fuel Uranium	^{235}U	^{233}U	^{235}U
4.	Fuel Density	90%	95%	95%
5.	Pellet Diameter (in.)	0.265 ± 0.002	--0.260 ± 0.002--	
6.	Smear Density	81	82	82
7.	Clad Size	---0.300-in.-o.d. x 0.010-in.-wall----		
8.	Clad Type	316SS	316SS	316SS
9.	Max Clad Temp, °F(°C)	1250(677)	1275 (690)	1250 (677)
10.	Max Fuel Centerline Temp. °F (°C)*	2130(1165)	2550(1399)	2100(1149)
11.	Burnup	---------- 3 at.% to 10 at.% ----------		

* Calculated for solid fuel pellet.

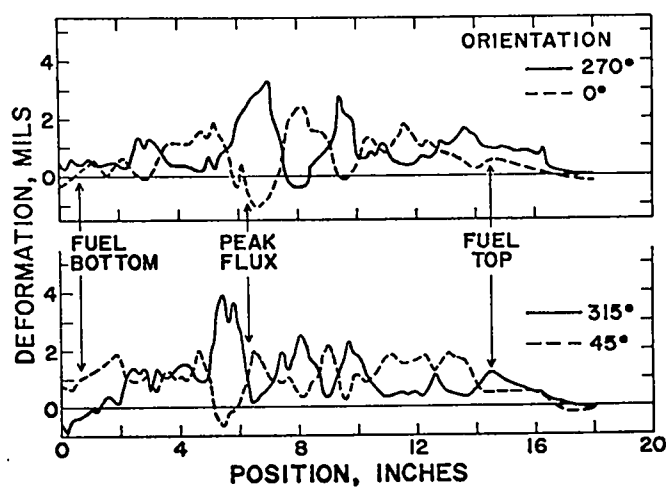

Fig. 463-3. Fuel element profilometry data from capsule K42B.

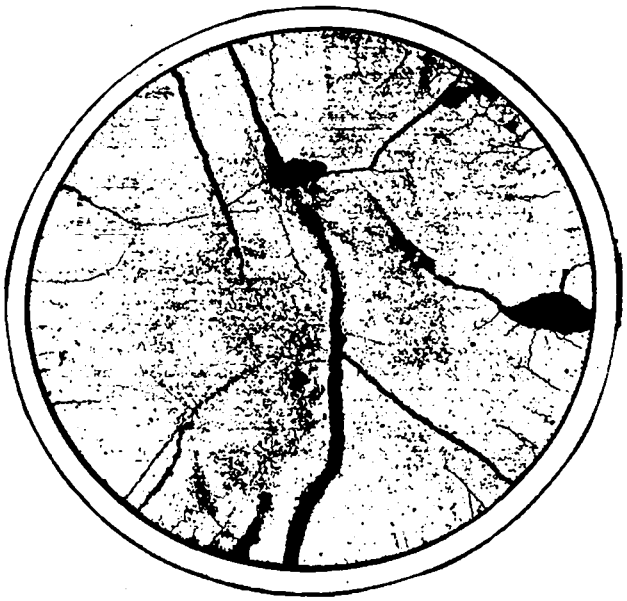

Fig. 463-4. As-polished mosaic of high fuel temperature, intermediate clad temperature (604°C mean), high burnup (~ 30 kW/ft) section of capsule K-42B. The inside diameter of the clad is 0.28 in.

5. The fission gas release from the fuel was low: 6.9 to 7.7%. The resulting operational hoop stress was also low: ~ 500 psi.

6. Thermal stresses result in major fuel splitting on initial reactor startup and general fragmentation as the fuel is weakened by fission product recoil and fast neutron damage. Fuel fragmentation is more severe in the high burnup, high temperature regions of the fuel. (See Fig. 463-4.)

7. Fission gas bubble nucleation (Fig. 463-5) and the depletion of beta-gamma activity in the central sections of fuel near the core midplane (Fig. 463-6) indicate that these sections operated at temperatures higher than would be calculated for a solid fuel pellet. This condition could result from a decrease in the rate of heat transfer through the fragmented fuel.

8. No new phases were observed in the fuel.

9. A slight amount of carburization of the cladding was observed. The degree of carburization increased with increasing cladding temperature (Figs. 463-7 and 463-8).

10. No evidence of reactions between uranium,

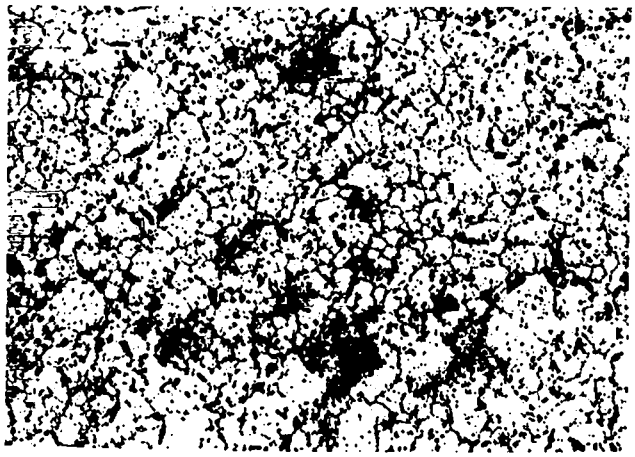

Fig. 463-5. As-polished photomicrograph of high fuel temperature, high burnup, section of capsule K-42B. Note fission gas "bubble necklaces" around grains. Dark areas are due to sodium stains. Maximum dimension of photomicrograph corresponds to an actual length of 0.0067 in.

plutonium, or fission products and the cladding was observed.

Three capsules from Series 1, designated K-37B, K-38B, and K-39B; and two capsules from Series 3, designated K-43 and K-44 began irradiation in EBR-II in subassembly X086 at the start of reactor run 45. The first interim examination of these capsules at a maximum burnup of 3.2 at.% was started at the end of run 49 and is in progress.

The three capsules from Series 2, designated K-49, K-50, and K-51; and two additional capsules from

Fig. 463-6. Beta-gamma autoradiograph of high fuel temperature, high burnup region of capsule K-42B.

Fig. 463-7. Photomicrograph of 0.010 in. thick cladding from low cladding temperature (515°C mean) region of capsule K-42B.

Fig. 463-8. Photomicrograph of 0.010 in. thick cladding from high cladding temperature (665°C mean) region of capsule K-42B.

Series 3, designated K-45 and K-46, were charged into EBR-II in subassembly X119 for the start of reactor run 49. The first interim examination will be done at a maximum burnup of 3.0 at.%. One capsule will be destructively examined at that time.

An approval-in-principle has been requested from the AEC for a combination carbide-nitride, singly encapsulated series of 19 elements. The fuel will be 95% dense, single-phase $(U_{0.8}Pu_{0.2})C$ and $(U_{0.8}Pu_{0.2})N$. The carbide fuel will be fabricated from material synthesized using arc melting and carbothermic reduction processes. The nitride fuel will be supplied by Battelle Memorial Institute. Both solution annealed and 20% cold worked Type 316 stainless steel will be utilized for cladding. Smear densities will be 80 and 85%. Heating rates will be in the range from 35 to 45 kW/ft for elements 0.310 in. in diameter.

An improved heat treating and hot eddy-current testing apparatus was designed and built during the year. Design of a xenon tagging apparatus was started.

C. Thermal Irradiations of Sodium-Bonded Mixed Carbides

(J. C. Clifford and J. O. Barner)

High purity, solid-solution $(U_{0.8}Pu_{0.2})C$, sodium-bonded to Type 316 stainless steel, has been irradiated in the Omega West Reactor, a 6 MW, MTR-type facility, to determine whether fuel, clad, and sodium remained mutually compatible at burnups of 10-15 at.%. While fast spectrum irradiations are preferred in order to produce power densities and radial temperature gradients anticipated in LMFBR's, thermal irradiations appeared useful in this case because the fuel regions of prime interest (those nearest the clad and in contact with sodium) for compatibility studies could be maintained at realistic temperatures.

Fuel for the experiments is $(U_{0.8}Pu_{0.2})C$, fully enriched in ^{235}U and containing approximately 4.7 wt% carbon, 270 ppm oxygen, and 370 ppm nitrogen.[3] The material is essentially single phase monocarbide with no

higher carbides and approaches 95% of theoretical density. Fuel pellets, 0.265 in. in diameter and 0.250 in. thick, are contained in Type 316 stainless steel capsules, each 2.5 in. long and 0.300 in. in diameter with a 0.010 in. wall. Each capsule contains three fuel pellets, a stainless steel insulator pellet, and approximately 0.3 gm of sodium. Two such capsules are used in each experiment.

Experiments were operated to estimated fuel surface burnups of 4.4, 7.3 and 13.0 at.%. Operating conditions are shown in Table 463-IV. A complete topical report on this series of experiments is in preparation. The results for the final experiment, 13 at.% surface burnup, have not been reported and therefore will be summarized here.

Metallographic examination of the irradiated fuel structures showed no significant alterations except for sodium logging, intergranular cracking, and a number of white intergranular inclusions.

The appearance of the inclusions was similar to ones which are occasionally present in very small amounts, < 0.5 vol%, in as-fabricated fuel. Microprobe analysis has been used to show the as-fabricated inclusions to be enriched in plutonium and silicon and depleted in uranium and carbon. These inclusions were not observed in the metallography samples for the chemical batch of fuel used in the fabrication of the experiment. It is not possible, however, to stipulate positively that no inclusions were present in the as-fabricated fuel, but it is clear that a substantial increase in the number of inclusions has occurred. In addition, the location of the inclusions was principally confined to the outside, high burnup zone of the fuel. Post-irradiation microprobe analysis showed that, in addition to the plutonium and silicon, the noble metals, Ru, Rh, and Pd were concentrated in the inclusions. No heterogeneity in the distribution of other fission products was observed. No evidence was found to indicate that uranium or plutonium had migrated or that these elements had interacted with the cladding.

TABLE 463-IV

OPERATING CHARACTERISTICS OF THERMAL NEUTRON IRRADIATION EXPERIMENTS

Linear Power	22.2 kW/ft
Specific Power (w/g of fuel)	
Outer 0.001 in. of surface	670
Centerline	50
Fuel Temperature (^{o}C)	
Surface, max.	730
Surface, min.	610
Centerline, max.	930
Centerline, min.	810
Clad Temperature (^{o}C)	
Inner surface, max.	720
Inner surface, min.	600

Metallographic examination of the irradiated cladding showed that light, intermittent grain boundary precipitation of an $M_{23}C_6$-type phase had occurred along the inner surfaces adjacent to the fuel in those sections which operated at temperatures in the range from 600 to 700^{o}C. Cladding which operated above an estimated inner surface temperature of 700^{o}C exhibited a microstructure which was characterized by (1) grain boundaries that were not delineated by the oxalic acid etchant and consequently appeared white, (2) a grain boundary phase generally associated with triple points, which was attacked by the etchant, and (3) a mottled appearance in the grains. Microprobe examination of the specimen revealed no compositional features that could be associated with these microstructural features. It is probable, however, that the grain boundaries were too small to resolve. In addition, the phase associated with the triple points occurred so rarely that detection is unlikely for scans made on an unetched sample.

Similar changes were observed in out-of-pile compatibility tests of cladding samples which had not undergone carburization. The structure was found to contain the Sigma phase (an iron-chromium intermetallic) at the triple points, no grain boundary precipitates of the $M_{23}C_6$-type carbides, and a mottled appearance in the grains which was probably caused by precipitation of $M_{23}C_6$. When clad carburization occurred in the out-of-pile studies, the Sigma phase did not form.

By analogy, then, the structure of the cladding irradiated at high temperature resulted from the normal aging of Type 316 stainless steel. Carbon transport to the cladding from the fuel, if any, was not sufficient to suppress the formation of the Sigma phase.

Those areas which operated at lower temperatures showed intermittent grain boundary precipitates. This probably resulted from the transport of small amounts of carbon from the fuel to the cladding.

It may be concluded that no significant fuel-clad interaction has occurred in tests where single-phase (U, Pu)C specimens were irradiated to surface burnups of 13 at.% at clad temperatures of 600-720°C. In addition, some carburization of the Type 316 stainless steel by the fuel may be beneficial in that it appears to prevent the formation of the Sigma phase and the concomitant increase in the chemical activity of nickel in the matrix austenite.

D. TREAT Irradiation Testing

(J.F. Kerrisk, R.E. Alcouffe, D.G. Clifton, K.L. Walters, and J.O. Barner)

In order to assess the behavior of carbide and nitride fueled elements under fast reactor accident conditions, transient irradiations will be conducted in the TREAT facility. Investigations will be conducted on both irradiated and unirradiated fuel pins to determine (1) the threshold power levels at which damage or failure occurs, (2) the effect of bond and cladding defects, and (3) the failure propagation mechanism in multipin assemblies.

A cooperative effort has been initiated with the United Nuclear Corporation in the area of TREAT testing. Four unfiltered experiments are planned. Two sodium bonded pins prepared by UNC will be tested: one irradiated and one unirradiated. Also, two UNC helium bonded pins will be examined; again, one irradiated and one unirradiated. Neutronic and heat transfer analysis of these experiments is being carried out.

The first experiments utilizing LASL fabricated fuel pins will be directed toward defining the threshold conditions at which boiling occurs in the sodium bond, and also determining the behavior of the thermal bond after the onset of boiling. These tests will be run in a pressure vessel assembly incorporating a thermal neutron shield to provide for power generation and temperature distributions in the fuel that are more typical of fast reactor systems.

1. Neutronic Analysis

(R.E. Alcouffe and K.L. Walters)

A neutronic analysis is being carried out on the experiments and the reactor system in order to scope the experimental procedure and to aid in interpreting experimental results. Three types of fuel pin configurations are currently being investigated: (1) United Nuclear-designed helium bonded pin, (2) United Nuclear-designed sodium bonded pin, and (3) LASL-designed sodium bonded pin. Essentially the same type of neutronic information is determined for all three experiments except that, in the case of the LASL pin, the feasibility of a thermal neutron filter has also been investigated. With an eye toward doing an accurate job of computing the effects of a thermal neutron filter, a 29-group library including five thermal groups was derived from ENDF-B neutron cross section data. Particular emphasis in this group structure is placed on the thermal and epithermal groups.

Preliminary objectives of the neutronic analysis are to (1) determine the power shape in the fuel pin, (2) compute the so-called figure of merit, that is, the ratio of the power density in the fuel to the total power in the reactor; and (3) determine the effect of selected thermal neutron filters on the reactor and the experiment. The DTF-IV one-dimensional transport theory code was used with the 29-group library to compute the radial flux distributions. The results of several such calculations for the different pins and filters are summarized in Table 463-V. From these results, it was concluded that a selected TREAT reactor transient would be able to deposit enough fission energy in the fuel pin to melt the fuel for all cases shown. Also, from these results and other considerations, it is concluded that gadolinium is a

TABLE 463-V

TREAT EXPERIMENT
ONE-DIMENSIONAL CALCULATIONAL RESULTS

Pin Type	Filter Type	k_{eff}	Pin Power Dist. Edge to Center	Figure of Merit
none[a]	none	1.0536	---	-----
UNC[b]	none	---	7.94	1.340×10^{-4}
UNC[c]	none	---	8.12	1.374×10^{-4}
LASL	none	---	7.66	$1.1[illegible] \times 10^{-4}$
LASL	Gd (0.010 in.)	1.0133	1.30	3.323×10^{-3}
LASL	BN (0.100 in.)	0.9934	1.21	2.211×10^{-3}

[a] Experiment replaced by reactor fuel.
[b] Helium bonded pin.
[c] Sodium bonded pin.

TABLE 463-VI

PRELIMINARY TWO-DIMENSIONAL CALCULATIONAL RESULTS

Theory	Pin Power Dist. edge/center	Figure of Merit
Diffusion	10.8	1.814×10^{-4}
Generalized Diffusion	6.96	1.623×10^{-4}

satisfactory filter and will not degrade the performance of TREAT for those experiments.

The figure of merit computed using the one-dimensional transport code is only an estimate because the flux shape in the axial dimension is not accounted for. In order to compute an accurate figure of merit, a two-dimensional analysis is necessary. This has been done to date using both diffusion theory and a generalized diffusion theory which takes into account the transport effects due to the experiment. The results for one calculation, the unfiltered LASL experiment, are shown in Table 463-VI. Further analyses are being carried on to predict the transient behavior of the system in order to choose the transients necessary to achieve the objectives of the experiment. For this purpose the reactor kinetics code ANCON[9] is being used.

2. Heat Transfer Analysis
(J. F. Kerrisk)

Heat transfer calculations are being performed to predict the behavior of (U, Pu)C fuels subjected to energy generation transients. The calculations are aimed at simulating the behavior of sodium bonded fuel pins during transient tests in the TREAT reactor. The CINDA-3G heat transfer code[5] has been programmed for one-dimensional (radial) calculations with space and time dependent energy generation rates, temperature dependent physical properties, phase changes, and radiative heat transfer where appropriate.

Initial calculations investigated the heat transfer in a fuel pin contained in a capsule. Table 463-VII lists the materials and radial dimensions of the components. The following parameters were investigated:

1) heat sink material - Na, Al, and Ni,

2) space energy generation in the fuel - uniform to flux depressions of 12 to 1,

3) time energy generation - step function and two typical TREAT transients,[6]

4) total energy deposited - 0 to 300 cal/gm fuel,

5) initial system temperature - 150 to 650°C,

6) fuel pin sodium bond behavior - bond ejection or bond remaining liquid.

A study of the results of these initial calculations has led to the following conclusions:

1) As compared to a gas bonded oxide fuel, a larger fraction of the energy generated in a sodium bonded carbide fuel will be lost to the cladding and heat sink as long as the fuel pin bond remains liquid. This is due to the higher conductivities of the carbide fuel and sodium bond compared to the oxide fuel and gas bond respectively.

2) Large flux depressions increase the fraction of energy generated that is lost by the fuel since the high conductivity liquid sodium bond provides a good heat transfer path for energy generated near the fuel surface. Thus large flux depressions should be avoided, which indicates that a neutron filter is advisable.

3) The behavior of the fuel pin sodium bond is critical in predicting the outcome of a transient. The two limiting cases of (a) the bond remaining liquid at all temperatures, and (b) the bond being ejected when the sodium vapor pressure exceeds the fuel pin cover gas pressure, produce radically different results since the conductivity of liquid sodium is a factor of 40 greater than the vapor. If the bond is assumed to remain liquid,

TABLE 463-VII

TREAT FUEL PIN AND CAPSULE

Component	Material	Radius, in. Inside	Radius, in. Outside
Fuel Pin			
Fuel	$(U_{0.8}Pu_{0.2})C$, 95% TD	0	0.1325
Bond	Na	0.1325	0.140
Clad	316 Stainless Steel	0.140	0.150
Capsule			
Bond	Na	0.150	0.1875
Heat Sink	Ni, Al, Na	0.1875	0.4625
Bond	Na	0.4625	0.5135
Clad	316 Stainless Steel	0.5135	0.5625

fuel melting (2300°C) and fuel pin clad melting (1400°C) are initiated about the same time with flux depressions less than 2 to 1 and with a transient of 250 msec width at half maximum. A total energy of 300 cal/gm of fuel would be required to completely melt the fuel, but clad failure would probably occur near energy depositions of 200 cal/gm of fuel. When the fuel pin sodium bond is assumed to eject, essentially all the subsequent energy generated in the fuel remains there. Approximately 200 cal/gm of fuel are then required for complete fuel melting. In this case the fuel pin cladding would probably remain intact. Since these two limiting cases predict such different outcomes, the initial TREAT tests should be designed to probe the sodium bond behavior.

4) Nickel is the best choice as a heat sink material, mainly because of its large volumetric heat capacity and high melting point.

5) Transients with a pulse width at half maximum of less than one msec will deposit essentially all the transient energy in the fuel before significant losses occur to the fuel pin sodium bond or cladding. Thus a transient in this range or faster is equivalent to a delta function input of the energy to the fuel.

Stress Analysis

A capability for calculating thermal stresses in the hollow cylindrical cladding of the fuel pin and capsule has been added to the heat transfer code. Initially only elastic stresses due to radial temperature gradients were calculated,[7] but a method of including plastic or viscoelastic behavior and accounting for internal pressures and axial loads is presently being included.[8]

Pressure Vessel - Neutron Filter Design

The capsule described in Table 463-VII provides only primary containment for the fuel pin. The secondary containment required for plutonium fuels has been met on oxide tests by a pressure vessel which contains the fuel pin and capsule and replaces one of the TREAT fuel elements.[9] In addition, this pressure vessel contains heaters for setting the initial fuel pin temperature, thermocouples, and thermal insulation. Preliminary design work has been started on a pressure vessel which would contain a neutron filter replacing an outer shell of thermal insulation. Four filter materials are being considered: boron as BN, and dysprosium, samarium, and gadolinium as the metals. Heat transfer and stress analysis calculations for the pressure vessel-fuel pin-capsule assembly subjected to some typical TREAT transients are in progress.

A series of four TREAT tests is to be run in cooperation with the United Nuclear Corporation. Heat transfer, stress analysis and neutronic calculations are being carried out to aid in the design and interpretation of these experiments.

III. FUEL PROPERTIES

A. Differential Thermal Analysis

(J. G. Reavis and L. Reese)

A program of differential thermal analysis (DTA) observations of irradiated oxide fuel materials has been initiated. The samples have been sealed in tungsten capsules and observed while heating and cooling over the range 1300 to 2900°C. Selected compositions in the Pu-C system have been observed by DTA and the Pu-C phase diagram has been revised. Selected compositions in the U-Pu-C system have been observed by DTA and metallographic examination of quenched samples in an attempt to determine the phase boundaries of the single phase region near $U_{0.8}Pu_{0.2}C$.

1. DTA of Irradiated Samples

DTA measurements have been made on oxide specimens sealed in W capsules having re-entrant wells for optical pyrometric temperature measurement. The melting of ZrO_2 in a sealed capsule was observed periodically to recheck the temperature calibration of the system. Two samples of UO_2-20% PuO_2 (NUMEC B-9-56) irradiated in EBR-II to 6.2 at.% burnup were observed under identical conditions, as was an archival sample of the fuel. Results of DTA of the three samples are shown in Table 463-VIII.

The "solidus" temperatures listed in Table 463-VIII for the irradiated samples may not be the temperatures of first liquid formation. Indeed, it is expected that certain of the fission products are present as microscopic metallic inclusions which melt at much lower temperatures. The "solidus" temperatures listed are the temperatures of major thermal arrests. It can be seen

TABLE 463-VIII

RESULTS OF DTA OF UO_2-20% PuO_2 SAMPLES IN SEALED W CAPSULES

Sample	Solidus, °C	Liquidus, °C	Other, °C
NUMEC B-9, No. 1	2725±30	2825±30	2685±30
NUMEC B-9, No. 2	2740±25	2840±25	2685±25
Archival Material	2750±25	2840±25	None

from Table 463-VIII that any change in solidus or liquidus temperatures produced by irradiation is smaller than the uncertainties of the determinations. The only remaining difference between DTA curves of archival and irradiated materials is a weak but reproducible thermal arrest seen for the irradiated samples at 2685 ± 25°C. The nature of the transformation producing this arrest is not known. Visual observations of thermally cycled samples have shown, however, that significant slumping does not occur at this temperature. Indeed, little slumping of these samples can be seen before the liquidus temperature is closely approached. Examination of samples taken to higher levels of burnup may provide more information about the arrest which occurs at 2685°C.

Arrangements have been made with GE-Sunnyvale for a cooperative program whereby LASL has been furnished specimens of irradiated UO_2-PuO_2 for DTA. Seven irradiated specimens varying in burnup from 4.3 to 10.6 at.% have been received. Three archival specimens have also been received. Examination of these specimens will begin in the near future.

2. Single Phase Boundaries of $U_{0.8}Pu_{0.2}C$

An attempt has been made to determine the boundaries of the single phase region near $U_{0.8}Pu_{0.2}C$. This work has used the techniques of DTA and of metallographic and x-ray powder diffraction studies of quenched samples. The DTA furnace was used for cycling, annealing, and quenching a series of $U_{0.8}Pu_{0.2}C$ specimens having selected C concentrations.

The temperature range 1400-2100°C has been most extensively studied. The phase boundary between single phase $U_{0.8}Pu_{0.2}C$ and the two-phase region containing liquid metal and solid monocarbide appears to be at a C/M ratio of 0.96 ± 0.01 at 1400°C and 0.95 ± 0.01 at 2100°C. Seemingly contradictory observations were made during the studies, but it now appears that carbon was lost from samples annealed in carburized Ta for long periods at high temperatures. This effect would account for the apparent contradictions.

The boundary between the single phase monocarbide and the phase field containing monocarbide and sesquicarbide appears to be at a C/M atomic ratio of 0.99 ± 0.01 at 1400°C and at a slightly higher value at 1900°C. There are strong DTA indications that specimens containing sesquicarbide and monocarbide undergo a phase transformation at 2050°C. Quenching experiments did not confirm this, but indicated a transformation producing a dicarbide phase which could be identified by x-ray powder diffraction in samples quenched from above 2150°C. Thermal arrests were not shown by DTA cycles through this temperature range. Metallographic studies are in agreement with the x-ray observations.

B. DTA of Pu-C Compositions

Samples of Pu, $PuC_{0.23}$ and $PuC_{0.51}$ were investigated using a low temperature DTA apparatus in which temperature measurements are made with thermocouples. Seven additional samples in the composition range from $PuC_{0.72}$ to $PuC_{1.91}$ were thermally cycled in the high temperature DTA apparatus. The data produced by these measurements were combined with previous data to reconstruct the Pu-C phase diagram as shown by Fig. 463-9. The accuracy of the horizontal phase boundaries below 1000°C is ± 5°C. The temperatures of horizontal phase boundaries above 1000°C are accurate to ± 10°C. Liquidus temperatures are known with an accuracy of better than ± 25°C. The composition limits of the single phase monocarbide were estimated to be at C/M atomic ratios of 0.80 ± 0.02 and 0.90 ± 0.02 over much of the range 1000 to 1500°C. These estimates are based on metallographic studies of quenched samples. No definitive data were obtained below 1000°C because of the slowness of approach to equilibrium. The upper limit of the single phase sesquicarbide field appears to occur at O/M ratio of 1.50 ± 0.01, but the lower limit could not be accurately determined. A range of stoichiometry was indicated, however, by the variation of lattice dimensions

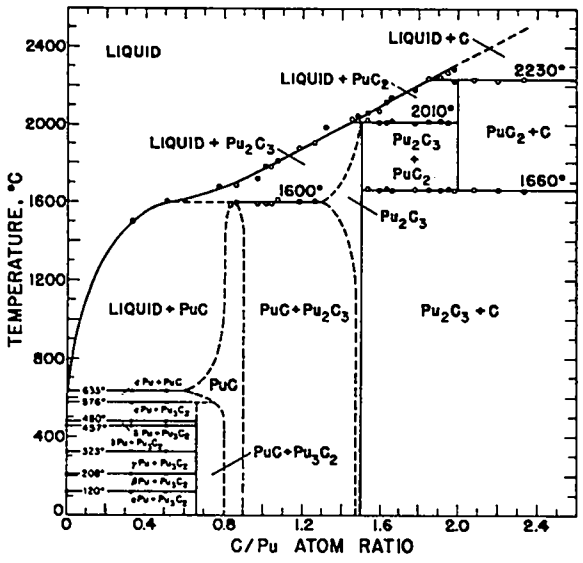

Fig. 463-9. The plutonium-carbon system.

determined by x-ray powder diffraction studies of quenched samples. Metallographic data indicates that the dicarbide has a C/M atomic ratio of 2.00 ± 0.02.

No further investigations of this type are planned for the Pu-C system.

C. High Temperature Calorimetry
(D. G. Clifton)

High temperature drop calorimetric enthalpy measurements are currently being made on irradiated and unirradiated samples of UO_2-20% PuO_2. The materials, obtained from the Nuclear Materials and Equipment Corporation (NUMEC), are considered to be representative of typical commercial grade LMFBR oxide fuels.

The high-temperature-drop calorimeter used for these measurements is installed in a LASL hot cell. The basic design of the receiving block, constant temperature bath, and instrumentation is the same as that described by Ogard and Leary[10] with the exception of two major modifications: (1) a tungsten mesh heating element is used in the furnace and (2) the furnace body and the sample holding-dropping mechanism has been changed to facilitate remote handling of the system. A full account of the design, installation, and manipulation of this hot cell apparatus has been reported.[11]

Samples being measured in the calorimeter are placed in W capsules 3/4 in. o.d. x 2 in. long. The lid is welded in place under a reduced pressure of Ar and He. The temperature of the sample in the furnace is measured by sighting an optical pyrometer onto a black-body hole drilled radially into the side of the capsule. Because the pyrometer measurements are made through the windows of the hot cell and furnace, absorption corrections are sizeable: 132 and 365°C for temperatures of 1195 and 2265°C, respectively. All of the measurements reported here were made with the calorimeter operating under a gas pressure of 200 mm of argon.

The energy equivalent of the calorimeter, with an empty W capsule in the block, has been determined by electrical calibration to be 2376.4 ± 0.26% s.d. calories per millivolt output of the block temperature-sensing resistance bridge network. This constant was determined with varying total energy inputs and varying powers.

Table 463-IX lists apparent enthalpy determinations of empty W capsules with the same geometry as the sample capsules. These values are denoted as apparent enthalpies for W because no corrections are included for radiative heat losses during the drops, hence the values are less than the true enthalpies for W. These data are used directly to correct for the enthalpy of the

TABLE 463-IX

MEASURED APPARENT ENTHALPY OF TUNGSTEN

T, °C	Apparent Enthalpy ($H_T - H_{25°C}$) cal/gm
1198	40.3
1348	45.5
1461	49.9
1582	54.9
1641	57.0
1719	60.7
1763	62.3
1767	62.7
1811	63.9
1833	65.1
1969	70.8
2125	77.9
2265	83.6

TABLE 463-X

MEASURED ENTHALPY OF
IRRADIATED U_{02}-20% PuO_2 (NUMEC B-9)

T, °C	H_T-H_{25} °C cal/gm
1195	86.0
1330	101.3
1368	101.2
1473	110.9
1539	116.5
1622	125.5
1673	129.6
1734	134.3
1846	147.5
1970	153.1
1987	158.5
2143	174.6

W capsules during a sample measurement; it is assumed that the radiative losses are the same for the loaded and empty capsules having the same geometry.

Tables 463-X and 463-XI list the measured enthalpy values for an irradiated and an unirradiated sample of UO_2-20% PuO_2, respectively. The irradiated sample, 40.006 gm, was taken from the NUMEC-B-9 fuel capsule[12] that had been irradiated in EBR-II to a burnup of 56,600 MWD/Te, 6.2 at.%. The unirradiated specimen, 42.3345 gm, was made from equal amounts of archival UO_2-20% PuO_2 taken from two batches of material obtained from NUMEC designated Batch Run No. 12 and Batch Run No. 25. NUMEC advised that the irradiated fuel for NUMEC-B-9 had been made from equal quantities of these two batches.

TABLE 463-XI

MEASURED ENTHALPY OF
UNIRRADIATED UO_2-20% PuO_2 (NUMEC ARCHIVE)

T, °C	H_T-H_{25} °C cal/gm
1245	90.3
1348	97.1
1508	110.0
1589	118.9
1725	130.2
1889	147.7
1974	154.9
2096	169.2
2223	177.4

Before making enthalpy measurements on these samples, measurements were made in the calorimeter of the radioactive decay self-heating to provide the necessary data to correct the enthalpy experiments. Self-heating determinations for the irradiated sample gave a value of $6.31 \times 10^{-3} \pm 2.7\%$ s.d. watts/gm of sample. The values obtained from an analysis of the slopes of the temperature-rise versus time curves agreed very well with those obtained by analysis based on the convergent temperatures. Determination of self-heating for the unirradiated sample, which practically results only from the Pu content, gave a value of 2.1×10^{-3} watts/gm Pu. This is good agreement with independently determined values for Pu.

Figure 463-10 is a plot of the measured enthalpy points versus temperature, with the exception of two recently measured points that have been included in Tables 463-X and 463-XI: namely at 2143 and 2223°C. Also shown in Fig. 463-10 are enthalpy data reported by Ogard and Leary[10] for samples of unirradiated $U_{0.802}Pu_{0.198}O_{2.00}$ and $U_{0.802}Pu_{0.198}O_{1.98}$ that were provided by the General Electric Company.

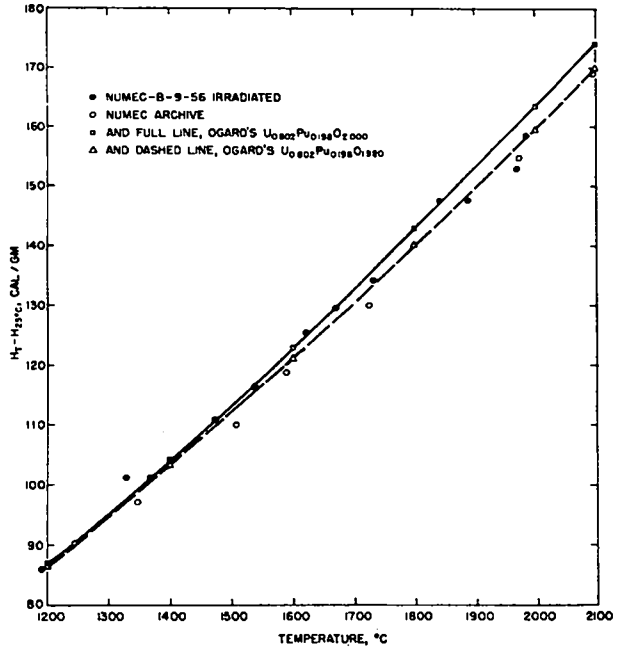

Fig. 463-10. Enthalpy vs. temperature for some uranium-plutonium oxide solid solutions.

Several tentative conclusions are drawn from the data of Fig. 463-10:

1) Generally the data for the irradiated NUMEC sample agree closely with those for the unirradiated stoichiometric $U_{0.802}Pu_{0.198}O_{2.00}$ except for one of the high temperature points at 1970°C and one of the lower temperature points at 1330°C. Further experimental confirmation of these points is being undertaken. The last high temperature point at 2143°C, listed in Table 463-X but not shown in Fig. 463-10, combined with the data near 1970°C seems to indicate that the data for the irradiated sample may be diverging toward values lower than Ogard's measurements for the stoichiometric compound.

2) The data for the unirradiated NUMEC specimen are consistently lower than those for the irradiated material as well as for the unirradiated $U_{0.802}Pu_{0.198}O_{1.98}$ data.

3) Ogard's data show a definite enthalpy decrease in going from the stoichiometric to the hypostoichiometric mixed oxide.

These observations suggested that the NUMEC unirradiated material may be hypostoichiometric, in fact, with an O/M ratio < 1.98. Therefore, a sample of the archival material was analyzed for U, Pu, and O. These measurements yielded an O/M ratio of 1.95 ± 0.02, which is not too surprising since it has been reported[12] that the fuel fabrication variables for the NUMEC Series B fuel were the same as for the Series A fuel and for the latter, the oxygen-to-metal ratio varied from about 1.94 to 2.004.

The 2 to 4% difference between the enthalpies of the irradiated and unirradiated NUMEC materials is attributed to burnup effects. The close agreement of the irradiated NUMEC and unirradiated GE $U_{0.802}Pu_{0.198}O_{2.00}$ is considered to be fortuitous.

In binary fission, each fissioned atom gives rise to two fission fragment atoms, thus increasing the total number of atoms in the sample. From the Dulong-Petit approximation, one can assign an enthalpy value per atom and thereby postulate an increase in the total enthalpy corresponding to the increase in the number of atoms. For 6.2% burnup, the total number of atoms increases by 2.1%; therefore, approximately a 2.1% increase in enthalpy would be expected assuming no losses of gaseous or volatile fission products since such losses would reduce this "increased number of atoms effect."

Fission products can be expected to provide other effects which may increase the observed enthalpy, such as heats of fusion, sublimation, vaporization, or chemical interactions.

For the irradiated sample examined, some of the anticipated characteristics of the fission products are listed in Table 463-XII. Columns 1 and 2 give the individual chemical species and their expected fission yields in number of atoms per 100 fissions. These yields were calculated under the following conditions: The U in the NUMEC, UO_2-20% PuO_2, fuel was enriched to about 91.4% in ^{235}U and the Pu is assumed to be ^{239}Pu. Fission reaction rate calculations as reported[13] for the core center of the EBR-II reactor give a reaction ratio of 1.184 for $^{239}Pu/^{235}U$. The NUMEC-B-9 fuel capsule was put into

TABLE 463-XII

SOME FISSION PRODUCT PARAMETERS
FOR 6.23 at.% BURNUP OF UO_2-20% PuO_2

Fission Product	Atoms per 100 Fissions	Atoms for 6.23 Fissions	State at Operating Temp.	O Atoms United with Fission Products (b)	O Atoms United with Fission Products (c)
Se	0.298	0.0186	vapor	0	0
Br	0.0996	0.0062	vapor	0	0
Kr	2.375	0.1480	gas	0	0
Rb	3.189	0.1987	vapor	0	0
Sr	6.858	0.4273	SrO	0.4273	0.4273
Y	3.563	0.2220	oxide	0.3330	0.4439
Zr	26.164	1.6300	ZrO_2	3.2600	3.2600
Nb	0.031	0.0019	Nb_2O_5	0.0048	0.0038
Mo	24.907	1.5517	oxide or metal	(a)	(a)
Tc	5.973	0.3721	metal	0	0
Ru	15.686	0.9772	metal	0	0
Rh	4.527	0.2820	metal	0	0
Pd	5.767	0.3593	metal	0	0
Ag	0.516	0.0321	metal (l)	0	0
Cd	0.434	0.0270	vapor	0	0
In	0.048	0.0030	vapor	0	0
Sn	0.615	0.0383	vapor	0	0
Sb	0.233	0.0145	vapor	0	0
Te	2.508	0.1562	vapor	0	0
I	1.360	0.0847	vapor	0	0
Xe	22.111	1.3775	gas	0	0
Cs	18.590	1.1582	vapor	0	0
Ba	6.276	0.3910	BaO	0.3910	0.3910
La	5.942	0.3702	oxide	0.5553	0.7404
Ce	11.480	0.7152	oxide	1.0728	1.4304
Pr	5.088	0.3170	oxide	0.4756	0.6340
Nd	19.400	1.0286	oxide	1.8129	2.4172
Pm	1.746	0.1088	oxide	0.1632	0.2176
Sm	3.772	0.2350	oxide	0.3525	0.4700
Eu	0.317	0.0198	oxide	0.0296	0.0395
Gd	0.084	0.0052	oxide	0.0078	0.0105
Total	199.90	12.457		8.8857	10.4466

(a) All Mo assumed to be present as the metal.
(b) All rare earths assumed to be present as the sesquioxides.
(c) All rare earths assumed to be present as the dioxides.

EBR-II in November 1966 and removed around March 1969: therefore, the approximation has been made that the fuel had an in-reactor time of 2 years and an out-of-reactor time of 2 years. This roughly accounts for variations in the reactor power, the assembly being out of the reactor temporarily, and the enthalpy measurements being made during the last few months of 1970 and the first half of 1971. Tables presented by Varteressian and Burris[14] give the fission product spectra for 1 MeV neutron fission of ^{235}U and for 2 MeV neutron fission of ^{239}Pu as a function of both in-reactor and out-of-reactor time. Interpolations were made from these tables for the 2 year in-core and 2 year out-of-core case for the yields of both ^{235}U and ^{239}Pu. These yields were then weighted by the respective concentrations and fission reaction ratios of the two fissioning nuclides to give the yields of column 2 of Table 463-XII.

Column 3 of this table converts the yields to the number of atoms for 6.23 fissions. Column 4 shows the anticipated state of the fission products at operating temperature of the fuel. Columns 5 and 6 are counts of the number of O atoms that may be expected to be tied up in the form of oxides with the fission products. In column 5 the rare earths, R.E., are assumed to be of the form $(R.E.)_2O_3$, whereas in column 6 they are $(R.E.)O_2$. The sums at the bottom of these columns give the expected total for the O atoms tied up with the exception of any O atoms combined with Mo.

The final average stoichiometry of the unburned fuel can be estimated. Calculations show that if the initial fuel had an O/M ratio of 1.95, a 6.23% burnup, and the residual fuel had an O/M ratio of 2.00 then only 7.460 O atoms would be released. This is not enough to provide all the O atoms for the stable fission product oxides listed in either column 5 or 6 (exclusive of the Mo). In fact, further calculation reveals that to allow all the oxides (exclusive of Mo) of either column 5 or 6 to form results in an average stoichiometry for the residual fuel of $MO_{1.99}$ or $MO_{1.97}$, respectively, with all of the Mo present as metal. Of course this is a consequence of the originally low O/M ratio of 1.95. If the O/M ratio of the residual fuel is lower than about 1.97, or if the stoichiometry of the original fuel has an O/M ratio > 1.95, there will be additional oxygen released which generally will be associated in a shifting reaction involving Mo (s), MoO_3 (g), MoO_2 (s)[15] and the residual fuel of MO_{2-x}. The heats of these reactions may then be a contributory factor in enthalpy measurements; however, for the low O/M ratio involved in the experiments reported here, effects of this nature are not expected to be seen.

Several expected heat effects associated with the present measurements that can help account for the 2 to 4% enthalpy increase are:

1) The volatile species, Cs, Rb, Te, I, Se, Cd, and Sb all boil below 1500°C; neglecting any major losses of these from the fuel sample used in the experiments, one can estimate a 1% increase in enthalpy contributed by the heats of fusion and boiling.

2) O'Boyle et al.[16] have found metallic ingots in irradiated $U_{0.8}Pu_{0.2}O_{2.00}$ that are an alloy of the metal fission products whose oxides are not stable under operating conditions. The alloy consists of Ru, Mo, Tc, Pd, and Rh and is expected to melt between about 1800 and 1900°C. Estimates of the heat of fusion for this alloy could contribute about 0.5% increase in the enthalpy.

3) The residual fuel stoichiometry is expected to have a higher O/M ratio than the unirradiated material with a concomitant increase in enthalpy of possibly 1-2%.

4) BaO, SrO, and some form of Ce oxide seem to appear in a "grey phase" in the equiaxed region adjacent to the columnar grains according to O'Boyle et al.[17] Dependent on the form of the cerium oxide, the melting of this grey phase could occur between about 1750 and 2400°C, contributing its heat of fusion.

More experimental data will be taken to confirm some of the data reported here and to extend the temperature to higher values. Measurements also are being made on a standard sample of Al_2O_3 to provide an accuracy check. Future measurements should be made on irradiated mixed oxide fuel with higher burnup and also on fuels with initial O/M ratios nearer 2.00; these systems should display more effects due to the oxygen-molybdenum-fuel interactions.

C. Transport Properties

(K.W.R. Johnson and J.F. Kerrisk)

1. Thermal Conductivity

The thermal conductivity apparatus is in the process of being moved to a new location. The glovebox that had contained the thermal conductivity apparatus has been removed. Modifications of a new inert atmosphere glovebox to house the apparatus have been completed. These include a new baseplate and bell jar cover which should reduce the furnace atmosphere contamination by oxygen and water. The new glovebox is in place but the installation of services has not begun.

2. Thermal Diffusivity

Design work has been completed on the apparatus for measuring the thermal diffusivity of plutonium-containing ceramic fuels from room temperature to 2700°C by the flash method. This includes drawings for the modification of an inert atmosphere glovebox to house the furnace, and installation drawings for the glovebox, furnace, and associated equipment. Modification of the glovebox is complete and it has been moved into place, but installation has not begun. All major equipment necessary for the installation is on hand.

During the design period the thermal diffusivity apparatus, including the high temperature furnace, lasers, monitoring devices, and associated equipment, was set up for non-radioactive operation in a location which simulates the physical arrangement it would assume in a glovebox. The initial work centered around a continued investigation of the laser beam energy distribution, and how it can be made as uniform as possible over the sample face. Two techniques were employed to examine the beam energy distribution: (1) replacing the sample with a thin, fast response foil whose temperature rise at a point was indicative of the energy deposition, and (2) photographing a magnified image of the beam with infrared film.

The technique of replacing the sample with a thin (0.005 in.) copper foil and measuring the temperature rise of the back face with a thermocouple (0.01-in.-diam thermocouple legs spaced approximately 0.05 in. apart) when the front face is flashed with the laser, has proven to be a quantitative method of determining the relative energy distribution in the laser beam. The maximum temperature rise measured at a particular point (averaged over at least a 0.05-in.-diam circle) is proportional to the energy deposited by the laser beam because the response of the foil is much faster than the time required for significant radial heat flow to occur. Figure 463-11 (a) shows a relative energy curve obtained from seven measurements (seven separate laser shots), along a horizontal diameter of the foil with no optical components between the laser and the foil. For the 0.4-in. diam sample used for the diffusivity measurement, the energy deposited at the edge is about 80% of that at the center. Other sets of measurements in similar configurations gave an energy at the edge of a 0.4-in. diam circle from 70 to 80% of the maximum energy. The range is due to uncertainty in the measurement of the temperature rise and shot-to-shot variations of the laser. The shape of the relative energy curve in Fig.463-11(b) is in line with

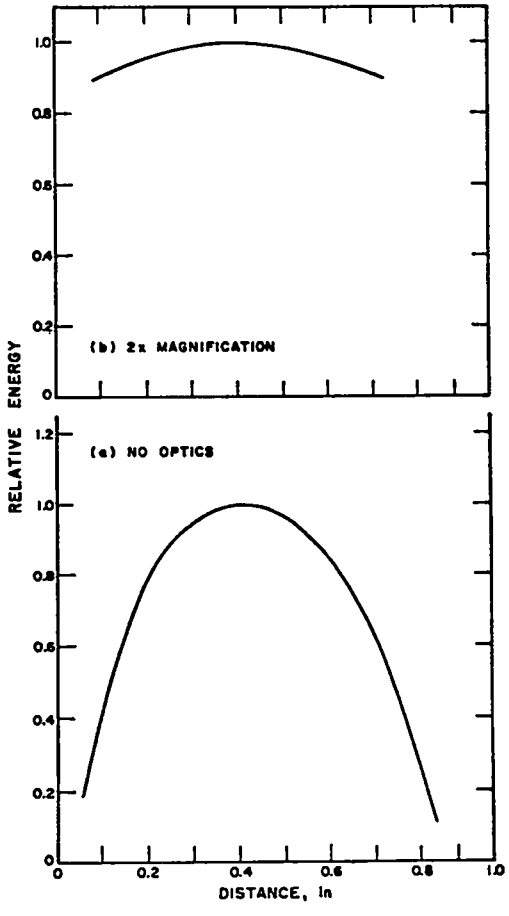

Fig. 463-11. Relative energy distribution in the thermal diffusivity laser beam.

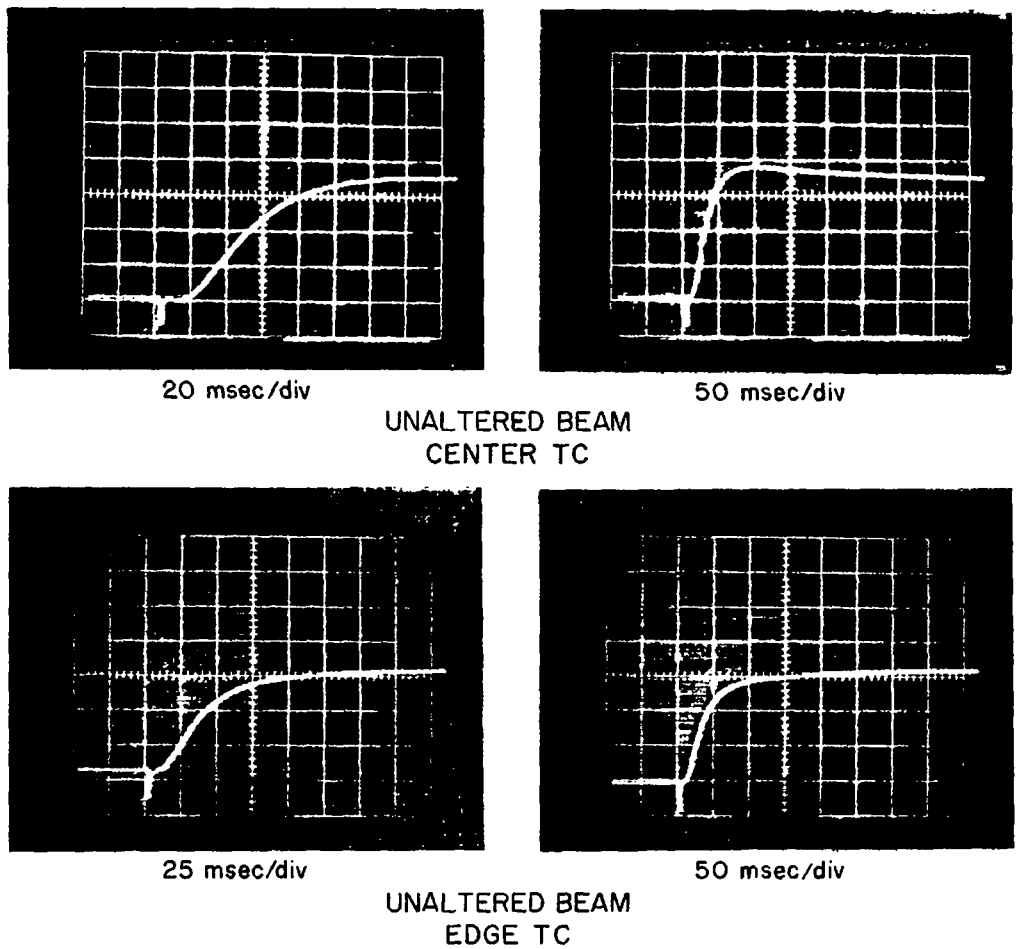

Fig. 463-12. Temperature rise of thermal diffusivity sample back face using an unaltered laser beam.

the predictions of Fox and Li[18] for a laser cavity with circular mirrors.

The usual relation for calculating the thermal diffusivity of a sample from the temperature rise of the back face assumes that the front face of the sample is illuminated uniformly.[19] If a pulse of the shape shown in Fig. 463-11(a) is actually used, with the maximum energy at the center of the sample, radial heat flow will occur along with heat flow through the sample. The symptoms of this problem can be seen in Fig. 463-12 which shows sample back face temperature rises (from 25°C) as a function of time taken at the center and edge of a 0.0765 in. thick Armco Iron Specimen, 0.40 in. in diam. The slow decrease of the center temperature and increase of the edge temperature are due to radial heat flow. The curve of the center temperature rise gives the appearance of heat losses, which should not be occurring at a significant rate at room temperature with a properly designed sample holder. Errors of 10 to 20% were encountered when the thermal diffusivity was calculated from the half-time (time required to reach half the maximum temperature rise) of curves similar to Fig. 463-12.

The problem of a circular sample flashed by a non-uniform pulse with cylindrical symmetry has been treated mathematically,[20] so that it is possible to predict or fit the behavior shown in Fig. 463-12. A number of curves, similar to those shown in Fig. 463-12, were least-squares fitted to a function which describes the back face temperature rise of a sample flashed by a laser pulse with a parabolic energy distribution. The thermal

diffusivity obtained from these fits was in better agreement with the values expected for Armco Iron at room temperature than those obtained from only half-time measurements, but the effort expended in preparing the data and computer time are prohibitive for routine work. A second problem encountered when using the unaltered laser beam is one of alignment. In the current apparatus design the laser beam travels 1 ft horizontally, is deflected 90° through a prism, and travels 3 ft vertically to the sample face. It is extremely difficult to keep the beam energy maximum centered on the sample because the full sample diameter subtends an arc of only 8×10^{-3} radians at 4 ft. Deviations of the energy maximum from the sample center would result in the shape of the back face temperature profile being a complex function of the location on the sample.

The problems of using a laser beam with the energy distribution shown in Fig. 463-11(a) for thermal diffusivity measurement are not insurmountable, but a uniform energy distribution would simplify both the experimental operation and data treatment. The simplest means of producing a more uniform distribution is to place a ground glass diffuser in front of the sample. Scattering from the diffuser produces illumination that is uniform, but the intensity decreases rapidly with distance so that the sample must be within about 1 in. of the diffuser to produce an acceptable temperature rise on the back face. This is practical up to $400\text{-}500^{\circ}$C, but since the apparatus described here can operate to a much higher temperature, other methods must be found. It is possible that other materials which are transparent to the laser radiation and can be used at high temperature could serve as diffusers, but this approach was not investigated.

A number of other techniques were tried to produce a uniform energy distribution in the laser beam at the sample front face, but the most successful amounted to expanding the beam with simple lenses so that only the central portion of the beam was used. This technique wastes some of the laser energy, but it has not proved to be a problem since the Korad K-2 laser used in this apparatus has a maximum energy of 125 joules, well above the energy necessary to give acceptable temperature rises in 0.40-in.-diam samples. Figure 463-11(b) shows a relative energy curve obtained in the same manner as Fig. 463-11(a), except that a double convex lens was used to magnify the beam approximately 2X at the copper foil. The energy at the edge of a 0.4-in.-diam circle (the sample size) is about 95% of the maximum energy. A more uniform beam can be obtained by greater magnification, but more of the total laser beam energy is lost. For a given diameter, a thin sample requires a more uniform illumination than a thick one, since there is less time for radial redistribution of the energy as it travels through the thin sample. But a thin sample also requires less total energy to achieve the same temperature rise as a thick one. Thus as the sample thickness increases, the laser beam magnification can be reduced, giving a less uniform beam (which is acceptable for a thicker sample) with more energy. Magnifications in the range of 2X to 3X were found to be acceptable from the standpoint of uniformity for samples 0.20 to 0.03 in. thick. An acceptable temperature rise curve showed no apparent drop in temperature, after the maximum had been achieved, for 10 to 30 half-times.

The location of a double convex lens in the path between the laser and the sample, and the focal length of the lens, determine the magnification of the beam at the sample face. Considering the sample front face as the image plane of the lens, it was found empirically that the most uniform beam was obtained when the focal length and placement of the lens were such that the object plane of the lens was within the laser cavity between the front mirror and the front face of the laser rod. No explanation of this result has been found.

Additional evidence of the non-uniformity of the laser beam was obtained by masking portions of the beam and measuring the energy of the unmasked portion with a laser calorimeter.

During these investigations a procedure was developed which gave a semiquantitative indication of the laser beam intensity distribution. In place of a sample at the image plane, a screen was mounted at a relatively long distance from the front mirror. With a 2-64 optical filter over the lens of a Crown-Graphic camera to remove the visible spectrum and with infra-red film which is

sensitive to 1.06μ radiation, photographs of the beam image were made by the open flash technique. Visual comparison of a series of photographs made by moving the double convex lens progressively farther from the front mirror indicated the optimum lens position for maximum beam uniformity. As previously noted, the lens position was such that the object plane was between the laser rod and the front mirror. Densitometer scans of the photograph negatives confirmed this observation. Subsequent thermal diffusivity measurements were made with the optical system which produced maximum beam uniformity.

As a comprehensive test of the entire apparatus, the thermal diffusivity of molybdenum and tungsten samples was measured from room temperature to 2000°C. The parameters investigated by these measurements were:

1) Sample thickness. Two samples of molybdenum (0.1024 in. and 0.1505 in. thick) and two samples of tungsten (0.1020 in. and 0.2510 in. thick) were used.

2) Furnace atmosphere. Measurements were made in helium, argon and vacuum.

3) Sample temperature rise detector. From room temperature to 1150°C a chromel-alumel thermocouple was used while from 800 to 2000°C a central spot on the back face of the sample was imaged onto the face of an RCA 7102 photomultiplier tube.

Both materials were characterized by a chemical analysis of the as-received material and a metallographic examination before and after the measurements. Table 463-XIII lists the analytical results along with densities calculated from the sample dimensions and mass. Metallographic examination of the as-received samples indicated considerable cold working. During the measurements recrystallization occurred. The final crystallite size of the samples ranged from 20 to 100μ.

The sample back face temperature rises from both detectors were recorded on a storage oscilloscope screen and subsequently photographed. Time mark generator traces were used to check the time scale. The thermal diffusivity, α, was calculated from the measured

TABLE 463-XIII

CHEMICAL ANALYSIS AND DENSITY OF Mo AND W

	Mo	W		Mo	W
C*	80	80	Co	< 30	< 10
Fe	40	220	Ni	< 10	< 1
O	45	35	Cu	< 3	<100
Si	< 3	30	Zn	<100	--
K	<30	100	Sr	< 30	< 10
Ca	<10	30	Zr	<100	< 30
Mn	< 3	10	Nb	<100	<300
Li	< 3	< 3	Mo	--	<100
Be	< 1	< 1	Ag	< 1	< 1
B	<10	< 3	Tl	--	< 10
Na	<30	< 3	Cd	< 10	--
Mg	< 1	< 1	Sn	< 10	< 10
Al	<10	<10	Ba	< 10	--
Ti	<30	<30	Pb	< 10	< 10
V	<30	<10	Bi	< 30	--
Cr	<10	<10	Cs	--	< 3

* Numbers expressed as ppm.

half-time, $t_{1/2}$, as

$$\alpha = \omega \ell^2 / t_{1/2},$$

where ℓ is the sample thickness and $\omega = 0.139$ when heat losses may be ignored.[19] Corrections for heat losses were made by the method proposed by Cowan.[21] The sample thickness (ℓ) was also corrected for thermal expansion.

Fig. 463-13 shows the thermal diffusivity, α, of molybdenum and tungsten plotted as a function of temperature. There were no significant differences observed in the results due to sample thickness, furnace atmosphere, or type of detector. A problem of excessive detector noise was observed with an argon furnace atmosphere and the photomultiplier detector, but this was attributed to convection currents in the argon distorting the image of the back face of the sample. No such problem was observed with helium.[22] The overall precision of the diffusivity results is estimated to be ± 4%.

The measured thermal diffusivities, specific heat, C_p, data taken from the literature,[23] and the measured densities, ρ, corrected for thermal expansion, were used to calculate the thermal conductivity, K, of molybdenum and tungsten as

$$k = \alpha \rho C_p.$$

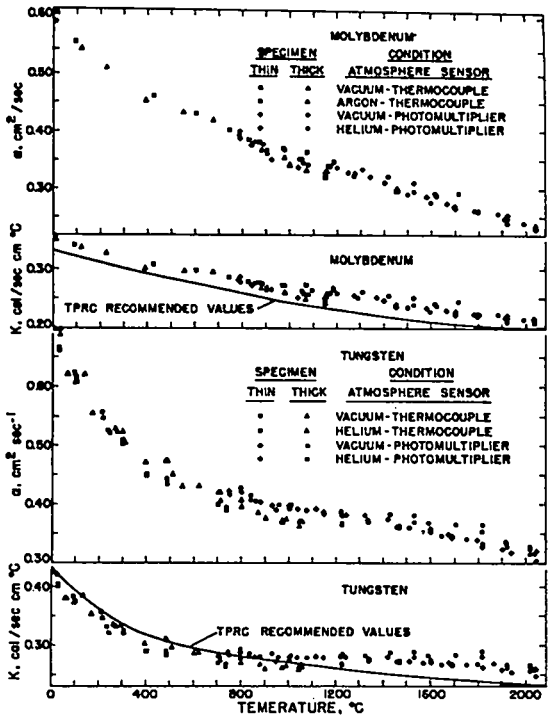

Fig. 463-13. Thermal diffusivity and conductivity of Mo and W.

These results are also plotted in Fig. 463-13 as a function of temperature. Shown with the data are curves obtained from the Thermophysical Properties Research Center recommended values for the thermal conductivity of Mo and W.[24] These values are assigned an accuracy of ± 4% of the true values near room temperature and ± 4 to 10% at other temperatures. It can be seen that a curve representing calculated thermal conductivity from measured thermal diffusivity lies well within the accuracy of the recommended values. Subsequent investigations[24,25] indicate that the measured thermal conductivity values may represent an accuracy of better than 4%.

3. Electrical Resistivity

No additional electrical resistivity measurements were made this period. Work on the electrical resistivity apparatus was terminated. The high temperature furnace originally purchased for electrical resistivity measurements will be installed in an inert atmosphere glovebox. Current plans are to use the furnace for preparative work.

D. Mechanical Properties
(M. Tokar)

1. Compressive Creep

Creep specimens of $(U_{0.79}Pu_{0.21})C_{1.02}$ with a sintered density of 11.8 g/cm^3 have been tested in compression at 1300, 1400 and 1500°C under stresses of 2000, 4000 and 6000 psi. The equipment and test procedures have been described in detail elsewhere.[26] In brief, solid cylindrical specimens, approximately 0.5 in. long and 0.4 in. in diam, were heated in a graphite susceptor and compressed between two graphite rods. The end surfaces of the specimens were separated from the graphite rods by thin B_4C discs to reduce carbon transfer. For this series of tests, specimen deformation was determined from micrometer measurements (± 0.0001 in.) made before and after each run. Temperatures were measured optically by sighting through a hole in the susceptor onto the specimen surface.

Some typical creep curves are shown in Fig. 463-14. The primary creep regions are extensive, but this may have been at least partially due to the specimen's

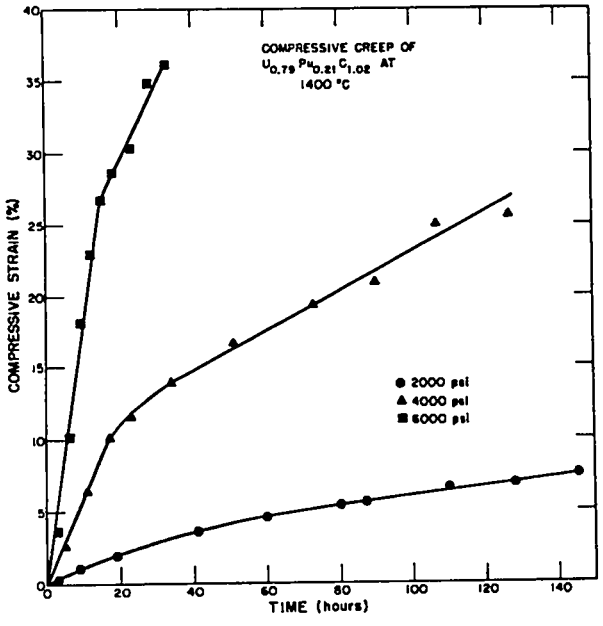

Fig. 463-14. Compressive creep of $(U_{0.79}Pu_{0.21})C_{1.02}$ at 1400°C as a function of time and applied stress.

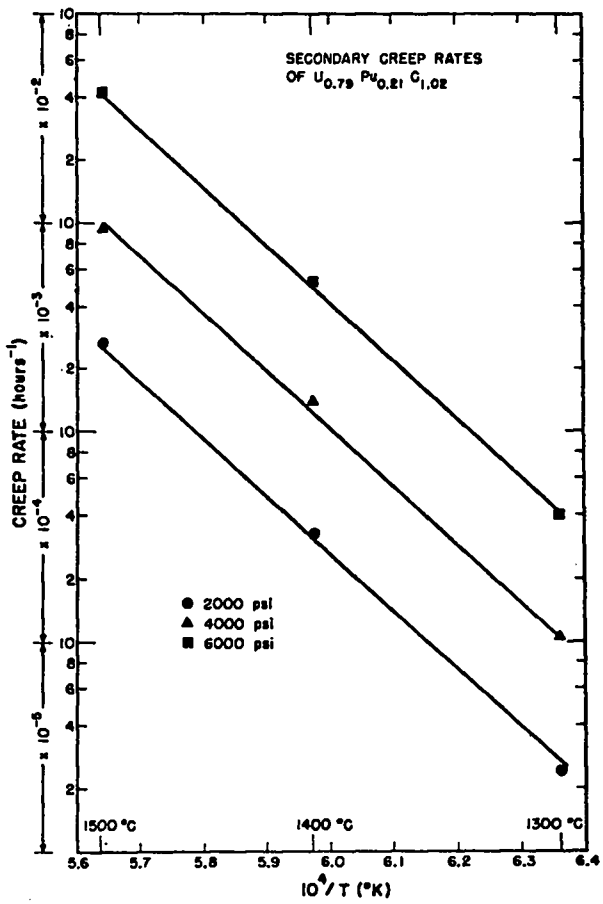

Fig. 463-15. Secondary compressive creep rates of $(U_{0.79}Pu_{0.21})C_{1.02}$ as a function of 1/T and applied stress.

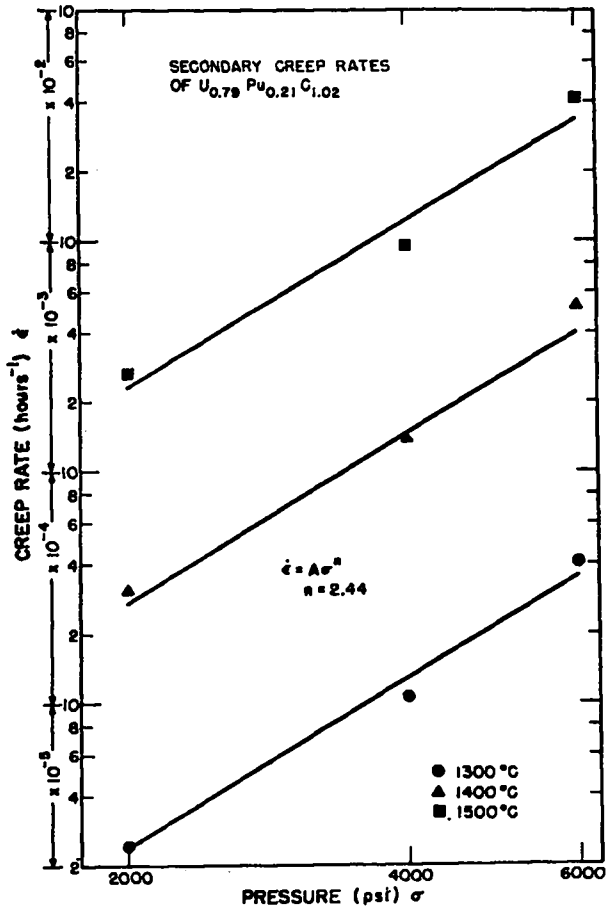

Fig. 463-16. Secondary compressive creep rates of $(U_{0.79}Pu_{0.21})C_{1.02}$ as a function of applied stress and temperature.

relatively low sintered density (~ 87% theoretical). Densification up to 92% of theoretical density was observed during the tests, and most of this increase in density occurred prior to the onset of secondary creep.

The effects of stress and temperature on the steady-state creep rates are shown in Figs. 463-15 and 463-16. The creep data were fitted by a least squares method to an equation of the form

$$\dot{\epsilon} = A\sigma^n \exp(-Q/RT) \qquad (1)$$

where

$\dot{\epsilon}$ = creep rate (hr^{-1})

A = a constant

σ = stress (psi)

n = stress exponent

Q = activation energy (kcal/mole)

R = gas constant

T = temperature (^{o}K).

The equation which best fitted the data was

$$\dot{\epsilon} = 7.96 \times 10^4 \sigma^{2.44} \exp\left(\frac{-126.4 \text{ kcal/mole}}{RT}\right). \qquad (2)$$

The standard deviations for the stress exponent and activation energy were 0.20 and 5.1 kcal/mole respectively. Creep rates calculated from this equation were within 30% of the experimentally determined values.

In a recent paper[27] the activation energy for creep of $(U_{0.85}Pu_{0.15})(C_{0.65}N_{0.35})$ was reported as 100 ± 10 kcal/mole, and in a study of creep in UC and (U, Pu)C, Killey et al.[28] reported an activation energy on the order of

100 kcal/mole for creep in (U, Pu)C_{1+x}. Other investigators[29,30,31] of creep in UC have reported activation energies between 44 and 90 kcal/mole.

The value of the stress exponent, n, in the general creep equation is often useful in interpreting creep behavior because the stress exponent should, according to theory, have certain discrete values dependent on the particular creep mechanism. For example, creep by dislocation climb[32] should yield a stress exponent of about 5, whereas Nabarro-Herring stress-directed vacancy migration[33,34] results in a linear stress dependence. Creep by grain boundary sliding is conventionally thought to result also in a linear relationship between creep rate and stress. Recently, however, Langdon[35] pointed out that reported examples of a linear relationship between $\dot{\epsilon}_{GBS}$ (creep rate due to grain boundary sliding) and σ are restricted to very low stress conditions and that, consequently, models which treat sliding as a Newtonian viscous phenomenon appear incapable of accounting for data obtained under the usual conditions of high temperature creep. Langdon proposed a grain boundary sliding model in which sliding occurs by the movement of dislocations along, or adjacent to, the boundary by a combination of glide and climb, and in which the strain rate due to sliding is proportional to σ^2/d, where d is the average grain diameter. The theoretical stress exponent for this mechanism is close to the experimentally determined value in the overall equation for creep in (U, Pu)C, Eq. (2), and is also close to most of the literature values of n for creep in UC.[29,30,31]

It should be noted, however, that whereas the overall stress exponent resulting from a fit of all the data to the empirical creep equation was 2.44, the data points in Fig. 463-16 could be connected by two sets of straight lines instead of one; one set of lines could connect the 2000 and 4000 psi points, and another set could connect the 4000 and 6000 psi points, thereby providing two stress exponents, a value of about two for the lower stresses and a value greater than three for the higher stress region. This would, therefore, correspond to a change in creep mechanism, possibly from grain boundary sliding to dislocation climb or even glide. Since only three stresses were used in this investigation, it would be premature to interpret the data in this fashion. Further work, performed over a wider stress range, would be required to establish whether different creep mechanisms prevail at low and high stresses.

Ceramographic studies of crept $U_{0.79}Pu_{0.21}C_{1.02}$ specimens support the indication that grain boundary sliding may be a major creep mechanism in (U, Pu)C. A quantitative evaluation of the amount of grain boundary sliding can be made from measurements of the average grain shape, defined in terms of the parameter (L/B) where L is the average grain length and B is the width relative to the compressive stress direction.[36,37] Assuming an initial value for L/B of unity (equiaxed grains), the grain strain, i.e., deformation within the grains due to slip or dislocation climb, is

$$\epsilon_g = (L/B)^{2/3} - 1. \qquad (3)$$

The relative contributions of the two processes, grain strain and grain boundary sliding, to the overall specimen deformation can be obtained from the ratio of grain strain to total strain, ϵ_g/ϵ_T. If the deformation is due only to straining of the grains, then $\epsilon_g/\epsilon_T = 1$, but if the deformation is due only to relative translational movements of the grains, with no change in the average grain shape, then $\epsilon_g/\epsilon_T = 0$.

Taking as an example a specimen deformed 25.0% (at 1400°C, 4000 psi), the L/B was determined to be 0.99. Hence, from Eq. (3), the grain strain was practically zero, indicating that almost all the creep strain resulted from grain boundary sliding. In another example a specimen deformed 50.6% (at 1500°C, 6000 psi) had an L/B of 0.86, from which ϵ_g was calculated to be 0.10. Thus grain boundary sliding accounted for about 80% (ϵ_g/ϵ_T = 0.10/0.51) of the total deformation in this specimen, which was deformed to an extreme degree. In the literature on grain boundary sliding, some writers have suggested that sliding accounts for all of the initial deformation until some critical strain is reached at which slip first occurs. The grain shape studies of crept (U, Pu)C specimens appear to support this suggestion.

Changes in pore shape have also been observed which support the above indications that grain boundary sliding may be a major creep mechanism in (U, Pu)C.

Pores in as-sintered pellets are typically rounded and non-oriented, whereas pores in severely deformed specimens are elongated and aligned in a direction parallel to the compressive stress direction. This would be the expected configuration in grain boundary pores caused by, or at least shaped by, the movement of ledges in the boundaries. Of course, grain boundary sliding cannot contribute to deformation indefinitely without auxiliary processes, because some intragranular deformation is necessary to maintain geometrical continuity between the grains. In a specimen which is porous initially, however, changes in grain boundary pore shape could facilitate sliding by alleviating the grain strain requirement.

It is interesting to note that Stellrecht et al.[31] did obtain evidence of extensive grain strain in creep in UC, but their material was arc-cast with a grain size of about 200 to 300 μm, compared to 20 to 30 μm for the sintered (U, Pu)C used in this study. It seems reasonable for grain boundary sliding to be more important in the material which has the larger number of sliding interfaces. Thus there may be some critical grain size below which grain boundary sliding is the predominant creep mechanism and above which dislocation climb is of major importance.

A comparison of the secondary creep rates measured in $U_{0.79}Pu_{0.21}C_{1.02}$ with literature values for $UC_{1.08}$ tested under the same conditions of stress and temperature is given in Fig. 463-17. It is apparent that the uranium carbide had greater creep resistance than the solid-solution carbide tested under the conditions shown.

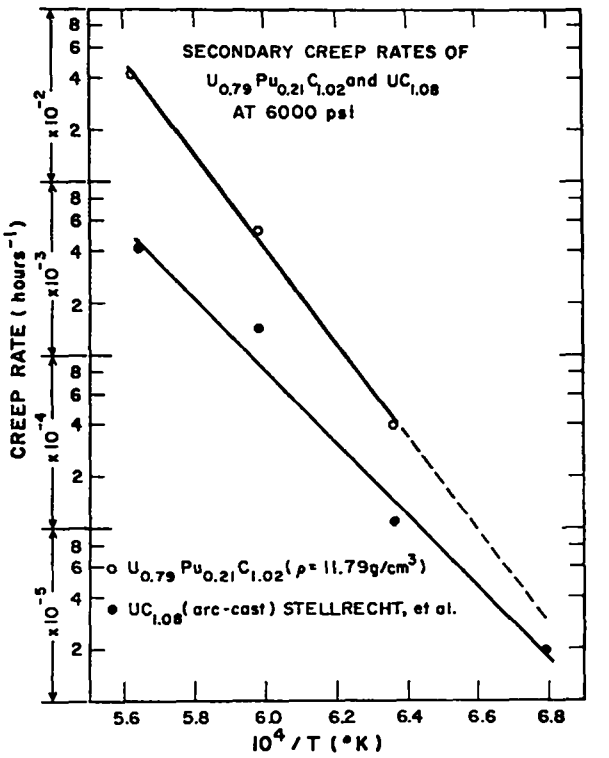

Fig. 463-17. Secondary creep rate vs. 1/T for $(U_{0.79}Pu_{0.21})C_{1.02}$ and $UC_{1.08}$.

2. Hot Hardness

The hardness of several monocarbides with various U/Pu ratios has been measured from room temperature to 1300°C. Plots of log hardness versus temperature for some of these compositions are shown in Fig. 463-18. Each point represents the mean of 5 to 15 readings taken over 1 to 4 runs. The hardness decreases gradually as the temperature rises to approximately 400 to 500°C. There is then an increase in softening rate with increasing temperature after which the materials again soften less rapidly.

For pure metals, plots of log hardness versus temperature often have a distinctive shape; viz. two straight line segments which intersect at approximately half the melting point, 0.5 T_m.[40] Hardness plots for certain intermetallic compounds have been found to have the same shape, but the point of intersection varies between 0.4 to 0.75 T_m.[41] This form of the log hardness versus temperature plots may be represented by the so-called Ito-Shishshokin equation[42,43]

$$H = A e^{-BT} \qquad (4)$$

where H is the hardness, A is a constant, B is the "softening coefficient," and T is the temperature. The constants A and B have different sets of values at low and high temperatures. It is theorized that different mechanisms of deformation are operative above and below the intersection temperature; below this temperature, slip processes predominate, while above this temperature, diffusion controlled processes prevail.

A plot of some of the hardness data as a function of homologous temperature, T/T_m, is shown in Fig. 463-19.

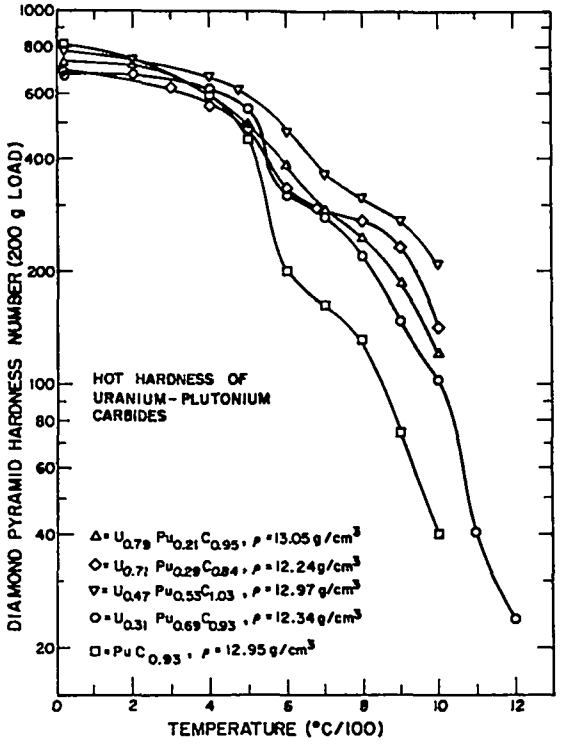

Fig. 463-18. Hot hardness of uranium-plutonium carbides.

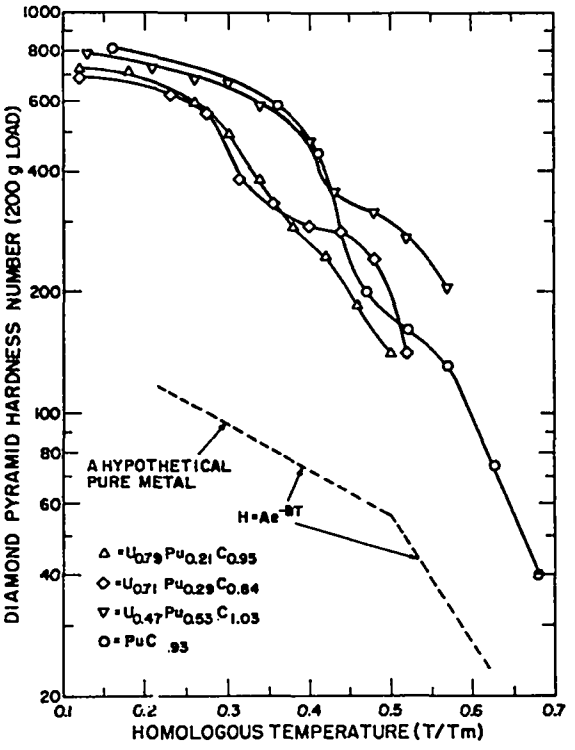

Fig. 463-19. Hot hardness of uranium-plutonium carbides as a function of homologous temperature.

For the solid solution carbides which melt over a temperature range, solidus temperatures were arbitrarily chosen as a basis for calculating the homologous temperature.

At temperatures below 0.5 T_m, the Ito-Shishshokin relationship is clearly not followed in these materials, but sufficient data are not yet available at temperatures above 0.5 T_m to establish the applicability of this relationship at high temperatures. At temperatures below 0.5 T_m the non-linearity of the log H versus T plots is possibly the result of dislocation-impurity interactions such as have been reported for UN.[43]

The effect of solid solution hardening at 1000°C in alloys of UC and PuC is shown in Fig. 463-20. Although the composition survey is incomplete, it appears that most of the solid solution carbides are significantly harder than UC at 1000°C (the UC hardness value was taken from the work of DeCrescente and Miller[45]). If this pattern held at higher temperatures, the solid solution carbides would be expected to be more creep resistant than UC, but as shown in Fig. 463-17, the (U, Pu)C creep-tested as part of this investigation had higher creep rates than reported for UC by Stellrecht et al.[31] If the creep data were extrapolated to lower temperatures, however, the lines would cross at about 1050°C; i.e., the creep rate of UC would be equal to that of the solid solution carbide.

A possible explanation for these results lies in the theory of solid solution strengthening. At very high temperatures the deformation mechanism is almost certainly diffusion-controlled, but if in (U, Pu)C the diffusivity of the solute Pu ions is sufficiently high, there may be no "impurity" retardation of dislocation motion. At intermediate temperatures, however, the drift velocity of the solute Pu ions might be expected to decrease to a point where dislocation motion is hindered, yielding a higher

hardness than that obtained for pure UC. Since self-diffusion data for Pu in the solid solution carbides are not available, this hypothesis remains unsupported, but similar dislocation-solute atom interactions have been held responsible for anomalous mechanical property measurements in other materials in the temperature range from 0.25 to 0.45 T_m.[28,44,49]

It should be noted that in a recent study on self-diffusion and actinide diffusion in uranium monocarbide ($UC_{1.07}$),[47] the diffusivity of plutonium in $UC_{1.07}$ was found to be higher than that of uranium in the temperature range 1700 to 2300°C. An extrapolation of the diffusion data to 1000°C, however, is not straightforward. Grain boundary diffusion may be significant at temperatures below 1700°C.[48,49] Moreover, there appears to be little justification for using diffusion data obtained on a particular monocarbide composition such as $UC_{1.07}$ for a solid solution carbide containing almost 20 mole% PuC.

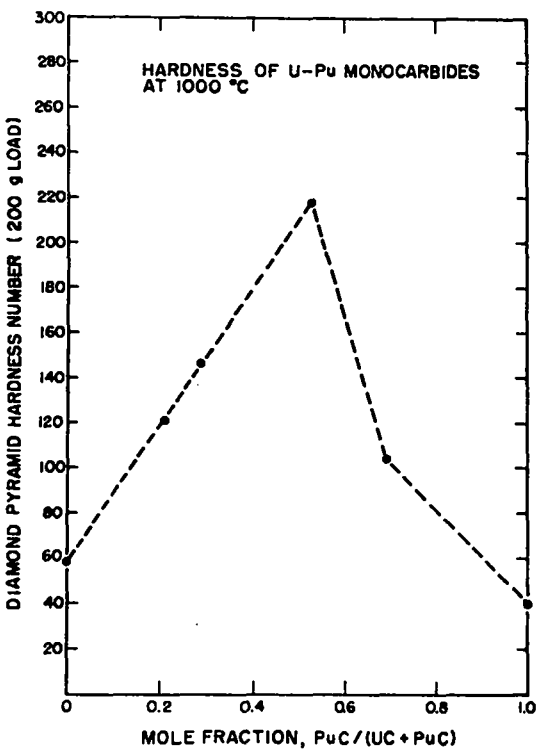

Fig. 463-20. Hot hardness of uranium-plutonium carbides at 1000°C showing the effect of solid solution hardening.

E. Mass Spectrometric Studies of the Vaporization of Pu Compounds

1. The Plutonium-Carbon System

Among the parameters required for the design of fuel materials for fast breeder reactors are the thermodynamic properties of these materials at high temperatures. From these properties, one can calculate the chemical activities of the individual fuel components and the stabilities of these fuel materials with respect to the cladding. Included among the fuel forms being considered are the solid solution uranium-plutonium-carbides. This study of the vaporization behavior of the binary Pu-C system was undertaken as an initial step in the investigation of the U-Pu-C ternary system.

Our study of the vaporization behavior of the Pu-C system has been concluded and a description of the experimental techniques and some of the preliminary results have been published.[50,51] In this report, the results obtained are compared with those obtained in various other investigations.[51,55]

(a) Vapor Pressure Results

The results of this investigation indicate that there are four composition regions of the Pu-C system that give rise to invarient but non-congruent vaporization: monocarbide plus sesquicarbide, sesquicarbide plus carbon, sesquicarbide plus dicarbide, and dicarbide plus carbon. The Pu-C phase diagram is shown in Fig. 463-9. The vapor species produced above each of these regions is gaseous Pu.

Throughout this section of the report the following symbols are employed: < > for solid, { } for liquid, and ( ) for gas.

Monocarbide plus Sesquicarbide

The vapor pressure of gaseous Pu above this two-phase region is given by

$$\log_{10} P_{Pu}(\text{atm}) = (5.118 \pm 0.027) - (18,919 \pm 72)/T^{\circ}K, \quad (1450\text{-}1850^{\circ}K). \qquad (1)$$

For the decomposition reaction

$$2.5 \langle PuC_{0.9} \rangle = (Pu) + 1.5 \langle PuC_{1.5} \rangle$$

the free energy is given by

$$\Delta G_T = 86,570 - 23.42T \text{ (cal/mole)}. \qquad (2)$$

The vapor pressure results obtained for this region of the phase diagram by the various investigators are compared in Table 463-XIV.

TABLE 463-XIV

VAPOR PRESSURE DATA FOR THE REACTION
$2.5\ <PuC_{0.8}> = (Pu) + 1.5\ <PuC_{1.5}>$

Temp., °K	Pressure Pu (atm) This Work	Relative Pu Pressures (This Work/Other Data) Ref. 52	Ref. 53	Ref. 55
1500	3.20×10^{-9}	0.95	0.76	5.48
1600	1.97×10^{-7}	0.93	0.82	5.55
1700	9.75×10^{-7}	0.91	0.88	5.60
1800	4.05×10^{-6}	0.90	0.94	5.65
1900	1.45×10^{-5}	0.88	0.99	5.71

$\Delta G_{1873°K}$ for the Decomposition Reaction		
42.7	kcal/mole	this work
42.2	kcal/mole	ref. 52
42.6	kcal/mole	ref. 53
49.2	kcal/mole	ref. 55

TABLE 463-XV

VAPOR PRESSURE DATA FOR THE REACTION
$<PuC_{1.5}> = (Pu) + 1.5\ <C>$

Temp., °K	Pressure Pu (atm) This Work	Relative Pu Pressures (This Work/Other Data) Ref. 52	Ref. 54	Ref. 55
1600	3.93×10^{-8}	1.23	0.36	0.98
1700	2.25×10^{-8}	1.20	0.41	1.01
1800	1.06×10^{-7}	1.18	0.45	1.04
1900	4.24×10^{-7}	1.16	0.46	1.07

$\Delta G_{1973°K}$ for the Decomposition Reaction		
54.7	kcal/mole	this work
54.2	kcal/mole	ref. 52
57.7	kcal/mole	ref. 54
55.0	kcal/mole	ref. 55

The results listed in Table 463-XIV indicate good agreement in the range 1700-1900°K between three sets of data, obtained employing different techniques. The vapor pressure data of Marcon[55] are lower by a factor of about five and may be considered to be in error since the data from the present study yield results in good agreement with low temperature calorimetry studies as noted below.

Sesquicarbide plus Carbon

The pressure of gaseous Pu above this two-phase region is given by

$$\log_{10} P_{Pu}\,(atm) = (4.468 \pm 0.057) - (20,598 \pm 106)/T°K,\ (1668\text{-}1927°K). \quad (3)$$

For the decomposition reaction

$$<PuC_{1.5}> = (Pu) + 1.5\ <C>$$

the free energy is given by

$$\Delta G_T = 94,252 - 20.44T,\ (cal/mole). \quad (4)$$

The results obtained from this investigation are compared to those from other studies in Table 463-XV.

The data listed in Table 463-XV show satisfactory agreement between the results of this study and those from two others. The usual experimental uncertainty in measurements of this type is less than ± 20%. The vapor pressure data of Battles et al.[54] are lower by a factor of about 2 and lead to a difference in ΔG of about 3 kcal/mole. This difference cannot be resolved until the high temperature calorimetry data are available. It should be noted, however, that most of the experimental errors encountered in vapor pressure measurements lead to pressure values that are too low.

Dicarbide plus Carbon

The vapor pressure of gaseous Pu above this two-phase region is given by

$$\log_{10} P_{Pu}\,(atm) = (3.787 \pm 0.084) - (19,288 \pm 170)/T°K,\ (1933\text{-}2140°K). \quad (5)$$

The free energy of the decomposition reaction

$$<PuC_2> = (Pu) + 2\ <C>$$

is given by

$$\Delta G_T = 88,258 - 17.33\ T,\ (cal/mole). \quad (6)$$

At temperatures near 2100°K, trace amounts of gaseous PuC_2 were observed. The ratio of the observed ion currents Pu^+/PuC_2^+ was approximately 1000/1. The various vapor pressure data for the dicarbide decomposition reaction are compared in Table 463-XVI and are not in as good agreement as those for the other decomposition reactions.

Some of the discrepancies may be resolved once the high temperature heat content data are available. The various values for the free energy of decomposition at 1933°K agree within 3 kcal/mole. Again the vapor pressure data of Battles et al.[54] are lower by a factor of about two.

Sesquicarbide plus Dicarbide

The vapor pressure of gaseous Pu above this two-phase region is given by

$$\log_{10} P_{Pu}\,(atm) = (6.533 \pm 0.109) - (24,569 \pm 223)/T°K,\ (1933\text{-}2170°K). \quad (7)$$

TABLE 463-XVI

VAPOR PRESSURE DATA FOR THE REACTION
$<PuC_2> = (Pu) + 2 <C>$

Temp., °K	Pressure Pu (atm) This Work	Relative Pu Pressures (This Work/Other Data) Ref. 53	Ref. 54	Ref. 55
2000	1.39×10^{-6}	1.29	0.46	1.17
2100	4.00×10^{-6}	1.25	0.46	1.25
2200	1.05×10^{-5}	1.21	0.46	1.32
2300	2.52×10^{-5}	1.18	0.46	1.39

$\Delta G_{1933°K}$ for the Decomposition Reaction		
54.8	kcal/mole	this work
53.7	kcal/mole	ref. 53
57.8	kcal/mole	ref. 54
55.2	kcal/mole	ref. 55

For the decomposition reaction

$$4 <PuC_{1.5}> = (Pu) + 3 <PuC_2>$$

the free energy is given by

$$\Delta G_T = 112,423 - 29.89\,T, \text{ (cal/mole)}. \quad (8)$$

The data from this investigation are compared with those from other studies in Table 463-XVII. There is good agreement between the results of this study and those of Marcon.[55]

(b) Free Energies of Formation

$PuC_{1.5}$

If the free energy expression for the decomposition of the sesquicarbide, Eq. (4), is combined with that for the vaporization of Pu metal[56] at 1842°K, the average temperature for the sesquicarbide data, we have

TABLE 463-XVII

VAPOR PRESSURE DATA FOR THE REACTION
$4 <PuC_{1.5}> = (Pu) + 3 <PuC_2>$

Temp., °K	Pressure Pu (atm) This Work	Relative Pu Pressures (This Work/Other Data) Ref. 54	Ref. 55
2000	1.77×10^{-6}	0.49	1.12
2100	6.82×10^{-6}	0.53	1.08
2200	2.31×10^{-5}	0.57	1.05
2300	7.09×10^{-5}	0.60	1.02

$\Delta G_{1933°K}$ for the Decomposition Reaction		
54.6	kcal/mole	this work
57.6	kcal/mole	ref. 54
55.1	kcal/mole	ref. 55

$(Pu) + 1.5 <C> = <PuC_{1.5}>$; $\Delta G = -94,252 + 20.44T$, (cal/mole)

$\{Pu\} = (Pu)$; $\Delta G = 80,157 - 22.63T$, (cal/mole)

$\{Pu\} + 1.5 <C> = <PuC_{1.5}>$; $\Delta G_{f_{1842}} = -14,095 - 2.19T$, (cal/mole). (9)

Equation (9) cannot be corrected to 298°K until high temperature heat content data become available. A sample of single phase $PuC_{1.5}$ has been supplied to ANL for a determination of $\Delta H_{f_{298}}$ by means of oxygen-bomb calorimetry.

Equation (9), when extrapolated to 1000°K, yields $\Delta G_f = -16.3$ kcal/mole, the same value as that obtained from the emf study performed in this laboratory.[51]

PuC_2

If the free energy expression for the decomposition of the dicarbide, Eq. (6), at the average temperature of the data, 2026°K, is combined with that for the vaporization of Pu metal at the same temperature,[56] we have

$(Pu) + 2 <C> = <PuC_2>$; $\Delta G = -88,258 + 17.33T$, (cal/mole)

$\{Pu\} = (Pu)$; $\Delta G = 80,687 - 22.90T$, (cal/mole)

$\{Pu\} + 2 <C> = <PuC_2>$; $\Delta G_{f_{2026}} = -7,571 - 5.57T$, (cal/mole). (10)

Again, Eq. (10) cannot be corrected to 298°K until the high temperature heat content data are available.

Transformation Temperature

If the free energy expressions for the formation of the sesquicarbide and the dicarbide are assumed to hold to the transition temperature, we have, combining Eqs. (9) and (10)

$<PuC_{1.5}> = \{Pu\} + 1.5 <C>$; $\Delta G = 14,095 + 2.19T$, (cal/mole)

$\{Pu\} + 2 <C> = <PuC_2>$; $\Delta G = -7,571 - 5.57T$, (cal/mole)

$<PuC_{1.5}> + 0.5 <C> = <PuC_2>$; $\Delta G_{trans} = 6,524 - 3.38T$, (cal/mole). (11)

Equation (11) yields a transformation temperature of 1930°K (1657°C) in excellent agreement with the value, 1660 ± 10°C, obtained from DTA studies performed in this laboratory.[57]

If the free energy expressions obtained in this study are internally consistent, the values of ΔG given by Eqs. (4), (6), and (8) should be equal at the sesquicarbide to dicarbide transition temperature, 1933°K. This criterion is satisfactorily met as the values of ΔG calculated at 1933°K from these equations are 54.7 ± 0.6,

54.8 ± 0.9 and 54.6 ± 1.1 kcal/mole, respectively.

$PuC_{0.9}$

If the expressions for the decomposition of the monocarbide, Eq. (2), and the formation of the sesquicarbide, Eq. (9), are combined with that for the vaporization of Pu metal at 1662°K,[56] we can obtain the equation for the free energy of formation of the monocarbide. As noted above, we do not have the necessary heat content data to enable us to calculate ΔG_f for the sesquicarbide at 1662°K. However, we do have ΔG_f values at 1842°K from this work and at 1000°K from the emf study.[51] Interpolating, we have at 1662°K

$$1.5\langle PuC_{1.5}\rangle + (Pu) = 2.5\langle PuC_{0.9}\rangle; \quad \Delta G = -86,570 + 23.42\ T, \text{ (cal/mole)}$$

$$\{Pu\} = (Pu); \quad \Delta G = 79,716 - 22.38\ T, \text{ (cal/mole)}$$

$$1.5\{Pu\} + 2.25\langle C\rangle = 1.5\langle PuC_{1.5}\rangle; \quad \Delta G = -21,952 - 2.84\ T, \text{ (cal/mole)}$$

$$\{Pu\} + 0.9\langle C\rangle = \langle PuC_{0.9}\rangle; \quad \Delta G_{f\,1662} = -11,522 - 0.72\ T, \text{ (cal/mole)} \qquad (12)$$

Equation (12), extrapolated to 1000°K, yields ΔG_f = -12.2 kcal/mole as compared to the value, -12.5 kcal/mole, obtained from the emf data.[51]

When Eq. (12) is reduced to 298°K, employing published thermodymanic functions for Pu,[56,58] C,[59] and $PuC_{0.9}$,[60] we obtain for the monocarbide, ΔH^o_{f298} = -10.9 kcal/mole, ΔS^o_{f298} = + 2.9 eu and S^o_{298} = 17.3 eu. These results are in excellent agreement with those obtained from calorimetric studies,[60,61] ΔH^o_{f298} = 11.4 kcal/mole and S^o_{f298} = 17.33 eu.

The free energy of formation values for the plutonium carbides are compared in Fig. 463-21.

(c) Activities

Aside from the free energy expressions, the parameters of most importance in predicting reactions between the fuel material and the clad and/or fission products, are the activities of the individual components of the fuel. The vapor pressure data obtained in this investigation were combined with the emf data[51] to yield Pu activities as a function of composition. The carbon activities were then calculated by means of a Gibbs-Duhem integration.

Activities of Pu and C as a function of composition at 1800°K are listed in Table 463-XVIII. When the temperature is reduced to 1000°K, the values for the composition $PuC_{1.0}$ are α_{Pu} = 0.05 and α_C = 0.06. The values at 1000°K for the composition $PuC_{1.5}$ are α_{Pu} = 0.0002 and α_C = 1.0.

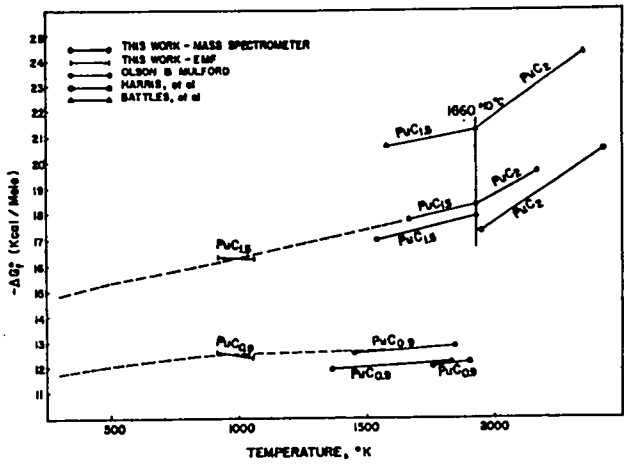

Fig. 463-21. Free energy of formation values for the plutonium carbides.

2. The Uranium-Plutonium-Carbon System

It was noted above in section 1 that the primary purpose for the investigation of the Pu-C binary system was to lay the groundwork for a study of the U-Pu-C ternary system. Of special interest are compositions near the stoichiometry $U_{0.8}Pu_{0.2}C_{1.0}$. One area of concern is that, if two condensed phases are present, one of the phases may be significantly richer in Pu. Although few experimental data are available for the U-Pu-C system, enough data do now exist for the U-C and Pu-C binary systems to allow some calculations and semiquantitative predictions to be made for the U-Pu-C system.

TABLE 463-XVIII

ACTIVITY VALUES FOR Pu AND C AT 1800°K

Condensate	α_{Pu}	α_C
$PuC_{0.70}$	0.95	0.02
$PuC_{0.76}$	0.85	0.03
$PuC_{1.00}$ [PuC + Pu_2C_3]	0.23	0.11
$PuC_{1.45}$	0.11	0.15
$PuC_{1.50}$ [Pu_2C_3 + C]	0.006	1.00

For the following calculations, the free energy expressions for the Pu-C compositions are given by Eqs. (9), (10) and (12). Free energy values for U,[62] the U-C compositions,[62,63] and Pu[56,58] are from published sources.

(a) Monocarbide plus Liquid

Consider a composition $U_xPu_{1-x}C_y$, where 1>y>0, consisting of two phases, $\langle U_{x_1}Pu_{1-x_1}C_{1.0}\rangle$ and $\{U_{x_2}Pu_{1-x_2}\}$.

For $\langle U_{x_1}Pu_{1-x_1}C_{1.0}\rangle$ we have

$$\Delta G_1 = x_1 \Delta G \langle UC\rangle + (1-x_1)\Delta G \langle PuC\rangle + RT[x_1 \ell n x_1 + (1-x_1)\ell n(1-x_1)] + E_1. \quad (13)$$

For $\{U_{x_2}Pu_{1-x_2}\}$ we have

$$\Delta G_2 = x_2 \Delta G\{U\} + (1-x_2)\Delta G\{Pu\} + RT[x_2 \ell n x_2 + (1-x_2)\ell n(1-x_2)] + E_2. \quad (14)$$

For these calculations it was assumed that plutonium monocarbide has a stoichiometry of $PuC_{1.0}$, and that both the monocarbide and the liquid are ideal, so that the regular solution interaction parameters E_1 and E_2 are zero.

If the monocarbide and the liquid are in equilibrium, the free energy of the system will be a minimum and

$$\frac{\partial}{\partial x_1}(\Delta G_1)_T = \frac{\partial}{\partial x_2}(\Delta G_2)_T. \quad (15)$$

Thus we have

$$\Delta G\langle UC\rangle - \Delta G\langle PuC\rangle - \Delta G\{U\} + \Delta G\{Pu\} = RT \ell n (1-x_1/x_1)(x_2/1-x_2). \quad (16)$$

Equation (16) was used to calculate the values listed in Table 463-XIX. Composition tie-line values at two temperatures are shown in Fig. 463-22. These results indicate that the liquid will be significantly richer in Pu. This phenomenon is more pronounced as the temperature is lowered and the Pu content is increased, as would be expected from a comparison of the melting points, 913°K for Pu and 1406°K for U.

For a sample consisting initially of $U_{0.8}Pu_{0.2}C_{1.0}$ heated to 2400°K, we calculate from Eq. (16) that the liquid would consist of 75% Pu and 25% U. This value is in excellent agreement with the results obtained from a microprobe analysis performed on a $(U_{0.79}Pu_{0.21})$-monocarbide sample that had been heated for two hours at 2100°C in the DTA apparatus.[64]

TABLE 463-XIX

SEGREGATION IN U-Pu-C AT THE M-MC BOUNDARY

Initial Ratio U/(U+Pu) in MC	Equilibrium Value of U/(U + Pu) in the Liquid					
	T = 1000°K	1200°K	1400°K	1600°K	1800°K	2000°K
0.99	0.098	0.26	0.44	0.62	0.73	0.81
0.95	0.020	0.062	0.13	0.24	0.34	0.45
0.9	0.010	0.030	0.067	0.13	0.20	0.28
0.8	0.004	0.014	0.031	0.061	0.098	0.15
0.7	0.003	0.008	0.018	0.036	0.060	0.092
0.6	0.002	0.005	0.012	0.024	0.039	0.062
0.5	0.001	0.003	0.008	0.016	0.027	0.042
0.4	0.0007	0.002	0.005	0.011	0.018	0.028
0.3	0.0005	0.001	0.003	0.007	0.012	0.018
0.2	0.0003	0.001	0.002	0.004	0.007	0.011
0.1	0.0001	0.0004	0.001	0.002	0.003	0.005

The activity of C at the liquid-monocarbide boundary is given by the equation

$$0.9\ RT \ell n \alpha_C = \Delta G\langle PuC\rangle - \Delta G\{Pu\} + RT \ell n (1-x_1) - RT \ell n (1-x_2). \quad (17)$$

Values for the carbon activity at the M-MC boundary are listed for various U/Pu ratios in Table 463-XX. The activity values for U and Pu will be proportional to

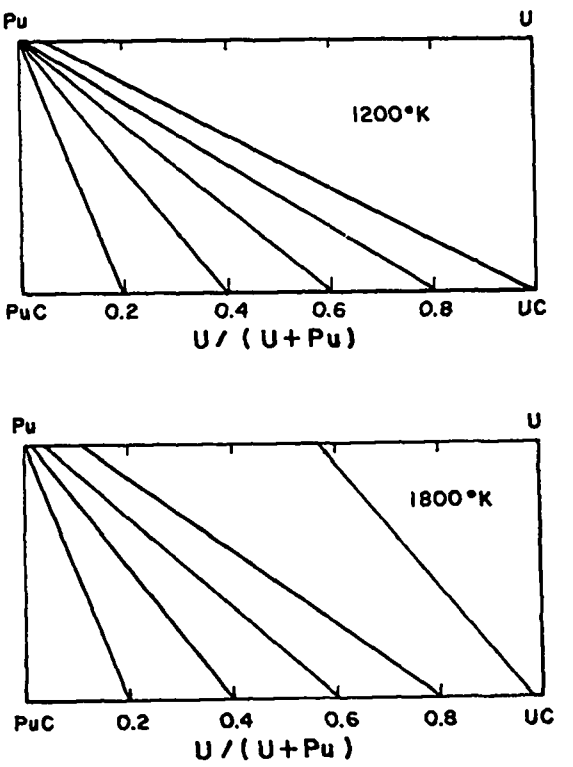

Fig. 463-22. Composition tie-lines at the M-MC boundary.

TABLE 463-XX

EQUILIBRIUM CARBON ACTIVITIES AT THE M-MC BOUNDARY

Initial Ratio U/(U+Pu) in MC	$\log \alpha_C = A + B/T$ A	B	Temp. Range, °K	α_C 1000°K	1500°K
0.8	-0.730	-2997	1000-1500	0.00019	0.0044
	-0.507	-3336	1500-2000		
0.6	-0.423	-2971	1000-1500	0.00040	0.0087
	-0.326	-3120	1500-2000		
0.4	-0.241	-2958	1000-1500	0.00063	0.013
	-0.196	-3024	1500-2000		
0.2	-0.105	-2954	1000-1500	0.00087	0.018
	-0.087	-2984	1500-2000		
$PuC_{0.9}$	-0.00085	-2950	1000-2000	0.0011	0.023

TABLE 463-XXI

SEGREGATION IN U-Pu-C AT THE MC-M_2C_3 BOUNDARY

Initial Ratio U/(U+Pu) in MC	Equilibrium Value of U/(U + Pu) in the Sesquicarbide T = 1000°K	1200°K	1400°K	1600°K	1800°K	2000°K
0.99	0.935	0.947	0.955	0.962	0.967	0.972
0.95	0.735	0.776	0.802	0.831	0.850	0.869
0.9	0.568	0.621	0.657	0.700	0.728	0.759
0.8	0.369	0.421	0.460	0.509	0.543	0.583
0.7	0.254	0.298	0.333	0.377	0.410	0.449
0.6	0.180	0.214	0.242	0.280	0.308	0.344
0.5	0.128	0.154	0.175	0.206	0.229	0.259
0.4	0.089	0.108	0.124	0.147	0.166	0.189
0.3	0.059	0.072	0.084	0.100	0.113	0.130
0.2	0.036	0.044	0.050	0.061	0.069	0.080
0.1	0.016	0.020	0.023	0.028	0.032	0.037

the amounts of these species in the liquid phase. These values are discussed in the following section.

In a separate series of calculations, the solubility of carbon in liquid Pu was taken into account,[65] but the effect on the values listed in Table 463-XIX was negligible.

(b) Monocarbide plus Sesquicarbide

Consider a composition $U_xPu_{1-x}C_y$, where $1.5>y>1.0$, consisting of two phases, $\langle U_{x_1}Pu_{1-x_1}C_{1.0}\rangle$ and $\langle U_{x_2}Pu_{1-x_2}C_{1.5}\rangle$.

For $\langle U_{x_2}Pu_{1-x_2}C_{1.5}\rangle$

$$\Delta G = x_2\Delta G\langle UC_{1.5}\rangle + (1-x_2)\,\Delta G\langle PuC_{1.5}\rangle + RT[x_2 \ln x_2 + (1-x_2)\ln(1-x_2)] + E_3. \quad (18)$$

The free energy expression for the monocarbide, ΔG_1, is again given by Eq. (13). If the monocarbide and the sesquicarbide are ideal, the interaction parameters E_1 and E_3 are zero, and at equilibrium between the monocarbide and sesquicarbide phases we have

$$\Delta G\langle UC\rangle - \Delta G\langle PuC\rangle - \Delta G\langle UC_{1.5}\rangle + \Delta G\langle PuC_{1.5}\rangle = RT \ln(1-x_1/x_1)(x_2/1-x_2). \quad (19)$$

Equation (19) was employed to calculate the values listed in Table 463-XXI. Composition tie-line values are shown in Fig. 463-23. These results indicate that the sesquicarbide will be richer in Pu, although to a lesser extent than is the liquid in equilibrium with the monocarbide.

The activity of C at the MC-M_2C_3 boundary may be calculated from the equation

$$0.6\,RT \ln \alpha_C = \Delta G\langle PuC_{1.5}\rangle - \Delta G\langle PuC_{0.9}\rangle + RT \ln(1-x_2) - RT \ln(1-x_1). \quad (20)$$

Values for the C activity at various U/Pu ratios are listed in Table 463-XXII. These calculated values for α_C are in good agreement with the experimental values obtained for similar compositions for the Pu-C binary system and listed in Table 463-XVIII.

The Pu and U activities may be obtained from the vapor pressure values. At the MC-M_2C_3 boundary, these

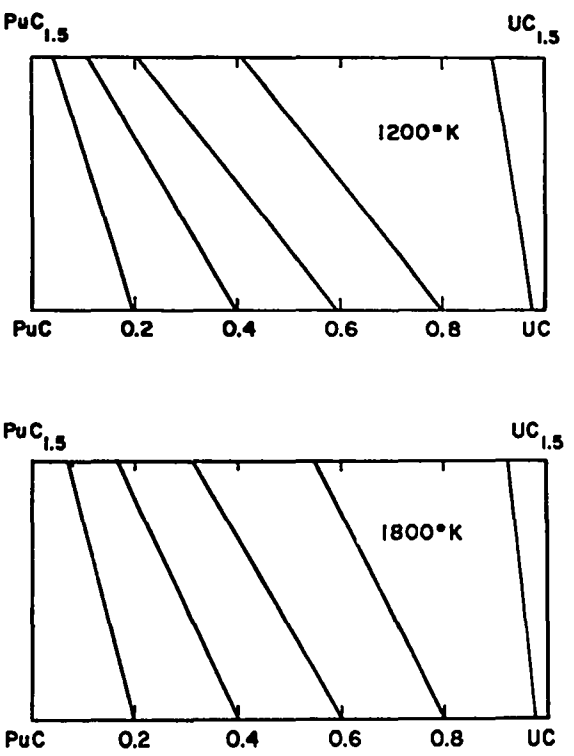

Fig. 463-23. Composition tie-lines at the MC-M_2C_3 boundary.

TABLE 463-XXII

EQUILIBRIUM CARBON ACTIVITIES AT THE MC-M_2C_3 BOUNDARY

Initial Ratio U/(U+Pu) in MC	$\log \alpha_C = A + B/T$			α_C	
	A	B	Temp. Range, °K	1000°K	1800°K
0.8	-0.089	-560	1000-1400	0.22	0.34
	-0.358	-189	1400-1800		
0.6	-0.255	-697	1000-1500	0.11	0.22
	-0.440	-410	1500-2000		
0.4	-0.354	-819	1000-1500	0.067	0.15
	-0.455	-659	1500-2000		
0.2	-0.446	-899	1000-1500	0.045	0.11
	-0.491	-827	1500-2000		
$PuC_{0.9}$	-0.531	-951	1000-2000	0.033	0.087

vapor pressure values are given by

$$RT \ln P_{Pu} = 2.5 \Delta G\langle PuC_{0.9}\rangle - \Delta G(Pu) - 1.5\Delta G\langle PuC_{1.5}\rangle + 2.5\, RT \ln(1-x_2) - 1.5\, RT \ln(1-x_1). \quad (21)$$

and

$$RT \ln P_U = 3\Delta G\langle UC\rangle - \Delta G(U) - 2\Delta G\langle UC_{1.5}\rangle + 3\, RT \ln x_1 - 2\, RT \ln x_2. \quad (22)$$

It was noted above that the Pu and U vapor pressures at the M-MC boundary are proportional to the equilibrium amounts of Pu and U in the liquid phase.

Vapor pressure values for Pu and U at the M-MC and MC-M_2C_3 boundaries at 1800°K, are shown for various U/Pu ratios in Fig. 463-24.

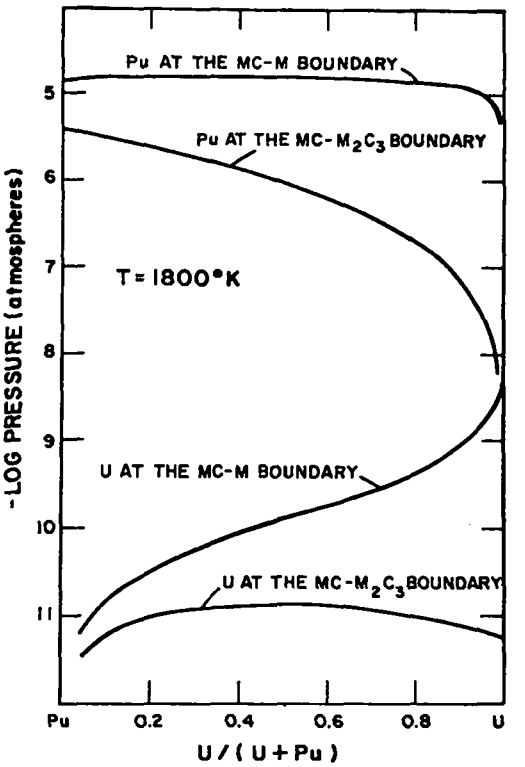

Fig. 463-24. Vapor pressure values for Pu and U at 1800°K at various compositions.

(c) Regular Solutions and Other Phase Boundaries

If one heats a sample of carbon-rich monocarbide (80% U-20% Pu), to 1800°K, the values given in Table 463-XXI predict that the composition of the sesquicarbide in equilibrium with the monocarbide will be $U_{0.54}Pu_{0.46}C_{1.5}$. These calculations are based on both the monocarbide and sesquicarbide being ideal solutions. Should the sesquicarbide be regular, the interaction parameter E_3, Eq. (18), must be taken into account. At present, the data available for the U-Pu-C system are insufficient to allow one to calculate E_3 accurately. Kaufman and Bernstien[66] have developed empirical techniques for the calculation of interaction parameters. These techniques, combined with the limited data for the U-Pu-C system, yield an approximate value for E_3 of -1.5 kcal/mole. When this is taken into account, the composition of the sesquicarbide in equilibrium with the monocarbide at 1800°K becomes $U_{0.7}Pu_{0.3}C_{1.5}$. At the present time, there are simply not enough data to allow one to accurately calculate the extent of deviation from ideality, if any.

One can, using the techniques outlined above, calculate equilibrium U-Pu segregation values at the MC-MC_2 and M_2C_3 boundaries. Qualitatively, the results indicate that at the MC-MC_2 boundary, the dicarbide will be richer in Pu, and that at the M_2C_3 boundary, the dicarbide will be slightly richer in U. It is likely, however, that there will be deviations from ideality at these boundaries. It is known, for example, that a MC-MC_2 miscibility gap exists in the U-C binary system. Again, there are not now sufficient data to allow one to accurately estimate the interaction parameters.

3. Irradiated Fuel Materials

During the near future, the intended usage of the existing quadrupole unit will be primarily in the area of

the study of post-irradiated materials. These investigations will allow the determination of the identities and relative amounts of fission products present, and, more important, the obtainment of information on the chemical form of specific fission products as they actually occur in typical specimens of irradiated fuels. The study of vapor pressure and vapor species identities will make it possible to define more positively the temperature regions of importance and mechanisms by means of which vapor phase transport of fission products occurs. In addition to information on fission products per se, the effect of the fission products and chemical restructuring during irradiation on the thermodynamic activity and vapor phase mobility of the basic fuel components can also be assessed. These studies will be integral in the sense that the actual system of interest is treated. This avoids the uncertainties involved in the mathematical synthesis of overall property effects from data on abbreviated simulations of irradiated materials.

Initially, the irradiated fuel materials will be studied using the quadrupole mass spectrometer. Because of the gamma ray emission from even small amounts of these materials, a number of modifications of the quadrupole apparatus must be made before irradiated samples can be studied. The major change is the installation of a radiation shield consisting of a one-inch thick cylinder of ^{238}U metal, mounted within the oven assembly.

The existing quadrupole unit has been in operation for approximately five years, and there has been a substantial deterioration in performance during this time. In order to upgrade the performance, several new components have been purchased and installed. Among these are a new ion source, new quadrupole rods and a 14-stage electron multiplier that has ten times the gain of the original 10-stage unit.

A number of modifications of the RM6-K mass spectrometer have been or are being made before the unit is installed in the glovebox-hood enclosure. Among these are changes in the pumping system required to accommodate the glovebox, modification of the vacuum measurement and interlock protection circuitry, replacement of the 10-stage electron multiplier with a 16-stage unit and replacement of the ion source with a Fox-type RPD unit. When this unit is in operation, it will be used primarily to study the vaporization behavior of fuel components and fission products when high resolution in the higher mass ranges is required.

As a preliminary step in the study of irradiated materials, a series of experiments is being performed in order to determine the reliability of published ionization cross section values. In practice, the study of the vaporization behavior of the fission products in irradiated fuel samples will involve complex systems containing many components. In order to allow the determination of absolute vapor pressures for these species, standard reference materials will be used and corrections will be made for the relative ionization cross sections.

The accuracy of vapor pressures calculated in this way depends on the reliability of the relative ionization cross section values. Ionization cross sections are usually calculated by means of quantum mechanics. Mann[67,68] has calculated values for the various elements at ionizing voltages ranging from 0 to 200 eV. National Bureau of Standards vapor pressure reference samples of Au and Ag have been obtained and a series of measurements has been made to check the validity of Mann's calculated cross sections. The results indicate that for Au and Ag the experimental and calculated data agree within experimental error.

F. B_4C Structural Study

(K. L. Walters and J. L. Green)

Neutron and x-ray diffraction studies on carbon saturated boron carbide have been completed. This work was carried out on high purity samples of carbon saturated boron carbide to allow a more complete definition of the crystallographic structure of that compound.

Final neutron diffraction data have been obtained and analyzed. Analytical data for the "B_4C" used in the preparation of the targets have been reported previously.[69] Peak intensity data for the neutron diffraction pattern have been least squares fitted to yield final values for both atomic position parameters and coherent scattering amplitudes for each crystallographic position in the structure. The results of these calculations are shown in Table 463-XXIII. Table 463-XXIV shows a comparison of

TABLE 463-XXIII

STRUCTURAL PARAMETERS FOR BORON CARBIDE*

Position Parameters (Hexagonal)

	x	z
BI	0.839 ± 0.001	0.359 ± 0.001
BII	0.893 ± 0.002	0.114 ± 0.001
C_1	------	0.382 ± 0.001

Coherent Scattering Amplitudes (x 10^{12} cm)

	Icosahedral Position	Terminal Chain Position	Central Chain Position
Preliminary Study	0.522	0.665	0.535
Current Results	0.533±0.015	0.668±0.016	0.533±0.011
	Natural C 0.661		
	Natural B 0.54		

* All error limits are calculated 1σ limits uncorrected for covariance.

TABLE 463-XXIV

RHOMBOHEDRAL POSITION PARAMETERS

	Clark and Hoard[70]		Present Study	
	x	z	x	z
BI	0.193	0.693	0.198	0.684
BII	0.007	0.325	0.007	0.327
CI	0.385	---	0.382	---

the results of this study with those from the original structure determination[70] in the rhombohedral coordinate system.

The position parameter results from the present study are not significantly different than those from the original determination. The identity of the atoms in each position, as has been reported before,[69] are not the same. Clark and Hoard identified all atoms in the icosahedral groups as B and all the atoms in the central chain as C. These assignments were presumptive in the sense that they were tailored to match the known stoichiometry of the compound. The authors stipulated that the differentiation between C and B was not possible from their data. The scattering amplitude results from the present study clearly indicate that the central 3-atom chain consists of two C atoms located on either side of a B atom, i.e., (CBC).

The chemical composition of the material used in the current study appears to require an overall stoichiometry of B_4C. The powder used in the neutron diffraction study contained excess carbon and a free carbon analysis is not yet available, so a carbide phase composition cannot be directly determined. However, high purity single crystals of "B_4C" containing no observable excess graphite are available which have been shown to have the stoichiometry B_4C. The lattice parameter for that material is essentially the same as for the powder used in the neutron diffraction target, implying that the carbide phase compositions are the same, i.e., B_4C.

Extensive x-ray powder diffraction data have been gathered for the high purity "B_4C" single crystals and for the material used for the preparation of the neutron diffraction target. Least squares fitted lattice parameters derived from these data are shown in Table 463-XXV. The x-ray powder pattern line list for the material derived from the single crystals is shown in Table 463-XXVI. It should be noted that this pattern contained no detectable x-ray impurities and no unindexable lines. Extraneous diffraction lines can no longer be ascribed to errors in the structure description. Unindexable lines and intensity anomalies must be accounted for in terms of phases other than pure, carbon-rich B_4C. Table 463-XXVII shows the chemical analysis for the powder derived from the single crystals. Optical and scanning electron microscopy showed that no detectable impurity inclusions were present.

Chemical analyses, x-ray, and metallographic data showed that the B/C ratio for the material used in

TABLE 463-XXV

LATTICE PARAMETERS, CARBON SATURATED B_4C

	Hexagonal[a]		Rhombohedral	
	a_o	a_o	a_o	c_o
Commercial Powder	5.6016±0.0010Å	12.072±0.003Å	5.1625Å	65.65 deg.
Single Crystal	5.6020±0.0003Å	12.075±0.001Å	5.1635Å	65.70 deg.

[a] Uncertainties are calculated 3σ error bars.

TABLE 463-XXVI

POWDER DIFFRACTION PATTERN OF CARBON SATURATED B_4C

HKL (Rhomb.)	Intensity Obs.	Intensity Calc.	d (Å)[c] Obs.[e]	d (Å)[c] Calc.
100	5	8	4.5063	4.5017
111	6	25	4.0293	4.0251
110	7	58	3.7681	3.7818
$10\bar{1}$	4	11	2.7976	2.8010
$21\bar{1}$	9	67	2.5629	2.5631
$11\bar{1}$	10	100	2.3805	2.3782
210	3	5	2.2998	2.2991
$22\bar{2}$	1	0.4	2.0132	2.0125
$20\bar{1}$	3	3	1.8112	1.8129
311	5	12	1.7100	1.7115
322	2	3	1.6245	1.6253
310	1	2	1.5655	1.5672
$22\bar{1}$, 300	5	12	1.5000	1.5006
320	6	19	1.4604	1.4604
332	6	17	1.4407	1.4413
$20\bar{2}$	6	16	1.3998	1.4005
$21\bar{2}$	4	12	1.3370	1.3373
$31\bar{1}$	4	12	1.3227	1.3227
$30\bar{1}$	4	11	1.3126	1.3133
422	3	4	1.2808	1.2816
421	4	10	1.2578	1.2564
432	3	2	1.2090	1.2100
$22\bar{2}$	3	6	1.1891	1.1891
410	2	2	1.1748	1.1754
431	3	5	1.1656	1.1654
420	3	3	1.1495	1.1496
400	1	0.8	1.1258	1.1254
$31\bar{2}$	1	0.5	1.0960	1.0946
442	1	2	1.0819	1.0810
$41\bar{1}$	3	4	1.0443	1.0443
441, 522	3	7	1.0323	1.0326
444	1	1.4	1.0060	1.0063
$531\alpha_1$	1	1.4	0.9696	0.9688
$30\bar{3}\alpha_1$	3	4.4	0.9335	0.9337
$544\alpha_1$	1	1.6	0.9126	0.9123
$412\alpha_1$	2	3.4	0.9097	0.9095
$412\alpha_2$	1	1.7	0.9069	0.9095
$40\bar{2}\alpha_1$		1.7		0.9065
$40\bar{2}\alpha_2$	1	0.8	0.9068	0.9065
$500\alpha_1$	2	2.9	0.8996	0.9003
$541\alpha_1$		2.2		0.8987
$530\alpha_1$	5	11.3	0.8959	0.8958
$530\alpha_2$	4	5.8	0.8959	0.8958
$42\bar{2}\alpha_1$	2	2.5	0.8773	0.8773
$42\bar{2}\alpha_2$	1	1.2	0.8773	0.8773
$41\bar{2}\alpha_1$	2	3.1	0.8692	0.8691
$553\alpha_1$	3	5.4	0.8675	0.8674
$553\alpha_2$	1	2.8	0.8676	0.8674
$32\bar{3}\alpha_1$	3	6.2	0.8627	0.8624
$32\bar{3}\alpha_2$	2	3.2	0.8625	0.8624
$51\bar{1}\alpha_1$	5	12.1	0.8572	0.8572
$622\alpha_1$	5	6.7	0.8550	0.8557
$51\bar{1}\alpha_2$		6.2		0.8572
522, $633\alpha_1$		5.1		0.8544
$632\alpha_1$	3	4.6	0.8505	0.8506
$632\alpha_2$	(d)	2.4	(d)	0.8506
$52\bar{1}\alpha_1$		2.0		0.8470
$44\bar{1}\alpha_1$		1.8		0.8457
$52\bar{1}\alpha_2$		1.0		0.8470
$44\bar{1}\alpha_2$		0.9		0.8457
621, $504\alpha_1$	3	5.6	0.8311	0.8311
621, $540\alpha_2$	2	2.8	0.8311	0.8311
$43\bar{2}\alpha_1$	(d)	1.4	(d)	0.8196
$631\alpha_1$		1.1		0.8184
$43\bar{2}\alpha_2$		0.8		0.8196
$642\alpha_1$		1.9		0.8172
$631\alpha_2$		0.6		0.8184
$611\alpha_1$		1.9		0.8162
$551\alpha_1$	4	8.8	0.8139	0.8139
$551\alpha_2$	2	4.6	0.8138	0.8139
$22\bar{4}$, $42\bar{2}\alpha_1$	3	5.1	0.8085	0.8086
$22\bar{4}$, $42\bar{2}\alpha_2$	2	2.6	0.8086	0.8086
$555\alpha_1$	1	2.8	0.8049	0.8050
$555\alpha_2$	1	1.4	0.8051	0.8050
$40\bar{3}\alpha_1$	2	2.7	0.7959	0.7958
$51\bar{1}$, $33\bar{3}\alpha_1$	9	24.3	0.7928	0.7927
$51\bar{1}$, $33\bar{3}\alpha_2$	8	12.8	0.7908	0.7927
$41\bar{3}\alpha_1$		5.9		0.7907
$41\bar{3}\alpha_2$	2	3.1	0.7907	0.7907
$653\alpha_1$	3	4.9	0.7806	0.7805
$653\alpha_2$	2	2.8	0.7805	0.7805
$41\bar{3}$, $31\bar{4}\alpha_1$	2	2.2	0.7769	0.7769
$41\bar{3}$, $31\bar{4}\alpha_2$	1	1.3	0.7769	0.7769

(a) Relative intensities based on visual estimates as assigned on a 10-step scale.
(b) Calculated intensities based on Table 463-XXIV
(c) Calculated interplanar spacings for $a_0 = 5.6020$ Å and $\alpha = 65.70$ deg.
For $2\theta < 90^\circ$, $\lambda(\bar{\alpha}) = 1.54178$ Å.
For $2\theta > 90^\circ$, $\lambda(\alpha_1) = 1.54051$ Å and $\lambda(\alpha_2) = 1.54433$ Å.
(d) Broad unresolved band; not measurable.
(e) Interplanar spacings for conglomerate lines calculated using $\lambda(\alpha_1)$.

TABLE 463-XXVII

ANALYTICAL DATA
B_4C SINGLE CRYSTAL

Element	Conc.[a]	Element	Conc.
B	79.0%		
C	20.53%		
Li	< 30		
Be	< 3	Fe	< 30
Na	<100	Co	<100
Mg	< 3	Ni	< 30
Al	< 30	Cu	< 10
Si	< 10	Zn	<100
K	<300	Sr	<100
Ca	<100	Zr	<100
Ti	<100	Ag	< 10
Cr	< 10	Cd	< 10
Mn	< 30	Ba	< 30
Sn	< 30	Bi	< 10
Pb	< 30		

[a]Chemical analysis reported as ppm by weight unless otherwise indicated.

the present study was essentially 4 to 1. This requires that the average content of the unit cell be $B_{12}C_3$. The neutron diffraction scattering amplitude data clearly showed that the central chain in the rhombohedral unit cell is a (CBC) group. Both density and composition require that an additional 11 B atoms and 1 C atom be contained in the unit cell. No diffraction effects were noted in the current study that indicate that any crystallographic positions are occupied other than those in the central chain and the icosahedral group. Preliminary results from the single crystal x-ray study that is in progress at LASL also indicate this to be the case.[71] The implication of this is that the icosahedral groups are, on the average, occupied by 11 B atoms and 1 C atom, rather than 12 B atoms as originally proposed. Thus, the formulation $(B_{11}C)CBC$ is consistent with all the experimental observations.

The NMR study reported by Silver and Bray[72] is consistent with our findings regarding the (CBC) central chain. A very recent publication of the results of another NMR study by Hynes and Alexander[73] is also consistent on this point and in addition lends experimental support to the postulate that one of the icosahedral positions is occupied by a carbon atom.

Theoretical investigation of the boron carbide structure has been previously done. Longuet-Higgins and Roberts[74] have investigated the electronic structure of the icosahedral boron groups. Their results, as interpreted by Scott,[75] indicate that of the 48 valence electrons present for bonding, 38 are associated with the icosahedral positions and 10 with the central chain. Scott further suggests that this preferred arrangement is achieved in boron carbide by randomly interchanging a boron atom in the icosahedral group with the carbon from the 1-b position. The formulation associated with this electronic structure would be $(CBC)^+(B_{11}C)^-$.

IV. PUBLICATIONS

1. J.O. Barner and J.L. Green, "Summary of Recent Work on Ceramic Plutonium Fuel Materials," 31st Meeting of High Temp. Fuels Committee, Dec. 1970.

2. J.O. Barner, "Behavior of Sodium-Bonded (U, Pu)C Fuel Elements after Moderate Burnup," LA-4669-MS, April 1971.

3. J.O. Barner, "Irradiation Testing of Potential LMFBR Fuel Element Systems by the Los Alamos Scientific Laboratory," Presentation for Program Review, Washington D.C., March 2, 1971.

4. J.O. Barner, "Behavior of Sodium-Bonded (U, Pu)C Fuel Elements after Moderate Burnups," Proc. of Conf. on Fast Reactor Fuel Element Tech., New Orleans, La., April 13-15, 1971.

5. J.O. Barner and J.L. Green, "Summary of Recent Work on Ceramic Plutonium Fuel Materials," 32nd Meeting of High Temp. Fuels Committee, May 1971.

6. J.C. Clifford, J.O. Barner, F.B. Litton, and M.W. Shupe, "Fabrication and Testing of Sodium-Bonded Mixed Carbide Fuel for Advanced LMFBR Application," Presentation at 17th Annual Meeting of Amer. Nucl. Soc., Boston, Mass, June 14, 1971.

7. J.F. Kerrisk, "The Thermal Diffusivity of Heterogeneous Materials," presented at 10th Thermal Conductivity Conf., Newton, Mass, Sept 28-30, 1970.

8. K.W.R. Johnson and J.F. Kerrisk, "Thermal Diffusivity and Laser Beam Uniformity," presented at 10th Thermal Conductivity Conf., Newton, Mass., Sept. 29-30, 1970.

9. L.R. Cowder, R.W. Zocher, J.F. Kerrisk, and L.L. Lyon, "Thermal Expansion of Extruded Graphite - ZrC Composites," J. Appl. Phys. 41, 5118 (1970).

10. J.F. Kerrisk, "The Thermal Diffusivity of Heterogeneous Materials," J. Appl. Phys. 42, 267 (1971).

11. J.F. Kerrisk, "The Thermal Diffusivity of Heterogeneous Materials, II. The Limit of the Steady State Approximation," submitted for publication.

12. K.W.R. Johnson, "Vacuum and the Actinide Elements," presented at the 1971 Symposium of the New Mexico Section of the Amer. Vacuum Soc., Albuquerque, N.M., March 23-26, 1971.

13. K.W.R. Johnson, "Materials for High Vacuum Technology," invited series of lectures at Sandia Laboratories, Livermore, Calif., May 18-20, 1971.

14. M. Tokar and J.A. Leary, "Compressive Creep and Hot Hardness of Uranium-Plutonium Carbide, (U, Pu)C," presented at the 73rd Annual Meeting and Exposition of the Amer. Ceramic Soc., Chicago, Ill, April 27, 1971.

15. M. Tokar, "High Temperature Compressive Creep and Hot Hardness of Uranium-Plutonium Carbides," LA-4704 (in preparation).

16. R.A. Kent, "Mass Spectrometric Studies of Plutonium Compounds at High Temperatures, V. The Plutonium-Carbon System," Recent Developments in Mass Spectroscopy, K. Ogata and T. Hayakawa, eds., (1970) pp. 1124-1131.

17. G.M. Campbell, R.A. Kent, and J.A. Leary, "Thermodynamic Properties of the Plutonium-Carbon System," Plutonium 1970 and Other Actinides, W.N. Miner, ed. (1970) pp. 781-790.

V. REFERENCES

1. M.W. Shupe, A.E. Ogard and J.A. Leary, "Synthesis and Fabrication of Pure, Single-Phase, Uranium-Plutonium Monocarbide Pellets," LA-4283, Los Alamos Sci. Lab. (1969).

2. "Quarterly Status Report on the Advanced Plutonium Fuels Program, April 1 to June 30, 1970 and Third Annual Report, FY 1970," LA-4494-MS, Los Alamos Sci. Lab. (1970) p. 24.

3. "Quarterly Status Report on the Advanced Plutonium Fuels Program, April 1 to June 30, 1969 and Third Annual Report, FY 1969," LA-4284-MS, Los Alamos Sci. Lab. (1969) p. 85.

4. "ANCON User's Manual," LA-4616, Los Alamos Sci. Lab., (1971).

5. D.R. Lewis et al., "Crysler Improved Numerical Differencing Analyser for 3rd Generation Computers," Crysler Corp. Space Division report TN-AP-67-287 (1967).

6. C.E. Dickerman et al., "Kinetics of TREAT Used as a Test Reactor," ANL-6458, Argonne Nat. Lab., (1962).

7. B.A. Boley and J.H. Weiner, Theory of Thermal Stresses, John Wiley and Sons (N.Y.) 1960, p. 288.

8. P.D. Schwiebert, Int. J. Mech. Sci. 7, 115 (1965).

9. G.E. Culley and D.O.Sheppard, "Hazards Analysis for the Battelle-Northwest EBR-II/TREAT Transient Irradiation Test Series," BNWL-1368 (1970).

T. Hikido and J.H. Field, "Molten Fuel Movement in Transient Overpower Tests of Irradiated Oxide Fuels," GEAP-13543, Gen. Electric Co. (1969).

10. A.E. Ogard and J.A. Leary, "Thermodynamics of Nuclear Materials, 1967," IAEA, Vienna, 1968, p. 651.

11. C.E. Frantz and J.W. Schulte, "Apparatus for Determining Heat Content on Irradiated Fuels," submitted for publication in the Proc. 19th Conf. on Remote Systems Tech., ANL Meeting, Oct. 1971.

12. "Development and Testing of PuO_2-UO_2 Fast Reactor Fuels," 16th Quarterly Rept. NUMEC-3524-67, Jan.-March 1969.

13. Reactor Development Program Progress Report, ANL-7553, Feb. 1969, p. 33.

14. K.A. Varteressian and L. Burris, "Fission-Product Spectra from Fast and Thermal Fission of ^{235}U and ^{239}Pu," ANL-7678, March 1970.

15. R.P. Burns, G. DeMaria, J. Drowart, and R.T. Grimley, "Mass Spectrometric Investigation of the Sublimation of Molybdenum Dioxide," J. Chem. Phys. 32, 1363 (1960).

16. D.R. O'Boyle, F.L. Brown and A.E. Dwight, "Analysis of Fission Product Ingots Formed in Uranium-Plutonium Oxide Irradiated in EBR-II," J. Nucl. Mater. 35, 257-266 (1970).

17. D.R. O'Boyle, F.L. Brown and J.E. Sanecki, "Solid Fission Product Behavior in Uranium-Plutonium Oxide Fuel Irradiated in a Fast Neutron Flux," J. Nucl. Mater. 29, 27-42 (1969).

18. A.G. Fox and T. Li, Bell System Tech. Journal 40, 453 (1961).

19. W.J. Parker et al., J. Appl. Phys. 32, 1679 (1961).

20. J.A. Cape and G.W. Lehman, J. Appl. Phys. 34, 1909 (1963).

21. R.D. Cowan, J. Appl. Phys. 34, 926 (1963).

22. J.B. Conway and A.C. Losekamp, Trans. Met. Soc. AIME 236, 702 (1966).

23. Y.S. Touloukian (ed.), "Thermophysical Properties of Matter, The TPRC Data Series, Vol. 5, Specific Heat--Metallic Elements and Alloys," Plenum Publishing Co. (1970).

24. R.E. Taylor, private communication.

25. V.E. Peletskii and Ya. G. Sobol, Proc. of 8th Conf. on Thermal Conductivity, C.Y. Ho and R.E. Taylor, eds., Plenum Press, New York, pp. 381-388.

26. M. Tokar, A.W. Nutt, and J.A. Leary, "Mechanical Properties of Carbide and Nitride Reactor Fuels," LA-4452 (Oct. 1970).

27. C.H. deNovion, B. Amice, A. Groff, Y. Guerin and A. Padel, "Mechanical Properties of Uranium and Plutonium-Based Ceramics," Plutonium 1970 and Other Actinides, Part 1, W.N. Miner, ed., Proc. 4th Int. Conf. on Plutonium and Other Actinides, Santa Fe, N.M. (Oct. 5-9, 1970) pp. 509-517.

28. N.M. Killey, E. King, and H.J. Hedger, "Creep of U and (U, Pu) Monocarbides in Compression," AERE-R 6486, presented at 4th Int. Conf. on Plutonium and Other Actinides, Santa Fe, N.M., (Oct. 7, 1970).

29. J.J. Norreys, "The Compressive Creep of Uranium Monocarbide," in Carbides in Nuclear Energy, Vol. 1, Harwell, England (1963).

30. M.H. Fassler, F.J. Huegel, and M.A. DeCrescente, "Compressive Creep of UC and UN," PWAC-482 (1965).

31. D.E. Stellrecht, M.S. Farkas, and D.P. Moak, "Compressive Creep of Uranium Carbide," J. Am. Ceram. Soc. 51(8), 455-458 (1968).

32. J.R. Weertman, "Theory of Steady-State Creep Based on Dislocation Climb," J. Appl. Phys. 26, 1213 (1955).

33. R.N. Nabarro, "Deformation of Crystals by Motion of Single Ions," Rept. Conf. Strength of Solids, University of Bristol, 75 (1948).

34. C. Herring, "Diffusional Viscosity of a Polycrystalline Solid," J. Appl. Phys. 21(5), 437-445 (1950).

35. T.G. Langdon, "Grain Boundary Sliding as a Deformation Mechanism During Creep," Phil. Mag. 22, 689-700 (1970).

36. W.A. Rachinger, "Relative Grain Translations in the Plastic Flow of Aluminum," J. Inst. of Metals 81, 33-41 (1952-53).

37. J.H. Hensler and R.C. Gifkins, "The Estimation of Slip Strain During Creep," J. Inst. Metals 92, 340 (1963-64).

38. V.S. Ivanova, Dokl. Akad. Nauk, U.S.S.R. 94, (2), 217 (1954).

39. Ya. R. Rauzin and A.R. Zhelezniakora, Fiz. Met. Metallov. 3, 146 (1956).

40. J.H. Westbrook, "Temperature Dependence of the Hardness of Pure Metals," Trans. Amer. Soc. Metals 45, 221-248 (1955).

41. E.R. Petty, "Hot Hardness and Other Properties of Some Binary Intermetallic Compounds of Aluminum," J. Inst. Metals 89, 343-349 (1960).

42. K. Ito, "The Hardness of Metals as Affected by Temperature," Toboken Sci. Repts. 12, 137 (1923).

43. V.P. Shishshokin, "The Hardness and Fluidity of Metals at Different Temperatures," Zeitschrift für Physikalishe Chemie 189, 263 (1930).

44. J.D. Harrison and R.P. Pape, "Factors Affecting the Hardness of Uranium Mononitride," Plutonium 1970 and Other Actinides, Part 1, 518-525 (1970).

45. M.A. DeCrescente and A.D. Miller, "High Temperature Properties of Uranium Carbide," in Carbides in Nuclear Energy, L.E. Russel, ed., Macmillan and Co., Ltd., London, 342-357 (1964).

46. N.R. Borch, L.A. Shepard, and J.E. Dorn, Trans. A.S.M. 52, 494 (1960).

47. Von Hans-Jürgen Hirsch, "Beitrage zur Selbstdiffusion und Aktinidendiffusion in Uranmonokarbid," PhD. Dissertation, Carolo-Wilhelmina Technical University of Braunschweig, 96 pp., (1970).

48. G.G. Bentle and G. Ervin, "Self-Diffusion of Uranium and Carbon in Uranium Monocarbide," A1-AEC-12726, (Aug. 1968).

49. R. Lindner, G. Riemer, and H.L. Scherff, "Self-Diffusion of Uranium in UC," J. Nucl. Mat. 23, 222-230 (1967).

50. R.A. Kent, "Mass Spectrometric Studies of Plutonium Compounds at High Temperatures. V. The Plutonium-Carbon System," Recent Developments in Mass Spectroscopy, K. Ogata and T. Hayakawa, eds., (1970) pp. 1124-1131.

51. G.M. Campbell, R.A. Kent and J.A. Leary, "Thermodynamic Properties of the Plutonium-Carbon System," Plutonium 1970 and Other Actinides, W.N. Miner, ed., (1970) pp. 781-790.

52. W.M. Olson and R.N.R. Mulford, Thermodynamics of Nuclear Materials 1967, IAEA, Vienna (1968) p. 467.

53. P.S. Harris, B.A. Phillips, M.H. Rand and M. Tetenbaum, UKAEA Report AERE-R-5353 (1967).

54. J.E. Battles, W.A. Shinn, P.E. Blackburn and R.K. Edwards, High Temp. Sci. 2, 80 (1970).

55. J.P. Marcon, J. Inorg. Nucl. Chem. 32, 2581 (1970).

56. R.A. Kent, High Temp. Sci. 1, 169 (1969).

57. J.G. Reavis and J.A. Leary, "Thermal Analysis Observations of the (U, Pu)C_2 System," Plutonium 1970 and Other Actinides, W.N. Miner, ed., (1970).

58. M.H. Rand, Atomic Energy Review, Vol. 4, Special Issue 1, (1966).

59. JANAF Thermochemical Tables, The Dow Chem. Co., Midland, Mich., 1965 and Supplement.

60. M.H. Rand, "A Thermochemical Assessment of the Plutonium-Carbon System," presented at a panel meeting, IAEA, Vienna (Sept. 1968).

61. G.K. Johnson, E.H. VanDeventer, O.L. Kruger and W.N. Hubbard, J. Chem. Thermodynamics 2, 617 (1970).

62. E.K. Storms, The Refractory Carbides, Academic Press, New York (1967).

63. C.E. Holley, Jr., and E.K. Storms, "Actinide Carbides: A Review of Thermodymanic Properties," Thermodynamics of Nuclear Materials 1967, IAEA, Vienna (1968) p. 397.

64. J.G. Reavis, private communication, unpublished work (1971).

65. D.F. Bowersox, Los Alamos Sci. Lab. Rept. LA-4559 (1971).

66. L. Kaufman and H. Bernstein, Computer Calculation of Phase Diagrams, Academic Press, New York (1970).

67. J.B. Mann, J. Chem. Phys. 46, 1646 (1967).

68. J.B. Mann, private communication (1970).

69. "Quarterly Status Report on the Advanced Plutonium Fuels Program, April 1 to June 30, 1970 and Fourth Annual Report, FY 1969," LA-4494-MS, Los Alamos Sci. Lab. (1970).

70. H.K. Clark and J.L. Hoard, J. Am. Chem. Soc. 65, 2115-2119 (1943).

71. A.C. Larson, Los Alamos Sci. Lab., private communication.

72. A.H. Silver and P.J. Bray, J. Chem. Phys. 31, 247 (1959).

73. T.V. Hynes and M.N. Alexander, J. Chem. Phys. 54, 5296 (1971).

74. H.C. Longuett-Higgins and M. deV. Roberts, Proc. Royal Soc. of London, Series A 250, 110-119 (1955).

75. J.L. Hoard and R.E. Hughs, "The Chemistry of Elemental Boron and Compounds of High Boron Content," The Chemistry of Boron and Its Compounds, Earl Muetterties, ed., J. Wiley and Sons, Inc., New York (1967).

PROJECT 472

ANALYTICAL STANDARDS FOR FAST BREEDER REACTOR OXIDE FUEL

Person in Charge: R. D. Baker
Principal Investigator: C. F. Metz

I. INTRODUCTION

Necessary to the development of the high quality fuel and cladding required by the LMFBR/FFTF program are reliable analytical methods for the chemical characterization of the raw materials and the manufactured fuel and for the examination of irradiated fuel.

The more immediate objectives of this project are (1) the evaluation of existing analytical methods used by potential producers of FFTF fuel, (2) the upgrading of those methods found to be inadequate and the development of new methods as required by additional specifications, (3) the preparation of standardized calibration materials required by various analytical methods used for specification analyses and the distribution of these materials to producers of FFTF fuel, (4) the publication of continuously updated analytical methods for FFTF fuel, (5) the development of a statistically designed quality assurance program for the chemical characterization of FFTF fuel as required by commensurate specifications, and (6) provide aid, as requested, for the prequalification programs of potential FFTF fuel producers.

These more immediate objectives will be continued, as required by the development of new fuel compositions for FBR demonstration plants and the new or additional chemical specifications that will be necessary for their characterization.

Additional objectives of this program involve studies of irradiated fuel including (1) the development of fuel burnup measurement methods based on conventional and spark source mass spectrometric determinations of actinide and fission product isotopes, (2) the development of faster fuel burnup measurement methods based on chemical analysis techniques for use for larger routine sample loads, (3) the applications of burnup methods correlated with other measurement techniques including gamma-ray spectrometry, microprobe, and metallographic examination to assess the irradiation behavior of FBR fuels, (4) the development of analytical methods for gases including hot cell techniques for the evaluation of their effects on cladding stability, (5) the development of mass spectrometer methods, including hot cell techniques, for studies of the gas retention properties of fuels as a function of temperature-time cycling, and (6) the application of ion emission microanalysis to elucidate migration mechanisms in irradiated fuels.

At the request of RDT, a program was initiated in March, 1971 to evaluate the status of analytical methods for the chemical characterization of boron carbide, the proposed neutron absorber material for the LMFBR/FFTF control rods.

II. ANALYTICAL CHEMISTRY PROGRAM FOR LMFBR/FFTF FUEL

(J. E. Rein, G. R. Waterbury, G. M. Matlack, R. K. Zeigler, R. T. Phelps, C. F. Metz)

Major features of this program include:

(1) Aid in the qualification of fuel producer analytical laboratories prior to periods of fuel production

(2) Preparation of calibration materials to be used by all participating laboratories for calibration of the chemical methods of analysis

(3) Preparation of quality control samples to be used for the continuous evaluation of the reliability of

the analytical results obtained by laboratories during periods of fuel production

(4) Publication of a compilation of analytical methods covering all specification analyses

(5) Development of a quality control assurance program for the chemical characterization of the fuel, and

(6) Development of analytical methods, as required, for the specification analysis of fuel and source materials

A. Qualification of Analytical Laboratories

RDT Standard F2-6 entitled "Qualification of Analytical Chemistry Laboratories for FFTF Fuel Analysis" was issued July 1970. This document presents the factors that will be considered for qualifying a fuel producer's analytical chemistry laboratory. First, approved analytical methods must be used which meet stated reliability requirements for the analysis of uranium-plutonium mixed oxide pellets and uranium dioxide insulator pellets and the source materials of ceramic grades uranium dioxide and plutonium dioxide. Recommended methods have been published by WADCO[1] and LASL[2]; the LASL publication is discussed in later section II. D. The second factor considered is the use of specified materials for the calibration of all analytical methods. These materials will be discussed in the next section (II. B). Lastly, qualification requires that a laboratory satisfactorily analyze a series of test samples for 20 different specifications prior to the start of a fuel production period. These samples will be mixed oxide pellets and mixed oxide powder blends with measured levels of uranium, plutonium, and impurity elements.

B. Preparation of Calibration Materials

An important factor controlling the accuracy of analytical methods is the use of correct calibration materials. For a reactor fuel production program, the use of the same calibration materials by all the laboratories involved reduces between-laboratory differences which, in turn, reduces shipper-receiver differences. The only available materials useful for the calibration of methods for the analysis of FFTF fuel and source materials are assay and isotopic standards for uranium and plutonium distributed by the National Bureau of Standards. These are specified for use in this program. For metal and nonmetal impurities, calibration powder blends have been prepared and characterized.

These calibration blends consist of mixtures of impurity compounds and the matrix powders in which the impurities are present at five concentration levels generally covering the range of one-tenth to twice the specification values. The matrices are uranium-plutonium mixed oxide, uranium oxide, and plutonium oxide that have been supplied by WADCO as typical of the FFTF fuel and source materials. The blends were prepared by combined grinding and vibratory mixing operations. Extensive sampling and analysis has verified the accuracy and homogeneity of these blends. They now will be packaged and shipped to WADCO for distribution to the participating laboratories.

C. Preparation of Quality Control Samples

The most effective means to know the accuracy and precision of the results being turned out by an analytical laboratory is accomplished by a quality control program administered by an independent organization. During periods of FFTF fuel production, LASL-prepared and characterized quality control samples that match the fuel and source materials will be analyzed in the fuel fabrication and WADCO laboratories. The planned rate of analysis of these samples is one per 8-hour working shift for each analysis setup used during that shift. These quality control samples consist of powder blends for metal and nonmetal impurities that have been prepared and characterized similarly to the calibration materials. Batches of mixed oxide pellets supplied by WADCO will serve as the quality control samples for the determinations of the concentrations and isotopic abundances of uranium and plutonium and the O/M ratio. One such batch has been carefully characterized for these specifications by statistical sampling and analysis and additional batches are now being so characterized.

D. Compilation and Publication of Analytical Methods

The compilation of 24 analytical methods issued February 1971[2] was written expressly for the analysis of FBR mixed oxide fuel and source materials based on WADCO specifications for the FFTF. These methods are characterized by having been extensively tested and

found to be applicable for these materials containing all impurities up to the allowable specification limits. Other features include detailed directions for calibration using the calibration materials discussed in previous section II. B, information concerning the degree of precision obtainable with the method, and the use of notes in the step-by-step analysis section that explains the chemistry involved and that gives directions to obtain high reliability.

E. Quality Control Assurance Program

A quality assurance program for sampling and chemical analysis of nuclear fuels is essential to guarantee that the fuel meets the strict chemical specifications required for optimum reactor performance. A program based on a statistical design that utilizes to the fullest extent (a) the measured chemical concentrations of fissile materials and impurities, (b) the variability of these concentrations within a production lot, and (c) the precision and accuracy of the analytical methods used to determine these concentrations should also result in minimum sampling and analytical costs. A statistically based program, known as the variable sampling plan, provides information about the magnitude and the variability of these chemical parameters that enables the fuel producer to balance costs between production quality and the number of samples that must be withdrawn from a lot to determine that quality. This plan, combined with a thorough knowledge of the precision and accuracy of the analytical methods, allows the producer to decide if improvement in the specified quality, improvement in the variability of that quality within a production lot, or improvement in the analytical precision will yield the minimum overall production costs (including sampling and analysis) while still ensuring the highest acceptance level of the lots.

Such a program has been developed for application to the production of uranium-plutonium mixed oxide fuel pellets[3].

F. Development of Analytical Methods

1. Fuel Burnup Measurement
(R. M. Abernathey, G. M. Matlack, J. E. Rein)

Stable fission product ^{148}Nd with nearly equal fission yields for ^{235}U and ^{239}Pu in thermal to fast reactor spectra and only a 10% higher yield for ^{238}U is an excellent monitor of total fissions in mixed oxide uranium-plutonium fuels. Relative (percent) burnup is mostly accurately measured on irradiated fuels based on analyses for ^{148}Nd and the postirradiation quantities of uranium and plutonium isotopes.

Several sequential separation methods have been reported in which fractions of these three elements are obtained which then are analyzed by thermal ionization mass spectrometry. These methods are characterized by lengthy procedures involving as many as five distinct separation operations. A method has been developed which involves only two separation operations. An aliquot of the dissolved fuel with added isotope spikes of ^{150}Nd, ^{233}U, and ^{242}Pu is fumed with perchloric acid and transferred in 12M hydrocloric acid to a 10X anion exchange resin column equilibrated with 12M hydrochloric acid. The effluent containing neodymium and most other fission products is fumed with nitric acid and transferred in a mixture of 1 volume of 8M nitric acid and 9 volumes of methanol to a 2X anion exchange resin column equilibrated with this same reagent. Elution with a mixture of 1 volume of 0.08M nitric acid and 9 volumes of methanol chromatographically separates americium and the rare earths giving a clean neodymium fraction for the mass spectrometric analysis. Plutonium is eluted from the 10X anion exchange resin column with a 12M hydrochloric acid mixture followed by uranium with 0.1M hydrochloric acid. Each of these fractions also is mass spectrometrically analyzed. Alternatively, with little sacrifice in reliability, plutonium and uranium can be eluted together with 0.1M hydrochloric acid and mass spectrometrically analyzed with one filament loading.

A spike isotope mixture of ^{150}Nd, ^{233}U, and ^{242}Pu, prepared for use on irradiated FBR fuel samples handled at LASL as part of Project 401, was calibrated. The precisions, expressed as relative standard deviation of the mean, for the three spike isotopes are 0.17% for ^{150}Nd, 0.13% for ^{233}U, and 0.07% for ^{242}Pu. This

set of values is as precise as any previously reported and will provide highly reliable burnup measurements.

2. Gas Analysis of Irradiated Fuels
(R. M. Abernathey, J. E. Rein)

The recently received mass spectrometer to be used for the quantitative analysis of cover gas and fuel pin gas including isotopic abundance of fission product krypton and xenon met LASL test specifications and is now operational. The instrument is being carefully calibrated for each gas component that may be present in the samples to provide highly reliable analyses.

3. Determination of the Isotopic Distribution of Uranium and Plutonium in Mixed Oxide Fuel
(G. M. Matlack. R. M. Abernathey, J. E. Rein)

A method was developed in which plutonium and uranium are sequentially separated on a single anion exchange column and individually analyzed for isotopic abundances by thermal ionization mass spectrometry. The separation factors are 300 for americium and > 1 x 10^5 for uranium in the plutonium fraction and 150 for plutonium in the uranium fraction. These factors permit the determination of the isotopic abundances of ^{238}Pu and ^{241}Pu at the required levels for the specification analysis of LMFBT/FFTF uranium-plutonium mixed oxide fuel in which the initial $^{238}U/^{238}Pu$ ratio is almost 2000 to 1 and the initial ^{241}Am content can be as much as 2400 μg per gram of plutonium.

An aliquot of the dissolved fuel sample containing about 100 μg of plutonium and 300 μg of uranium is fumed with perchloric acid and the solution is transferred in 12M hydrochloric acid to a highly cross-linked (10X) anion exchange resin column. Americium and impurity elements are eluted with 12M hydrochloric acid and discarded. Plutonium is eluted with a 12M hydrochloric acid-0.1M hydriodic acid mixture.

After a rinse with this same mixture to remove plutonium tailings, uranium is eluted with 0.1M hydrochloric acid. Portions containing about 0.5 to 1 μg of plutonium and of uranium from the separated fractions then are analyzed separately by thermal ionization mass spectrometry using a triple filament source and a Faraday cup detector.

4. Determinations of O/M Atom Ratios
(G. C. Swanson, J. W. Dahlby, G. R. Waterbury)

Investigation of the many problems involved in the measurement of O/M atom ratios was continued, following the development of a recommended thermogravimetric method. The recommended method included an oxidation of the oxide fuel in air at 1000°C to a hyperstoichiometric mixture which was reduced in He-8% H_2 at 1000°C to the exactly stoichiometric dioxide. The O/M ratio was calculated from the initial and final weights.

As the thermogravimetric method depended upon selection of the proper gas composition, temperature, and duration of reduction to produce exact stoichiometry of the final oxide, many reduction conditions were tested using samples of prepared oxides having known oxygen contents. These oxides were made by oxidizing high purity U and Pu metals (< 200 ppm total impurities) carefully in air and the oxygen contents were calculated from initial and final weights. Mechanical mixtures of these materials were then reduced under various conditions until proper gas mixtures and reduction temperatures were found. The results of many such analyses showed that reduction in He-8% H_2 at 1000°C for six hours, as stated in the recommended method, resulted in a product having an O/M ratio of 2.000.

The effects of selected impurities on the recommended method were determined. Those commonly found in mixed oxide materials, or stated in the fuel specifications were included. Test samples were prepared from a mechanical mixture of unsintered, high-purity, U_3O_8 and PuO_2, and also from finely ground, sintered $(U_{0.75}Pu_{0.25})O_2$ pellets. It was found that Ni, Ni_2O_3, Fe, and Al_2O_3, at levels ranging from 375 to 2000 ppm as the metal, did not change the measured O/M ratio of either the sintered or unsintered oxides by more than 0.003 (Table 472-I), but Ca, CaO, Fe_2O_3, Al, C, at metal or elemental concentrations of 400 to 1100 ppm, caused errors of 0.004 or greater.

Combinations of Al, Fe, Cr, Ni, Si, and Ti and combinations of their oxides at a total metal concentration of 1000 ppm caused much larger effects especially

TABLE 472-I

EFFECTS OF SELECTED IMPURITIES ON THE THERMOGRAVIMETRIC DETERMINATION OF O/M RATIO

Element	Form	Concentration[a]		Effect on O/M Ratio[b]	
		Unsintered	Sintered	Unsintered	Sintered
Ca	metal	1025	1100	- 0.006	- 0.006
	CaO	420	570	+ 0.004	+ 0.006
Ni	metal	1050	2000	- 0.003	- 0.003
	Ni_2O_3	535	890	+ 0.003	- 0.002
Fe	metal	965	775	- 0.003	0.000
	Fe_2O_3	595	615	+ 0.004	+ 0.006
Al	metal	995	1035	- 0.026	- 0.025
	Al_2O_3	375	565	0.000	- 0.001
C	elemental	965	855	+ 0.013	+ 0.014
Al, Cr, Fe, Ni, Si, Ti	metal	300 to 600 ppm each		- 0.009 to - 0.032	- 0.006
	oxides	50 to 150 ppm		+ 0.003 to - 0.001	+ 0.005 to + 0.003

[a] ppm of the element whether added as metal, oxide, or compound.
[b] Average of duplicate determinations.

in case of the Al. Addition of Na and S as Na_2SO_4 corroded the fused silica boat and furnace tube, and the results obtained were not considered reliable.

The recommended conditions for analysis were intended to apply to sintered (U,Pu) solid solution oxides and to ceramic grade U and Pu oxide powders. Although the reduction behavior of the ceramic powders might be expected to be similar to the reduction behavior of the prepared high-purity oxide mixture, there are no date to this effect. In addition, installation data do not exist to compare the reduction behavior of mechanical mixtures with solid solutions of mixed oxides. Preparation of solid solutions therefore was undertaken. Evaporations of various aqueous solutions of U and Pu, including chloride, sulfate, perchlorate, formate, and acetate solutions, were investigated but were not satisfactory because the salts either were deliquescent, decrepitated on drying, segregated on evaporation or on burning, or were insoluble. Evaporating nitrate solutions of U and Pu at room temperature produced crystalline salts which when dried very slowly at 100°C yielded a powder that burned cleanly to oxide. Analysis of the solid solution oxide prepared from nitrate will be completed as time permits.

5. Determination of Sulfur
(G. C. Swanson, T. K. Marshall, R. G. Bryan, G. R. Waterbury)

Sulfur, a recently added chemical specification for FFTF fuels, is determined spectrophotometrically as Lauth's Violet following separation from solution of UO_2, PuO_2, or $(U,Pu)O_2$ by distillation as H_2S. The samples are dissolved by repeated evaporations with HNO_3-HF or in HCl at 325°C in a sealed tube[4], and higher oxidation states of sulfur are reduced in boiling HI-H_3PO_2 to H_2S which is distilled into Zn ($C_2H_3O_2$) solution. The resulting ZnS is reacted with HCl, p-phenylenediamine, and $FeCl_3$ to form Lauth's Violet. The amount of sulfur is calculated from the absorbance of the Lauth's Violet at 595 nm using a standard curve prepared from data obtained by analyzing known quantities of K_2SO_4 added to solutions of U, Pu, and U plus Pu.

Preliminary reduction of nitrate with formic acid, and of Pu(IV) and Pu(VI) with NH_2OH improved the method by yielding more quantitative recovery of sulfur. As with many distillation methods, recovery of sulfur is influenced by the amounts of metals present in solution, and for this reason a calibration using solutions similar in composition to the sample solutions was found to be necessary. Relative standard deviations were 6 to 3% in measuring 50 to 600 $\mu g/g$ of sulfur in 0.1-g samples and 12 to 5% in measuring 10 to 120 $\mu g/g$ of sulfur in 0.5-g samples. Analyses of 64 UO_2 and 64 $(U,Pu)O_2$ samples were carried satisfactorily. None of the impurity elements for which maximum concentrations in FFTF fuels have been specified (Al, B, Be, Ca, Cd, Co, Cr, Fe, K, Li, Mg, Na, Ni, Ta, W, V, Cu, Si, Ti, Zn, Ag, Mn, Mo, Pb, and Sn) caused interference in the method even when present at twice their specified maxima.

Recently, the method was modified to decrease sample preparation time. The formic acid reduction of nitrate was eliminated, and the nitrate was reduced by NH_2OH simultaneously with the Pu(IV) and Pu(VI) reduction. The residue from the final HNO_3-HF evaporation was taken up in 3N HCl, and sufficient 20% NH_2OH was added to reduce nitrates and higher oxidation states of Pu. Beside shortening sample preparation time, this modification avoided possible particulate losses due to spattering during the formic acid reduction of dry

nitrate salts.

6. Determination of Phosphorus
(R. G. Bryan, T. Romero, G. R. Waterbury)

Measurement of phosphorus at low concentrations in PuO_2, UO_2, and $(U,Pu)O_2$ was necessary to ensure that the specified maximum of 100 μg/g in FFTF fuel materials was not exceeded. Analysis of solutions of the oxides was accomplished by reacting the phosphorus with $(NH_4)_2MoO_4$ to form phosphomolybdic acid which was extracted into n-butanol, reduced with $SnCl_2$, and measured spectrophotometrically at 725 nm. The phosphorus content was calculated from the measured absorbance and the average absorbance/μg phosphorus obtained for samples containing known amounts of phosphorus.

One of the main problems was the dissolution of the oxides without contamination or loss of phosphorus. Hot 15.6M HNO_3 containing a trace of HF dissolved UO_2 readily, sintered $(U,Pu)O_2$ slowly, and PuO_2 very slowly. Dissolution in HCl at 325°C in a sealed tube was recommended for high-fired PuO_2. Following dissolution, the solution was fumed with HF-$HClO_4$ to remove volatile acids and Si. Fuming with H_2SO_4 caused low and erratic results.

Repeated measurements of phosphorus added at concentrations between 10 and 200 μg/g to 50-mg samples of UO_2, PuO_2, and $(U,Pu)O_2$ showed that the method was unbiased. The relative standard deviation was no greater than 3% for phosphorus concentrations of 100 μg/g or more and increased to 4% at 40 μg/g and to 10% at 10 μg/g. The Beer-Lambert Law was obeyed in the range of 0.5 to 10 μg of phosphorus (10 to 200 μg/g).

At the maximum impurity specifications for the FFTF materials, only Sn and Ta interfered. These elements did not interfere when present at 0.1 of their specification maxima. The method was used to measure phosphorus satisfactorily in many oxide samples, including the calibration and quality control glends prepared at LASL.

7. Determination of Chloride and Fluoride
(T. K. Marshall, N. L. Koski, G. R. Waterbury)

Measurements of the concentrations of chloride and fluoride in UO_2, PuO_2, and sintered $(U,Pu)O_2$ were especially important because of the serious effects of the halides on the corrosion rates of stainless-steel cladding materials. Reliable methods existed for measuring chloride concentrations as low as 1 μg/g and chloride concentrations down to 10 μg/g on separate samples, but a new method involving the simultaneous measurement of fluoride and chloride was developed to reduce the analysis time and to improve the sensitivity of the measurement of each halide. The chloride and fluoride were separated simultaneously from the oxide sample by pyrohydrolysis at 1000°C in a Ni boat and furnace tube using a flow of Ar-steam mixture that produced 8 ml of condensate in 15 min. The fluoride was measured with a fluoride specific-ion electrode in a 1-ml aliquot of the condensate. The chloride in the remainder of the condensate was reacted with $Hg(CNS)_2$ and Fe^{+3} to form $Fe(CNS)_3$ which was measured spectrophotometrically at a wavelength of 460 nm.

Repeated measurements of chloride and fluoride added as NaCl and HF to 1-g samples of oxides showed that the relative standard deviations were approximately 5% for a single determination of 6 to 50 μgCl/g and 10% for 4 μgCl/g. Relative standard deviations were 7% for measuring 5 to 50 μgF/g oxide and 10% for 1 to 5 μgF/g. There was no bias. This reliability was considered adequate for the small quantities of halides measured. The method was used successfully in measuring chloride and fluoride in several oxide samples including the various calibration blends and quality assurance blends described previously.

8. Determination of Water and Gases
(D. E. Vance, M. E. Smith, G. R. Waterbury)

Gases released from reactor fuels contribute significantly to the internal pressures developed in sealed fuel capsules, and maxima for the contents of water and other gases are specified for FFTF mixed oxide fuel pellets. To determine if specifications are met, measurements of these gaseous contaminants are necessary. The quantity of water released from the sintered oxide pellets at 400°C is measured separately from the other gases that are evolved at 1600°C.

In the measurement of water, a fuel pellet is heated in a fused-silica furnace tube and the evolved water is swept by argon to a moisture monitor. Integration of the monitor signal provides a quantitative measure of the water. As some controversy existed concerning the optimum temperature for the quantitative release of water, the quantities evolved from several pellets at temperatures between 200 and 950°C were measured. It was observed that all the water was evolved from each pellet at a temperature of 400°C or lower. Water was evolved from some pellets in two distinct peaks, indicating that it might be present in two different states.

Certain published methods for measuring water recommend heating the pellet in a tungsten crucible. As reduction of water by tungsten at elevated temperatures was suspected, the reaction was studied by determining with a mass spectrometer the H_2 in the reaction products formed by heating water vapor in an Ar gas carrier with tungsten powder. A definite reaction at 400°C was observed, but the rate was so slow that 20 minutes at temperature were required to produce measurable quantities of H_2. At 350°C, no reaction occurred within 45 minutes.

These investigations showed that 400°C was adequate for quantitative evolution of water without risking a significant water-tungsten reaction. In the recommended method the use of a fused silica support for the pellet during heating is recommended.

The effects of the storage environment on the quantity of adsorbed water was demonstrated by drying three fuel pellets at 600°C in a stream of He for 10 h. One pellet was then stored over water for 24 h, another was exposed to the room temperature (40 to 50% relative humidity) for 24 h, and the last was placed in a dry atmosphere for 28 h. At the end of the storage period, each pellet was analyzed for water with results of 3 μg/g, 1 μg/g, and 0 μg/g, respectively. These data indicate the desirability for some type of uniform pretreatment of the fuel pellets. Following a comparison of several pretreatments, drying the pellets in air at 110°C for 1 h was selected as the most satisfactory. This treatment can be duplicated easily in any laboratory.

Gases other than water were evolved by heating the sintered mixed oxide inductively in a tungsten crucible to 1600°C. These gases were collected by a vacuum extraction apparatus, dried over anhydrous $Mg(ClO_2)_2$, and measured manometrically. Reaction of the hot tungsten crucible and any water evolved from the fuel pellets to form H_2, as described above, would cause erroneously high results.

Mass spectrometric analyses of the evolved gases showed that the main constituents were H_2 and CO. It has been suggested that the major portion of H_2 probably was adsorbed by the pellets from the sintering-furnace atmosphere during pellet manufacture[5]. The CO probably is a product of the reduction of the mixed oxide by carbon impurities.

Although these methods are free of known difficulties, exact measurement of their accuracy is not possible because suitable standards are not available. Consistent results are obtained if the recommended evolution and measurement conditions are carefully maintained.

9. Determination of Carbon
(C. S. MacDougall, M. E. Smith, G. R. Waterbury)

Analysis for carbon in U, Pu, and sintered U-Pu mixed oxides by igniting samples at 1000°C in O_2 for 10 min and manometrically measuring the CO_2 produced was shown to be reliable if the samples were finely ground. Low results were obtained for unground oxides. Tests were made to determine if grinding in a CO_2-free atmosphere was necessary. Repeated analyses of sintered $(U,Pu)O_2$ pellets ground in air and in a carbon dioxide-free atmosphere showed no significantly different results. In other tests, six measurements of carbon were made on each of the following materials prepared from one lot of sintered $(U,Pu)O_2$ pellets: (1) unground chunks, (2) powder ground in argon, (3) powder exposed to air one week and reground in air. Low values were obtained for the chunks and exposure of the ground sample to air for one week caused a very small pickup of carbon. Regrinding in air did not affect the carbon content.

It was concluded that oxides must be ground prior to measuring carbon and that the grinding can be done in air if exposure to air is minimized by making the analysis as soon as possible following grinding. Increasing the ignition temperature from 1000 to 1300°C did not increase the amount of CO_2 evolved from $(U,Pu)O_2$ powder samples. A temperature of 1000°C, therefore, was considered adequate and was used successfully in the repeated measurements of carbon in various U, Pu, and mixed U-Pu oxides including the calibration blends and quality assurance blends prepared at LASL.

10. Determination of Uranium in Plutonium Dioxide
(N. L. Koski, G. R. Waterbury)

Measurement of U at trace concentrations in ceramic grade PuO_2 is necessary to assure that the specified maximum of 2000 μg/g for FFTF material is not exceeded. A spectrophotometric method for measuring U in high-purity Pu metal[6] was improved and successfully applied to this measurement. This method uses a sample of 1 to 3 g to provide adequate sensitivity for the U measurement and two passes through an ion exchange resin column to assure clean separation of the trace of U. An investigation of the use of smaller samples and various modifications in the separation procedure showed that a 70-mg sample was adequate for the 300 to 3000 μg/g U concentration range of interest and that a single pass through the ion exchange resin column provided adequate separation. The method was modified also to use HNO_3 to dissolve the samples. Following dissolution and fuming to remove HNO_3, the Pu in 9M HCl was reduced to non-adsorbable Pu(III) with NH_2OH and $SnCl_2$, and the solution was passed through a Dowex-1 x 2 resin column to adsorb only the U(VI). Subsequent elution of the U with dilute HCl and reaction with Arsenazo I produced a U(VI)-Arsenazo I complex that was measured spectrophotometrically at a wavelength of 600 nm. The quantity of U was obtained from the absorbance using a standard curve. The high molar absorptivity of the complex (23,000) assured reliable detection of quantities of U as small as 3 μg.

The standard deviation was 5 relative percent for U concentrations between 1500 and 3000 μg/g and 10 relative percent for 300 to 1100 μg/g. Bias was eliminated by chemical calibration when present. At the impurity specification limits for PuO_2, none of the elements interfered.

11. Determination of Metal Impurities by Carrier Distillation Emission Spectroscopy
(J. V. Pena, W. M. Myers, C. J. Martell, C. B. Collier, R. T. Phelps)

Control of metal impurities in the mixed oxide pellets requires reliable analytical methods both for the fuel and the UO_2 and PuO_2 source materials. Spectrographic methods using the carrier-distillation technique previously were found satisfactory for determining 20 metal impurities in these materials[7]. Recent changes in the FFTF specifications for these materials has required further study and method modifications to include measurements for five additional metals, namely, Be, Co, K, Li, and Ta. These modified methods apply to the determination of the 25 elements listed in Table 472-II over the stated concentration ranges. The methods developed involve use of calibration materials (standards) prepared with U_3O_8, PuO_2 and sintered $(U_{.75}Pu_{.25})O_2$ matrix and with all 25 impurity elements present at the concentrations stated in Table 472-II. A U_3O_8 matrix is used because the analysis of UO_2 includes its conversion to U_3O_8. Microphotometry of the spectrogram was used to calculate the concentrations of the impurity elements. This practice is recommended if a precision better than 30% relative standard deviation is to be realized. The use of a suitable element as an internal standard is also recommended because it improves the precision to better than 20%. Evaluation of concentration by visual comparison of spectra yields results with about 50% relative standard deviation and is to be avoided unless previously verified by microphotometry.

TABLE 472-II

METAL IMPURITIES DETERMINED IN MIXED OXIDE, UO_2, AND PuO_2

Impurity	Concentration Range, μg/g
Al, Fe, Na, Ni, V	50-1000
Si, Ta	40-800
Ca, Cr	25-500
Cu, K, Ti, Zn	20-400
Ag, Mg, Mn, Mo, Tb, Sn, W	10-200
B, Be, Cd, Co	2-40
Li	1-20

a. Methods for Uranium Oxide

Two methods were developed for the analysis of UO_2 (Table 472-III). Most of the 25 impurity elements are determined using 4% Ga_2O_3 as the carrier. Added Co serves as an internal standard for determining impurities Al, B, Cr, Fe, Mn, Ni, and Si with a precision of 15% relative standard deviation. Cobalt and the refractory elements, Mo, Ta, Ti, V, and W, are determined with AgCl carrier and Pd internal standard. The elements measured by microphotometry but without an internal standard (Ag, Be, Ca, Cd, Cu, K, Li, Mg, Na, Pb, Sn) are determined with 20% relative standard deviation.

b. Methods for Plutonium Oxide

The determination of impurities in PuO_2 requires four methods, two using Ga_2O_3 carrier and two using AgCl carrier (Table 472-III). Two methods using Ga_2O_3 carrier are required because the spectral coverage of the spectrograph is not adequate to include the sensitive K lines at wavelengths 7665 Å with the lines of the other impurity elements. By determining K, Li, and Na separately, better detection sensitivity for Li and greater latitude of exposure conditions are obtained. Cobalt is used as an internal standard for most of the impurities determined by Ga_2O_3 carrier. Two AgCl carrier methods, using different concentrations of the carrier and electrode charge sizes, are needed to obtain adequate detection limits for Ta and W. Palladium serves as an internal standard for Co, Mo, V, and W. For the determination of Ta and Ti, Hf is added as the internal standard. An average precision of 20% relative standard deviation is obtained for the 25 impurity elements over the required concentration range of one-tenth to twice the specification values (Table 472-II).

TABLE 472-III

SUMMARY OF METHODS FOR THE CARRIER DISTILLATION SPECTROSCOPIC DETERMINATION OF UO_2, PuO_2, AND MIXED OXIDE

Material Analyzed	Impurity	Carrier	Internal Standard	Arc Atm	Electrode Charge, mg	Current Amp
UO_2	Ag, Al, B, Be, Ca, Cd, Cr, Cu, Fe, K, Li, Mg, Mn, Na, Ni, Pb, Si, Sn, Zn	4% Ga_2O_3 + 2.4% graphite	Co	Air	100	12
UO_2	Co, Mo, Ta, Ti, V, W	15% AgCl	Pd	O_2	130	7
PuO_2	Ag, Al, B, Be, Ca, Cd, Cr, Cu, Fe, Mg, Mn, Ni, Pb, Si, Sn, Zn	4% Ga_2O_3	Co	O_2	100	18
PuO_2	K, Li, Na	4% Ga_2O_3	-	O_2	100	10
PuO_2	Co, Mo, V, W	40% AgCl	Pd	O_2	50	7
PuO_2	Ta, Ti	15% AgCl	Hf	O_2	120	6
Mixed Oxide	Ag, Al, B, Be, Ca, Cd, Cr, Cu, Fe, Mg, Ni, Pb, Si, Sn, Zn, Mn	6.4% Ga_2O_3	Co	O_2	100	18
Mixed Oxide	K, Li, Na	6.4% Ga_2O_3	-	O_2	100	10
Mixed Oxide	Co, Mo, V, W	40% AgCl	Pd	O_2	50	7
Mixed Oxide	Ta, Ti	15% AgCl	Hf	O_2	120	6

c. Methods for Mixed Oxide

Four methods similar to those used to analyze PuO_2 are required (Table 472-III) for the analysis of mixed oxide. This was found necessary because of the spectral interference arising from the presence of both U and Pu. Cobalt serves as an internal standard for the impurities determined by Ga_2O_3 carrier except for Ag, Cu, K, Li, and Na. As with PuO_2, two AgCl carrier methods are needed to obtain adequate sensitivity for Ta and W. Palladium serves as an internal standard for determining Co, Mo, V, and W while Hf is used for Ta and Ti. The average precision for all impurity elements is 20% relative standard deviation.

12. Determination of Dy, Eu, Gd, and Sm by Emission Spectroscopy
(H. M. Burnett, O. R. Simi)

A TNOA (tri-n-octylamine) extraction method was modified to apply to the determination of Dy, Eu, Gd, and Sm in UO_2, PuO_2, and sintered mixed oxide. The method uses three extractions with 20% TNOA in xylene to remove U and Pu from a 6.7M HCl solution of the sample (0.2 g as oxide) to which has been added 5 mg H_3BO_3. The aqueous phase, which contains the rare earths, added yttrium internal standard, and other nonextracted impurity elements, is treated to remove residual amounts of boron by volatilization and organic matter by ignition. A portion of the residue is dried on copper electrodes and the characteristic spark spectra are excited in an argon atmosphere. This method is based on work reported by Ko[8] but with significant modifications to permit reliable analyses of materials containing maximum concentrations of impurities specified for FFTF sintered mixed oxide fuel and source materials.

The recommended procedure prescribes a complete processing of each calibration blend along with a reagent

blank. The calibration materials, which are blends of 29 metal impurities (the 25 metals listed in Table 472-II plus Dy, Eu, Gd, and Sm) in the appropriate matrix, are not completely soluble in either 15M HNO_3 - 0.05M HF, 12M $HClO_4$, or 6M HCl. The small amount of insolubles, however, does not interfere with the separation of the U and Pu nor the determination of the rare earths. An assessment of the calibration materials was made by processing and evaluating three portions of each blend. The extracted solutions from each of the three matrices are similar except for the amount of Am present. The amount of Am from the PuO_2 matrix caused spectral interference with the Dy analytical line (4000.5 Å) used in the analysis of UO_2 and mixed oxide matrices. Dysprosium concentration was evaluated in the PuO_2 materials by using the Dy 3531.7 Å line. Calibration curves (log-log plots of concentration vs intensity ratios) established from the three repeat analyses were linear over the concentration range of 10 to 200 μg/g with satisfactory slopes. An average precision of better than 10% relative standard deviation for the intensity ratio measurement of the rare earths in the calibration materials were verified by comparison with known samples prepared independently and in a different manner.

The calibration materials were used in the recommended fashion to evaluate specially prepared quality control samples. The results also showed a precision of better than 10% relative standard deviation. The amounts of rare earths found in the quality control samples were in excellent agreement with the makeup values. Repeat sampling and evaluation showed the materials to be homogeneous.

III. ANALYTICAL CHEMISTRY PROGRAM FOR BORON CARBIDE

The proposed neutron absorber material for LMFBR/FFTF control rods is boron carbide pellets. A program has been initiated to establish the status of analytical methods for the chemical characterization of boron carbide and to develop improved or alternate methods of analysis.

A. Status of Analytical Methods

(J. E. Rein, C. F. Metz)

Boron carbide pellets prepared by WADCO and pulverized samples were distributed to ORNL, LASL, and the WADCO analytical laboratories as round robin samples. Analysis of those materials will show the status of the proposed analytical methods for chemical specification analysis. The three laboratories have been given a sampling and analysis plan which will provide statistically computed estimates of pellet-to-pellet variability and the analytical method precision. The methods to be used are essentially those proposed by WADCO[9]. The laboratories, however, also have been requested to analyze the samples by their own methods as time permits. The requested completion of the round robin analyses is early August 1971 and the statistical analysis of the data should be complete two weeks after receipt of the analytical results. The analyses to be made are total boron, total carbon, soluble boron, soluble carbon, $^{10}B/^{11}B$ isotopic ratio, chloride, fluoride, and specified metal impurities.

B. Investigation of Methods

1. Determination of the $^{10}B/^{11}B$ Isotopic Ratio in Boron Carbide

(R. M. Abernathey, J. E. Rein)

The present method[9] used for the isotopic abundance measurement of boron involves a lengthy chemistry treatment prior to the mass spectrometric measurement. A greatly simplified method has been developed which is based on the ORNL method for the mass spectrometry of boron materials[10]. A weighed portion of a pulverized powder sample and a weighed quantity of pulverized sodium hydroxide are mixed in a plastic capsule in a Wig-L Bug blender for 30 seconds. An approximately 25-μg aliquot of the mixture is transferred to a canoe-shaped tantalum or rhenium filament and sufficient current is passed through the filament to fuse the mixture giving sodium metaborate or sodium tetraborate. The filament is transferred to the mass spectrometer where an extremely stable emission of $Na_2BO_2^+$ ions is obtained. This simple chemical treatment requires about 5 to 10 min and the mass spectrometry measurement takes about 15 min.

The ratio of sodium hydroxide/boron carbide affects the relative volatilization of ^{10}B and ^{11}B $Na_2BO_2^+$

ions. An increasing ratio gives a high $^{11}B/^{10}B$ ratio. This agrees with an NBS study[11] using varying ratios of sodium hydroxide and boric acid. The cause is attributed to preferential excitation of sodium ions which therefore requires a higher filament current to obtain the $Na_2BO_2^+$ ion spectra. At higher filament currents, the resulting increased temperature causes selective volatilization of the lighter $^{10}B\ Na_2BO_2^+$ ion resulting in an increasing $^{11}B/^{10}B$ ratio with time. Experiments were done with varying ratios of sodium hydroxide and boron carbide over the Na/B ratio range of 1/2 to 4/1. Excellent emission stability and correct $^{11}B/^{10}B$ ratios were obtained over the Na/B ratio range of 1/2 within a 30-minute scan period.

2. Dissolution of Boron Carbide
(R. D. Gardner, A. L. Henicksman, W. H. Ashley)

The classical method for dissolution of boron carbide is fusion with sodium carbonate. Several disadvantages are inherent such as, only a small sample can be fused at one time; a large ratio of sodium carbonate reagent to sample is necessary; the sample must be finely pulverized, an operation which introduces impurities; and the difficulty of avoiding mechanical loss in the fusion or in the subsequent acidification of the sodium carbonate solution. A different approach to this problem proved successful. The sample is digested overnight in quartz-distilled (concentrated) HNO_3 in a sealed quartz tube at 300°C. These conditions have been reported to dissolve BN, B_4C, and elemental B[12]. Carbon oxidizes quantitatively to CO_2 and boron converts to boric acid. None of the disadvantages of the alkaline fusion technique are encountered.

For the assay procedure for boron (or for the chemican determination of impurity elements) samples of 300 mg of boron carbide are dissolved by overnight heating at 300°C with 6 ml of quartz-distilled HNO_3. Fine subdivision of the sample is not required and this sample size is large enough to allow a precise boron assay. The introduction of impurities is eliminated except for a trace of silicon dissolved from the tube. Repeated determinations have shown that this amount is quite constant, about 0.25 mg, or about 0.1% of the recommended sample weight.

3. Determination of Total Boron
(R. D. Gardner, A. L. Henicksman, W. H. Ashley)

In the conventional volumetric determination of boron, the titration is normally carried out by neutralizing the solution to a visual indicator endpoint or a fixed pH, adding mannitol, and titrating to a different visual indicator endpoint or fixed pH. This technique is probably not capable of a relative standard deviation better than 0.1%. Improvements include the use of a second derivative technique for establishing the endpoints, the use of a large sample, the use of a weight buret, and the use of NBS boric acid (SRM 951) for calibration of the sodium hydroxide titrant. The last improvement also obviates the need for a blank correction. The methods with these changes, when applied to 16 portions of pure boric acid, gave a relative standard deviation of 0.012%.

Prior to the titration, the samples were boiled for 5 min in covered beakers to remove absorbed CO_2; absorption of CO_2 during the titration was prevented by floating pentane on the solution. The boiling treatment was tested for possible loss of boron by comparing two series of 6 titrations each of 300-mg H_3BO_3, one series in which the H_3BO_3 was dissolved in freshly boiled water and immediately titrated and the other series in which the samples were acidified, the beakers were covered, the solutions were boiled for 5 min, cooled, and titrated. The differences were insignificant.

The present tentative method for the determination of boron in B_4C includes dissolution of the sample by sodium carbonate fusion and subsequent dissolution of the melt in water. The large excess of sodium carbonate causes hydrolytic precipitation of most of the specification metal impurities, which if not removed would cause a positive bias. Since iron is usually the major impurity in B_4C, loss of boron may be caused from the carrying nature of ferric hydroxide. For this reason removal of metal ions by cation exchange is being investigated.

4. Determination of Total Carbon
(R. D. Gardner, A. L. Henicksman, W. H. Ashley)

The determination of carbon in boron carbide by direct combustion in oxygen is complicated by the fact

that the sample particles, even when very finely divided, form a glaze or protective film of boron oxide on the surface which prevents complete oxidation of the sample. Lead oxide, metallic tin, copper-coated metallic tin, and copper oxide were all tried as flux materials in an attempt to prevent formation of this protective coating. None of these materials promoted complete oxidation of the sample.

Vanadium pentoxide was found to be a satisfactory flux when the particle size of the sample was reduced to pass a 100 mesh sieve. In an attempt to improve the precision of the method, the sample size was increased from 35 to 100 mg. Using an oxygen flow of 0.25 l/min and a furnace temperature of 1100°C, 30 min is required for complete combustion.

Five lots of commercial boron carbide containing 20.7 to 30.4% carbon were analyzed using vanadium pentoxide as the flux. For eight determinations per lot, the relative standard deviation was 0.25%.

5. Determination of Soluble Carbon
(A. L. Henicksman, W. H. Ashley, R. D. Gardner)

Selective oxidation of the uncombined (soluble) carbon to CO_2, filtration and an analysis of the undissolved residue for weight percent carbon is the basis of a method for this determination. For a sample containing only B_4C and soluble carbon, it can be shown that the soluble carbon is calculated from the relationship:

$$C_s = \frac{T-Z}{1-Z}$$

in which:

C_s = decimal fraction soluble carbon in sample

T = decimal fraction total carbon in sample

Z = decimal fraction of combined carbon in the undissolved portion (B_4C),

so long as the value of Z is not changed by the selective oxidation reaction.

A 60% H_2SO_4 solution containing potassium dichromate is used at 100°C for the selective oxidation[13]. The rage of dissolution of boron carbide in this mixture is fairly rapid initially, but decreases with time. For example, one 368-mg sample required one week to dissolve completely. Portions of another boron carbide sample were subjected to the oxidation treatment for periods from one to 70 hours. Analysis of the undissolved portion gave a constant value for Z indicative that the method has promise.

Factors adversely affecting the method are the presence of impurities and the extent of soluble boron in the sample. These factors are being investigated.

IV. PUBLICATIONS

1. J. E. Rein, G. M. Matlack, G. R. Waterbury, R. T. Phelps, and C. F. Metz, "Methods of Chemical Analysis for FBR Uranium-Plutonium Oxide Fuel and Source Materials," LA-4622 (1971).

2. G. R. Waterbury, G. B. Nelson, K. S. Bergstresser, and C. F. Metz, "Controlled-Potential Coulometric and Potentiometric Titrations of Uranium and Plutonium in Ceramic-Type Materials," LA-4537 (1970).

3. D. E. Vance, M. E. Smith, and G. R. Waterbury, "The Determination of Water Evolved from FFTF Reactor Fuel Pellets," LA- report in press.

4. R. K. Zeigler, G. M. Matlack, J. E. Rein, and C. F. Metz, "Statistically Designed Program for Sampling and Chemical Analysis of Reactor Fuel Materials," LA- report in press.

V. REFERENCES

1. WADCO Report WHAN-IR-5, August 1970.

2. J. E. Rein, G. M. Matlack, G. R. Waterbury, R. T. Phelps, and C. F. Metz, USAEC Report LA-4622, February 1971.

3. R. K. Zeigler, G. M. Matlack, J. E. Rein, and C. F. Metz, "Statistically Designed Program for Sampling and Chemical Analysis of Reactor Fuel Materials," LA - report in press.

4. C. F. Metz and G. R. Waterbury, USAEC Report LA-3554, 1966.

5. W. H. Pechin and R. A. Bradley, USAEC Report ORNL-4520, Part III, 1970.

6. R. D. Gardner and W. H. Ashley, USAEC Report LA-3551, 1966.

7. W. M. Myers, J. V. Pena, C. B. Collier, C. J. Martell, and R. T. Phelps, LA-4494-MS, pp. 93-5, August 1970.

8. R. Ko, WADCO Report WHAN-IR-5, Method 20.9, August 1970

9. W. L. Delvin and R. W. Stromatt, Report HEDL-TME 71-54, April 1971.

10. E. J. Spitzer and J. R. Sites, USAEC Report ORNL-3528, 1963.

11. E. J. Catanzaro, C. E. Champion, E. L. Garner, G. Marinenko, K. M. Sappenfield, and W. R. Shields, NBS Special Publication 260-17, February 1970.

12. J. M. Donaldson and F. Trowell, Anal. Chem. 36, 2202 (1964).

13. S. Kitzhava, H. Asahara, and T. Atode, USAEC Report ORNL-tr-1778, 1958.

SPECIAL DISTRIBUTION

Atomic Energy Commission, Washington

Division of Reactor Development & Technology

Assistant Director, Nuclear Safety
Assistant Director, Program Analysis
Assistant Director, Project Management
Assistant Director, Reactor Engineering
Assistant Director, Reactor Technology
Chief, Fuels and Materials Branch (3)
Chief, Fuel Engineering Branch

Division of Naval Reactors

Division of Reactor Licensing (3)
Division of Reactor Standards (2)

Atomic Energy Commission, Oak Ridge

Division of Technical Information Extension (100)

Atomic Energy Commission, Richland

Assistant Director for Pacific Northwest Programs

Atomic Energy Commission -- RDT Site Offices

Argonne, Illinois
Idaho Falls, Idaho
Canoga Park, California
Sunnyvale, California
San Diego, California
Oak Ridge, Tennessee

Argonne National Laboratory

Director, LMFBR Program Office (2)
Director, Metallurgy Division (2)

Idaho Falls, Idaho

EBR-II Project Irradiations Manager

Atomics International

Director, LMFBR Technology Program
P. O. Box 1449, Canoga Park

Director, LMFBR Technology Program
P. O. Box 309, Canoga Park

Director, Liquid Metal Engineering Center

Atomic Power Development Associates, Detroit
Head, Fuels & Materials

Babcock & Wilcox

Director, Nuclear Development Center

Battelle Memorial Institute

Associate Manager

Materials Engineering Dept.

Brookhaven National Laboratory

Manager, Metallurgy & Materials Science Division

Combustion Engineering

Manager, Nuclear Laboratories

General Electric Company

Knolls Atomic Power Laboratory

Manager, Sodium Reactor Technology, Sunnyvale (2)

Director, Vallecitos Nuclear Center, Pleasanton

Gulf General Atomic, Inc.

Laboratory Assistant Director

Lawrence Radiation Laboratory

Division Leader, Inorganic Materials

NASA Lewis Research Center

Division Chief, M & S Division

Nuclear Materials & Equipment Corp.

Manager, Plutonium Chemistry & Ceramics Fuels Dev.

Oak Ridge National Laboratory

Director, Metals & Ceramics Div. (2)

Pacific Northwest Laboratory

Manager, FFTF Project (2)
FFTF Fuels Department (2)

United Nuclear Corporation

Manager, Plutonium Fuels Dept.

Westinghouse Electric Corporation

Bettis Atomic Power Laboratory

Advanced Reactor Division (2)

ALT/bc:418(25)